Master's thesis

NTNU
Norwegian University of Science and Technology
Faculty of Information Technology and Electrical Engineering
Department of Electric Power Engineering

Jose Armando Romero Amaya

Active Front End Converter Used in Adjustable Speed Hydro

Master's thesis in Electric Power Engineering
Supervisor: Roy Nilsen
July 2019

NTNU
Norwegian University of Science and Technology

Jose Armando Romero Amaya

Active Front End Converter Used in Adjustable Speed Hydro

Master's thesis in Electric Power Engineering
Supervisor: Roy Nilsen
July 2019

Norwegian University of Science and Technology
Faculty of Information Technology and Electrical Engineering
Department of Electric Power Engineering

NTNU
Norwegian University of
Science and Technology

Abstract

A consistent part of the research in the hydropower field in Norway is being done at NTNU. The Faculty of Information Technology and Electrical Engineering is an active player in this research through the Department of Electric Power Engineering. This research is established through a long-term plan and is organized in four main areas: hydropower structures, turbines and generators, markets and services, and environmental design.

For this purpose, NTNU is the host institution and the main research partner, through Hydrocen whereas SINTEF Energy Research and The Norwegian Institute for Nature Research NINA, also contribute in their respective areas.

At Hydrocen, the research in variable speed machinery based on converter-fed technology is one of the main topics.

The synchronous generator is controlled by an inverter and feeds a DC link, which is connected through the grid by means of the grid side converter, also called Active Front End Converter (AFE).

This Thesis is related to the controls used by the AFE.

The control of the AFE is a cascade control, which includes a hysteresis current and resonant voltage control loop, AC voltage and frequency droop, and other dynamic features as virtual damping and inertia effects.

The focus of this thesis has been the development of a tuning methodology of the resonant controller considering the PI control, resonant control and active damping by means of the Nyquist diagrams and robust control theory guidelines. Also, a delay compensation method has been developed and tested in a simulation environment. The impact of the most important variables has been evaluated and recommendations are given to continue the work.

Sammendrag

Norwegian translation of your English Abstract.

Preface

This thesis is the last step in my master at the Norwegian University of Science and Technology.

The thesis is a continuation of the specialization project from autumn 2018, and some parts of that project have been used and improved. The work has been under the supervision of Roy Nilsen from the Department of Electrical Power Engineering.

This has been a completely new and interesting topic which is highly relevant now that the power electronics based renewable energy sources are becoming widespread all over the world and when old-school generating sources such as pump storage hydropower can benefit from the development of the full frequency converters.

Therefore, I would like to thank my supervisor Roy Nilsen for the support in the completion of this thesis.

Table of Contents

List of Figures

List of Tables

List of Abbreviations and Symbols

$\alpha\beta$	alpha-beta frame coordinate system
dq	dq frame coordinate system
V_{dc}	DC voltage in the DC side of the AFE converter
m_f	Frequency modulation index
f_{cr}, f_{sw}	Carrier frequency or switching frequency
m_a	Amplitude modulation index
V_{m_peak}	Peak value of modulating wave
V_{cr_peak}	Peak value of triangular carrier wave
V_{mA}, V_{mB}, V_{mC}	Three-phase modulating waves
C	Capacitance
P_N	Rated Power of an Inverter
ω_1	Angular frequency at fundamental frequency
V_g	Grid voltage
L_1	Converter side inductor of an LCL filter
V_N	Rated voltage
I_N	Rated Current
L_2	Grid side inductor of an LCL filter plus grid inductance
L_g	Grid inductance
K_{res}	Resonant factor of an LCL filter
f_{res}	Resonant frequency
ω_{res}	Resonant angular frequency
K_P	Proportional gain
K_I	Integral gain
s	Variable in the s plane
ω_c	Angular frequency associated with damping factor
ω	Angular frequency
$G_{dq}(s)$	Integral part of a PI controller in the dq frame
$G_{\alpha\beta}(s)$	Transformation matrix from dq to $\alpha\beta$ frame
$G^{+}_{\alpha\beta}(s)$	Transformation matrix from dq to $\alpha\beta$ frame for positive sequence
$G^{-}_{\alpha\beta}(s)$	Transformation matrix from dq to $\alpha\beta$ frame for negative sequence
$G_{PR_h}(s)$	Proportional resonant controller for tracking a harmonic of order h
K_{P_h}	Proportional gain at harmonic h
K_{I_h}	Harmonic gain at harmonic h
h	Harmonic number
$C(s)$	Output of a closed-loop system
$R(s)$	Reference input of a closed-loop system
$G(s)$	Feedforward transfer function
$H(s)$	Feedback transfer function or continuous transfer function
$D(s)$	Disturbance transfer function
ζ	Damping factor
T_{sw}	Switching period
f_s	Sampling frequency
T_s	Sampling period

ϕ_h	Delay compensation angle
$LPF_{dq}(s)$	Low pass filter in the dq frame
T_{LP}	Time constant of low pass filter in the dq frame
$LPF_{\alpha\beta}(s)$	Equivalent dq frame low pass filter in the in the $\alpha\beta$ frame
$HPF_{\alpha\beta}(s)$	Equivalent dq frame high pass filter in the in the $\alpha\beta$ frame
ΔG	Gain Margin
$\Delta\phi$	Phase Margin
$\Delta\tau$	Delay Margin
ΔM	Modulus Margin
ω_{cr}	Crossover frequency
ω_{cr}^{i}	Crossover frequency when HOL crosses the unit circle at ith time
$\omega_{180°}$	Angular frequency at 180°
H_{OL}	Open loop transfer function
$H_{OL}(z)$	Open loop transfer function in z domain
$C_D(s)$	Output Response to the disturbance $D(s)$ when the input $R(s)$ is zero
$C_R(s)$	Output Response to the input $R(s)$ when the disturbance $D(s)$ is zero
S_{yp}	Output sensitivity function
$e(k)$	Error discrete signal
$u(k)$	Control sequence
$H_{ZOH}(s)$	Zero order hold transfer function in s domain
$H'(s)$	Global continuous transfer function
σ	Real part of a complex variable $s = \sigma + j\omega$
z	Variable of z transform
δ	Delta operator
Δ	Optimization parameter
w	Variable of w transform
$G_{PR_h}^{d}(s)$	Proportional resonant controller for tracking a harmonic of order h with delay compensation
$G_{PR_h}^{cd}(z)$	Proportional resonant controller for tracking a harmonic of order h with delay compensation and with Taylor approximation of $cos(h\omega_1 T_s)$
C_h	Corrected input for resonant controllers implemented with two integrators that improves the resonant frequency accuracy
ϕ_h'	Parameter to introduce delay compensation in a resonant controller transfer function. In the case of $G_{PR_h}^{d}(z)$ controllers, it is also the target (design) value for ϕ_h.
K_{P_T}	Proportional gain
$G_L(s)$	Transfer function of a L filter
v_c	Capacitor voltage in time domain
$I(s)$	Laplace transform of i
$V_c(s)$	Laplace transform of v_c
R_F	Filter equivalent series resistance (ESR)

L_F	Filter inductance
$G_{PL}(s)$	Z transform of a plant transfer function
ρ	Variable equal to $e^{\frac{R_F T_S}{L_F}}$
L^{-1}	Inverse Laplace transform
η	Minimum distance of H_{OL} to the critical point
η_P	Modulus of the minimum distance between the critical point $(-1,0j)$ and the Nyquist plot of $K_{P_T} G_{PL}(z)$
$1/\eta_P$	Sensitivity peak
η_h	Modulus of the minimum distance between the critical point $(-1,0j)$ and the Nyquist plot of a resonant controller tuned at harmonic order h
$D(z)$	Distance between the Nyquist plot and the critical point $(-1,0j)$
ω_η	Angular frequency where $\lvert D(z) \rvert$ has its global minimum η_P
γ_h	Angle between the asymptote at $h\omega_1$ and the real axis
ω_c	Crossover frequency
R_p	Resistance to obtain damping current
i_p	Current across resistance R_p for active damping
v_c	Capacitor voltage, t domain
$\angle$T	Angle of tangent line to resonant controller with damping in z plane
$\angle$D	Angle of line perpendicular to the vector distance of open loop transfer function to instability point
$\angle H_{OL}$	Angle of H_{OL} and the x axis in z plane
θ	Angle between H_{OL} and tangent line T of a resonant controller locus in z plane
$T_{eq,i}$	Time constant of an equivalent first order current control loop
k_d	Active damping gain
$RC(s)_h$	Resonant Controller in s domain
K_{Vh}	Gain in voltage resonant controller at harmonic h
i_h	Current reference for harmonic h before resonant gain K_{Vh}
f_{sw_avg}	Average switching frequency
Δf	Frequency variation related to relative damping factor
f_N	Nominal frequency
δ_{grid}	Grid angle
v_{c_ref}	Capacitor voltage reference in s domain
V_{c_ref}	Capacitor voltage reference in s domain
I_0	Load current in s domain
R_c	Capacitor resistance
K_{PV}	Proportional gain in the voltage control loop
K_{IV}	Integral gain in the voltage control loop
AFE	Active Front End Converter
IGBT	Insulated Gate Bipolar Transistor
SPWM	Sinusoidal Pulse Width Modulation
SHE	Selective Harmonic Elimination

NPC	Neutral Point Clamped
HVDC	High Voltage Direct Current
VSC	Voltage Source Converter
VSI	Voltage Source Inverter
THD	Total Harmonic Distortion
PCC	Point of Common Coupling
MIMO	Multiple Input Multiple Output
PLL	Phase Locked Loop
PI	Proportional Integral Controller
IIR	Infinite Impulse Response
ZOH	Zero Order Hold
ADC	Analog to Digital Converter
DFIIt	Direct Form II transposed structure

1 Introduction

1.1 Problem Background

The energy production in Norway is highly dependent on hydropower with a share of approximately 99% of the energy production. Also, Norway has a large potential for wind energy, which can be used at as much as possible if the Norwegian grid can deal with the intermittency of the wind.

In addition, the countries in Continental Europe are increasing their proportion of renewable generation such as wind and solar, in line with the demanding requirements imposed by the growing of population and the need of reducing the dependency of fossil fuels and other non-environmentally friendly energy sources in the energy mix.

The solution with large electric battery storage systems that helps with the variability of solar and wind is still far away from a practical solution.

In the meantime, Norway is aiming at providing flexibility of operation of its electric system to incorporate large amounts of wind energy and the European electric system and, in this way, help on increasing the penetration of renewable energies through the better use of the Norwegian existing hydropower plants, using pumped storage technology.

Several aspects of this technology are currently under research in NTNU, and one of these is the variable speed machinery based on converter-fed technology, a key technology for pump storage power plants.

There are several existing variable speed technologies in use in converters used in variable speed generators, but the most recently studied and developed is the full frequency converter, which is described briefly in the next lines and is shown graphically in Figure 1.1.

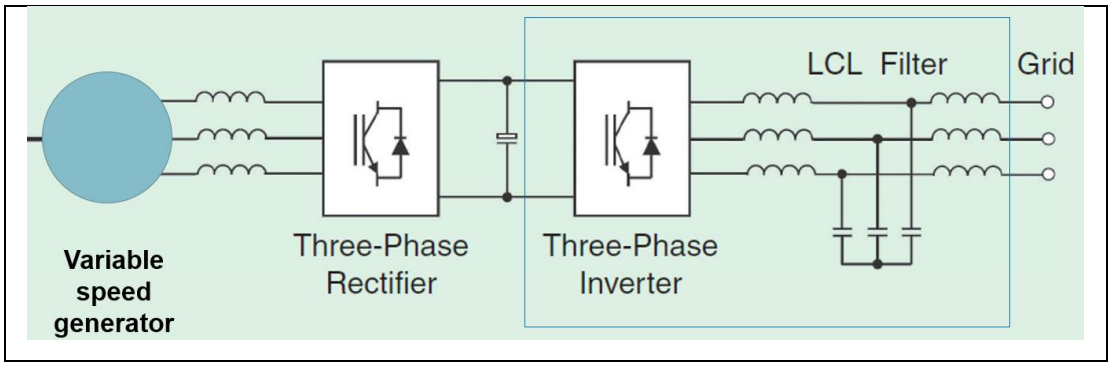

Figure 1.1: Full frequency converter

The full frequency converter used with the variable speed pump/turbine consists of two main parts; the machine side converter, which does the variable speed operation of the generator and that feeds a DC link, and the grid side converter, which inverts the energy from the DC side to an AC grid frequency and interacts with the electric grid.

The machine side converter allows the operation of the generator/motor at different rotational speeds, increasing the available range of operation of the pump storage power plant when operating in the generating/pumping mode. Hydropower turbines provide their best efficiency at rated head when they are operated at a fixed frequency; outside of this point, their efficiency decreases. Variable speed helps in this providing energy to the system or using energy to fill up the reservoir at better efficiency and heads lower than the rated head. Turbine ramping rates are also faster with a full frequency converter.

The grid side converter is the one which deals directly with the electric grid. In this sense, this is the one which must interact with the electric grid all the time. For this reason, its dynamic capabilities are of importance; grid side converters must operate and contribute to the operation of the electric grid.

The AFE takes the power of the DC link and converts it to AC. The control strategy of the switches in the inverter is the one that shapes the dynamic characteristics that the whole converter can provide.

The AFE control scheme consists of cascade control loops, which are the following:

- Inner Current Control Loop, consisting of a hysteresis current controller
- Voltage Control Loop, consisting of a resonant current controller
- Outer Control Loops, which contain other additional functions such as virtual impedance, unbalance control, active and reactive power frequency droop, harmonic compensation, synthetic inertia, islanding operation, among other features.

Being all features of the inverter control based, they are supposed to be to programmable to some extent. For instance, the inverter could behave as a generator in the AC grid if desired. This idea is important, since it is expected that several power electronics – interfaced energy production systems will be incorporated into the grid in the upcoming years, and a reduction of the dynamic properties of the system provided by synchronous generators, -such as inertia – is expected and must be compensated by the inverters through software implementation (this is the reason why the term "synthetic inertia" comes into play).

1.2 Scope of the Master Thesis

In this thesis, the current and voltage controllers of the LCL-type grid side converter, also called, Active Front End Converter (AFE) have been studied, with more emphasis in the proper tuning of the controllers for an stable operation, considering that the control system should be adaptable to variations in the system frequency caused by grid disturbances.

The stability analysis has been done by means of the Nyquist diagrams and Bode Plots.

A tuning procedure has been proposed to get a robust and stable solution. As part of the tuning procedure, a delay compensation method has been developed and proposed, considering the particular properties that the resonant controllers with and without damping, as well as with and without delay compensation, have in the z plane. The suitability of the proposed methodology has been assessed by means of simulations.

Practical aspects, such as the digital implementation, noise filtering, delay compensation, has been considered.

1.3 Outline of the Thesis Report

- Section 2 is a Theoretical Background of the available types of resonant controllers in the continuous domain and their digital implementation. The relevant theory and concepts of stationary and rotative reference frames, voltage source converters, LCL filters, and control theory, as well as any other control features such as active damping and the synchronization procedures of the voltage source converters to the electrical grid are presented. In addition to that, a literature review of the current tuning methodology for resonant controllers. The available digital implementations for resonant controllers with and without damping as well as with and without delay compensation are presented.
- Section 3 explains the proposed delay compensation method for resonant controllers with damping developed in this thesis.
- Section 4 is a detailed explanation of the Simulink models implemented for the control loops and the synchronization scheme.
- Section 5 explains the results of the simulations done in Simulink.
- Section 6 presents a summary of the simulations and discuss the findings, mainly on stability criteria, tuning methodology, the effect of active damping use and the implementation approach of the resonant controllers.
- Section 7 presents the conclusion of this thesis and proposes further work that is recommended to do to continue with the research done.

2 Theoretical Background

2.1 Reference Frame in Control Signal

The three-phase electrical systems are a proven technology to generate, transmit and distribute energy.

Most of the rotating electrical machines have three-phase winding in its stator, even for small machines. Some of the reasons are:

- In electrical machines, it is easy to get three sinusoidal electric fields shifted by 120 degrees. This physical configuration produces a rotating electromagnetic field constantly in amplitude at the desired frequency
- A non-pulsating and smooth torque is also obtained by using three-phase systems, which is a desirable feature in several applications.
- It is also possible to have higher order electrical configurations such as 6-phase or 9-phase machines, but these are very particular designs where there are high power requirements with voltage restrictions. However, the practical aspects of handling systems for more than three phases are difficult to overcome.

The analysis of such systems makes necessary the existence of a three coordinates reference frame.

A drawback for the analysis of the three-phase systems is that their oscillating nature may complicate the calculations. However, a three-phase balance system can also be represented by an orthogonal two-phase stationary system by means of the Clarke transformation as shown below:

$$\begin{bmatrix}\alpha\\ \beta\\ \gamma\end{bmatrix} = \frac{2}{3}\begin{bmatrix}1 & -\frac{1}{2} & -\frac{1}{2}\\ 0 & \frac{\sqrt{3}}{2} & -\frac{\sqrt{3}}{2}\\ \frac{1}{2} & \frac{1}{2} & \frac{1}{2}\end{bmatrix}\cdot\begin{bmatrix}a\\ b\\ c\end{bmatrix} \tag{1}$$

When the system is balanced, the γ quantities are zero, therefore the last row in the matrix is not necessary. Then:

$$\begin{bmatrix}\alpha\\ \beta\\ 0\end{bmatrix} = \frac{2}{3}\begin{bmatrix}1 & -\frac{1}{2} & -\frac{1}{2}\\ 0 & \frac{\sqrt{3}}{2} & -\frac{\sqrt{3}}{2}\end{bmatrix}\cdot\begin{bmatrix}a\\ b\\ c\end{bmatrix} \tag{2}$$

A stationary two reference system such as the $\alpha\beta$ system can be further transformed into a rotating reference system, where the magnitudes of both axes can be seen as fixed. This is done by means of the Park Transformation, which can be performed as indicated below:

$$\begin{bmatrix} d \\ q \\ 0 \end{bmatrix} = \begin{bmatrix} \cos(\omega t) & \sin(\omega t) & 0 \\ -\sin(\omega t) & \cos(\omega t) & 0 \\ 0 & 0 & 1 \end{bmatrix} . \begin{bmatrix} \alpha \\ \beta \\ \gamma \end{bmatrix} \quad (3)$$

$$\begin{bmatrix} \alpha \\ \beta \\ \gamma \end{bmatrix} = \begin{bmatrix} \cos(\omega t) & -\sin(\omega t) & 0 \\ \sin(\omega t) & \cos(\omega t) & 0 \\ 0 & 0 & 1 \end{bmatrix} . \begin{bmatrix} d \\ q \\ 0 \end{bmatrix} \quad (4)$$

Combining both Clark and Park transformation, a full transformation from abc to dq can be done in this way:

$$\begin{bmatrix} d \\ q \\ 0 \end{bmatrix} = \frac{2}{3} \begin{bmatrix} \cos(\omega t) & \cos(\omega t - 2\pi/3) & \cos(\omega t + 2\pi/3) \\ -\sin(\omega t) & -\sin(\omega t - 2\pi/3) & -\sin(\omega t + 2\pi/3) \\ 1/2 & 1/2 & 1/2 \end{bmatrix} . \begin{bmatrix} a \\ b \\ c \end{bmatrix} \quad (5)$$

$$\begin{bmatrix} a \\ b \\ c \end{bmatrix} = \frac{2}{3} \begin{bmatrix} \cos(\omega t) & -\sin(\omega t) & 1 \\ \cos(\omega t - 2\pi/3) & -\sin(\omega t - 2\pi/3) & 1 \\ \cos(\omega t + 2\pi/3) & -\sin(\omega t + 2\pi/3) & 1 \end{bmatrix} . \begin{bmatrix} d \\ q \\ 0 \end{bmatrix} \quad (6)$$

A graphical representation of the transformations can be seen in Figure 2.1. A unique set of three-phase abc quantities can be represented as a unique set of $\alpha\beta$ quantities and dq quantities. The practical aspect of this is that any phenomenon can be analyzed and studied in the rotating frame dq and then transferred back to the stationary abc frame.

2.2 Operating Principle of Voltage Source Converters

The primary function of a voltage source converter or voltage source inverter is to convert a fixed DC voltage into a three-phase AC voltage with variable magnitude and frequency. The most basic inverter that produces a three-phase output voltage is called a two-level voltage source converter or voltage source inverter [1]. Once the energy is available at DC voltage in the DC link and AC voltage is needed at the output terminals, the conversion to the desired AC voltage is done by switching action performed sequentially in each of the 6 switches, two pair of switches at the same time. The idea is to impress the existing voltage in the DC link on each phase in such a way that the waveform measured on each phase is shifted by 120 degrees. Of course, the energy stored in the DC voltage link is not infinite, it must be restored all the time by an external source. This DC link voltage can be the terminals of a battery, the endpoint of a passive or active rectifier, or the DC side of a speed drive. The switches can be of several types depending on the specific intended application (IGBT, for instance) but all of them have an essential characteristic; they can only conduct current in one direction. Therefore, when returning current to the source is necessary, diodes are considered. They are called free-wheeling diodes. This can be understood looking at Figure 2.2.

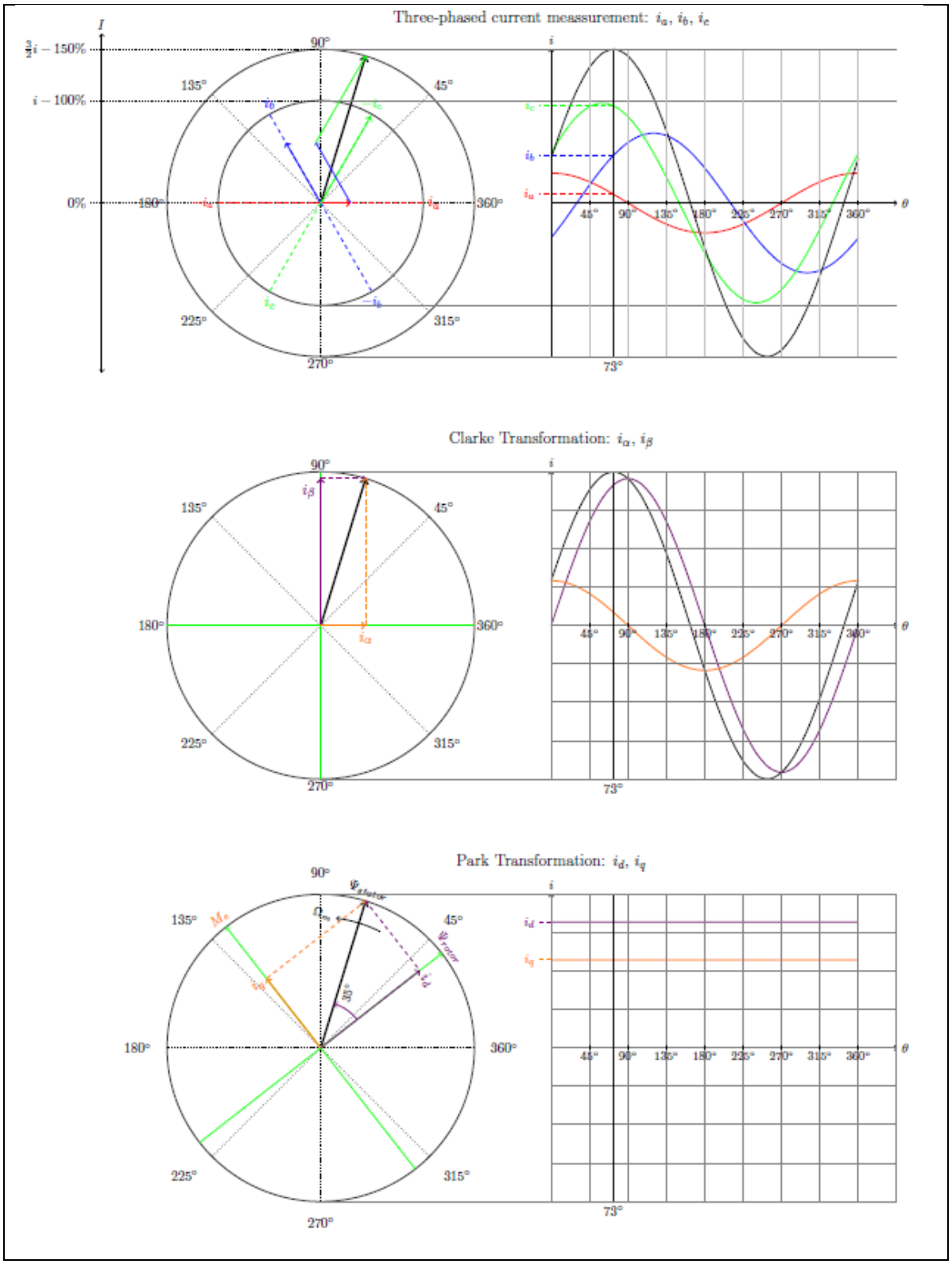

Figure 2.1: Relationship between abc, $\alpha\beta$ and dq reference frame for a three-phase current. [Yngve Solbakken, 2016]

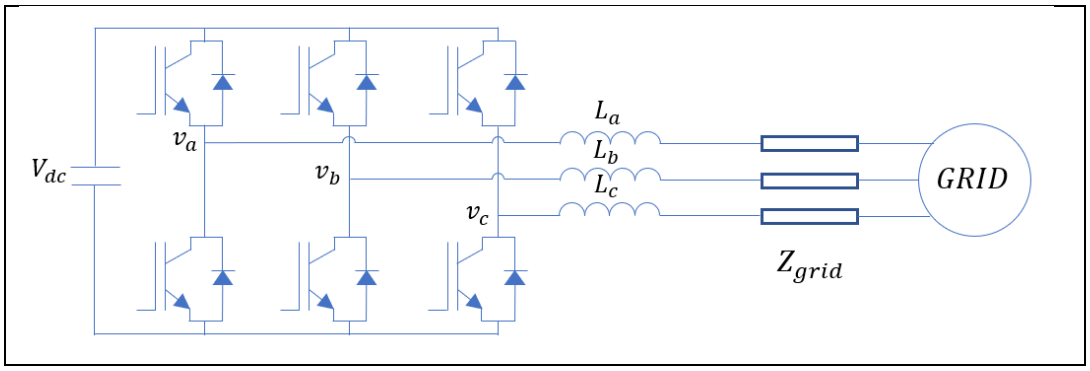

Figure 2.2: Grid Side Converter or Voltage Source Converter

Whatever the waveform produced in the AC side of the inverter is, the best strategy to activate the switches is the one that produces the highest fundamental voltage in the AC side. The most basic strategy to produce AC from DC voltage is to activate each of the switches by half cycle (180 degrees) and phase shifted 120 degrees between phase. This strategy produces a fundamental phase peak voltage of $\frac{2}{\pi}V_{dc}$ $(\frac{2}{\pi}\sqrt{\frac{3}{2}}V_{dc} \approx 0.78V_{dc})$ if line rms voltage is considered, where V_{dc} is the DC link voltage. The switching sequence for the 6 switches can be appreciated in Figure 2.3 and how the voltage V_{ab} is formed.

The three-phase waveform created in this way is not sinusoidal and produces high harmonic components. For this reason, this method is no longer used and because the magnitude of the output voltage cannot be modified [2].

2.3 Sinusoidal Pulse Width Modulation Method

A better strategy to produce a sinusoidal waveform is to involve a sinusoidal control signal as a signal reference. Over the years, a method called sinusoidal pulse width modulation has become the most popular method to produce sinusoidal waveforms. There are other well-known PWM strategies; for instance, selective harmonic elimination (SHE) and space vector modulation (SPWM) [2]. Only the SPWM method will be briefly explained.

The frequency of the output voltage is the same as the frequency of the sinusoidal signal reference (or also called modulating wave) and is controlled by means of a *frequency modulation index* which is defined as the quotient between the carrier wave frequency and the modulating wave frequency:

$$m_f = \frac{f_{cr}}{f_m} \tag{7}$$

The carrier frequency f_{cr} is also the switching frequency f_{sw}

Similarly, the amplitude of the output voltage is controlled by adjusting the *amplitude modulation index*, which is the quotient of the peak value of the sinusoidal signal reference and the peak value of the carrier wave:

$$m_a = \frac{V_{m\_peak}}{V_{cr\_peak}} \tag{8}$$

In the Figure 2.4, v_{mA}, v_{mB}, v_{mC} are the three-phase modulating waves and v_{cr} is the triangular carrier wave.

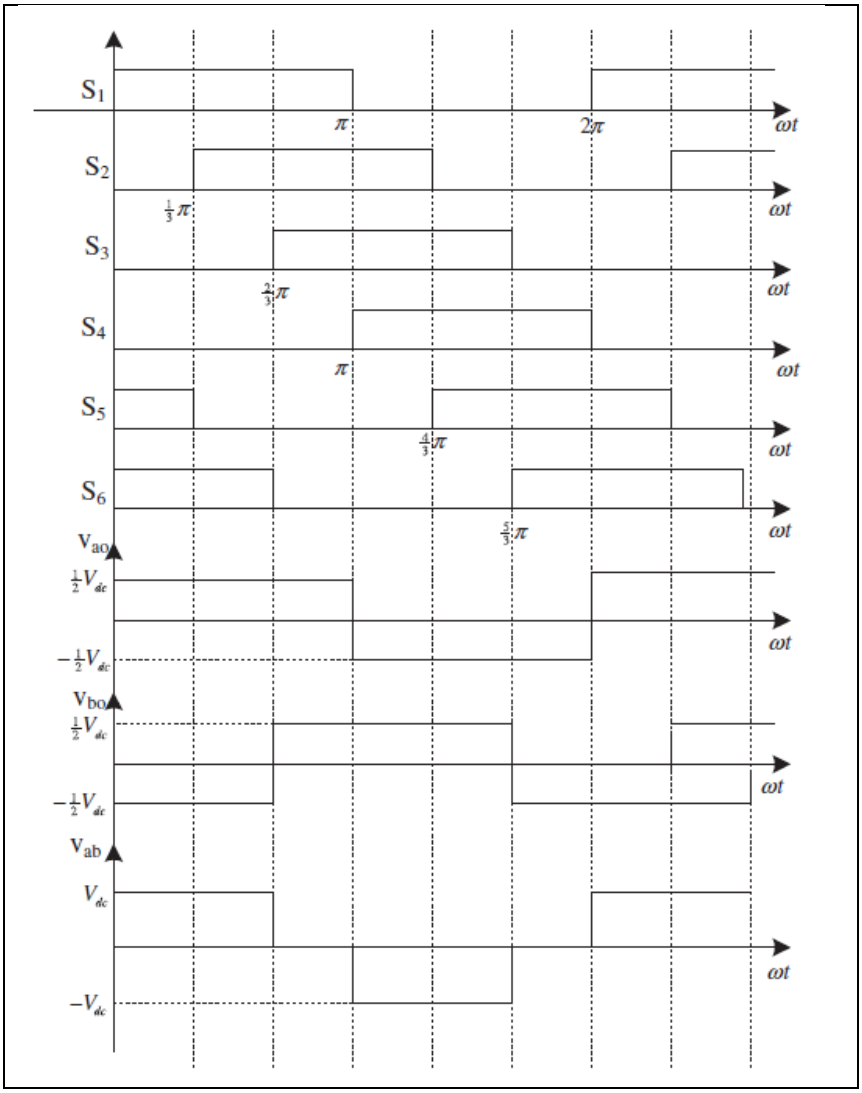

Figure 2.3: Gate signal mapping and converter output voltage for the 180º method [2]

For a linear increase of the fundamental output voltage, the amplitude modulation index should be less than one. In this case, the maximum value of the fundamental line rms voltage is $0.612V_{dc}$. An increase of the modulation index is possible up to the theoretical maximum produced by the square wave of $0.78V_{dc}$, as shown in Figure 2.5.

However, this operation is undesired because it creates difficulties with low order harmonics [1].

A good strategy to get a higher fundamental voltage is to increase the peak value of the fundamental component of the modulating wave without increasing the peak value of the modulating wave itself, adding a third harmonic component in such a way that the new peak value of the modulating wave including the third harmonic is less than the peak value of the carrier wave as shown in Figure 2.6.

The new three-phase modulating wave would be [4]:

$$V_{mA} = \sin(\omega t) + \frac{1}{6}\sin(3\omega t) \tag{9}$$

$$V_{mB} = \sin(\omega t - \frac{2\pi}{3}) + \frac{1}{6}\sin(3\omega t) \tag{10}$$

$$V_{mC} = \sin(\omega t - \frac{4\pi}{3}) + \frac{1}{6}\sin(3\omega t) \tag{11}$$

The third harmonic cancels out in both line and phase voltages. If the reference signal is cosinusoidal instead of sinusoidal, the third harmonic is subtracted [5].

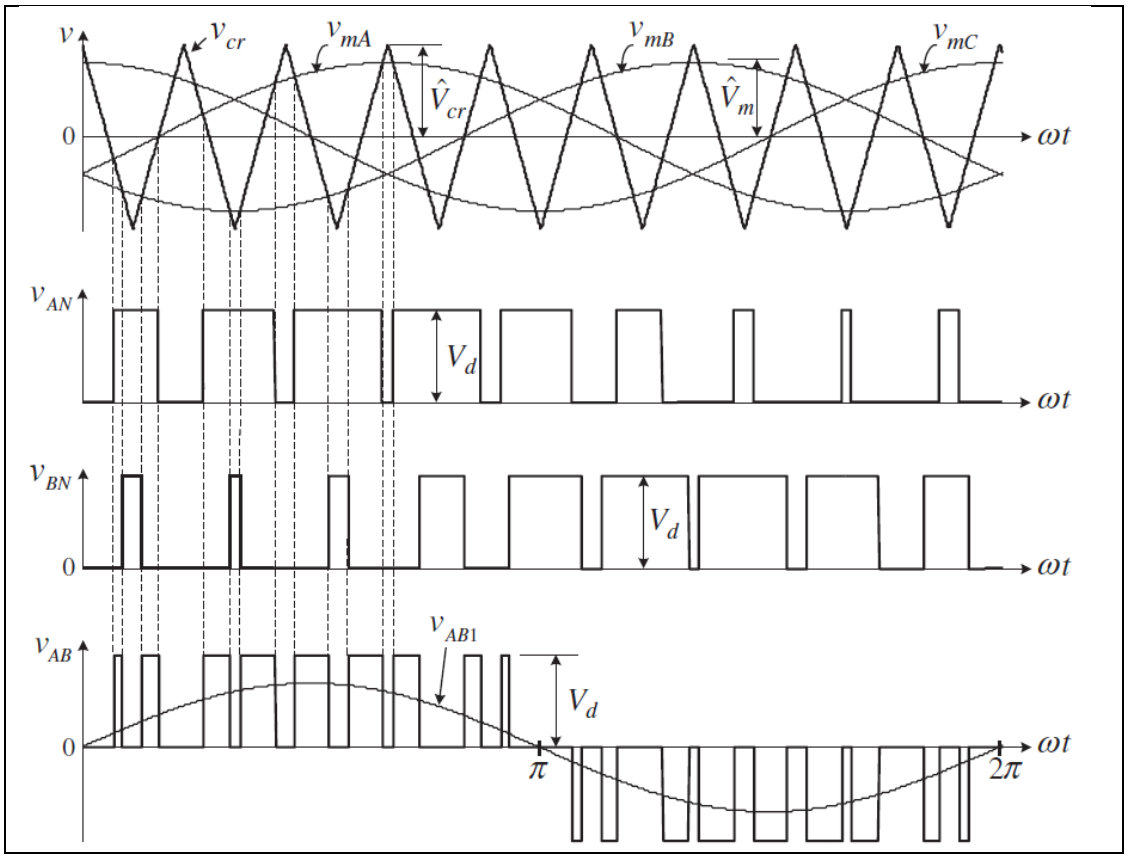

Figure 2.4: Sinusoidal pulse width modulation technique (SPWM). [1]

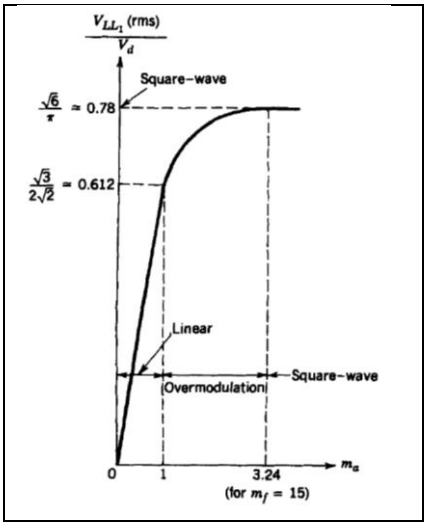

Figure 2.5: Three phase inverter $\frac{V_{LL_1}(rms)}{V_d}$ as a function of m_a [3]

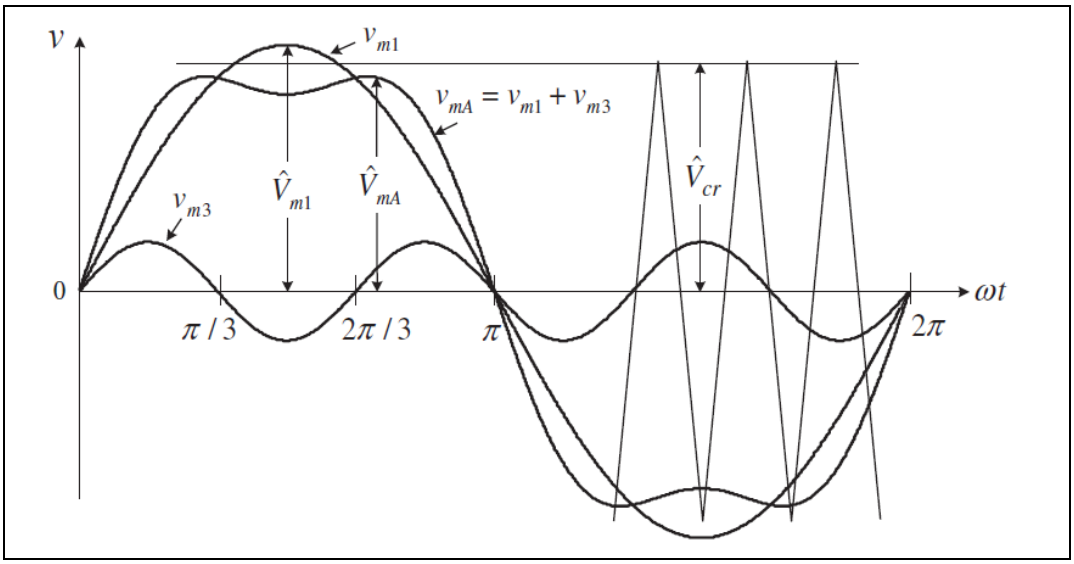

Figure 2.6: Modulating wave v_{mA} with 3rd harmonic injection. [1]

The maximum increase obtained by this strategy is 15.5% additional voltage [1].

Depending on the voltage, current and power level that must be converted to AC, there are several types of VSCs. For wind/solar inverters [6] and distributed generation [7] the most popular inverters are the ones described above. In the case of medium voltage and High Power industrial inverters, the neutral-point clamped (NPC) inverter [1] is a popular solution. The modular multilevel converters are the latest development in the field, and they are intended to produce very high voltages with minimal losses (between 0.9% to 1%) and minimal or no harmonic filtering requirements [8]. They are applied on creating AC voltages from DC links or as part of VSC-HVDC links.

Notwithstanding the popularity of the SPWM method, the control action necessarily causes delays that must be considered when the digital implementation is done, and other methods have also been explored. Hysteresis controllers have also been used as current controllers because of their simplicity and speed. The operating principle of the hysteresis controllers and their main features are explained in item 2.4. The hysteresis controller is the type of current controller that have been used in this thesis.

2.4 Hysteresis Controllers

Also called tolerant band controllers [3], hysteresis controllers are ones of the most basic control schemes available. It consists of a control that compares the measured signal with two references using hysteresis comparators, whose reference values are higher or lower than the measured signal by a value. The difference between the upper and lower reference value is called the hysteresis band. This hysteresis band can be fixed or adaptative. In the case of a fixed hysteresis band, when the measured signal (typically current in voltage source inverters) reaches the upper or lower limit, two switch actions are performed. For instance, considering a three-phase inverter with a hysteresis controller per phase, the activation of each hysteresis controller activates two of six switches. No more information than the hysteresis band is needed for control. The fixed hysteresis band applied over the measured signal causes that the switching action is not performed in a uniform way, as seen in Figure 2.7.

Therefore, the switching frequency of the hysteresis controller is not constant. In the case of a sinusoidal measured signal, the switching frequency is lower around the maximum or minimum value and higher when the measured signal is close to zero.

In the ideal case, the hysteresis controller should activate the switching action as soon as the current has reached the upper and lower limit. However, this is not possible in the digital implementation. Therefore, the actual operation of the hysteresis controller looks like as shown in the figure below:

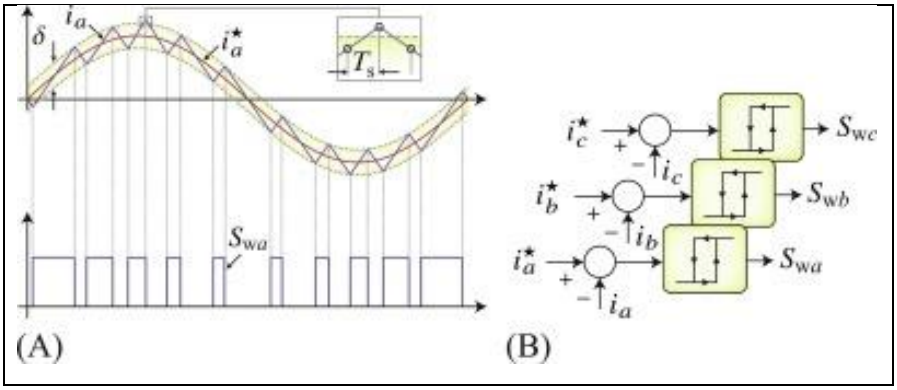

Figure 2.7: An hysteresis current control for a three-phase two-level power converter: (A) operation principle and (B) block diagram. [9]

The simplest hysteresis control is performed in the natural frame abc, but it can also be performed in the $\alpha\beta$ (stationary reference frame) and dq frame (synchronous reference frame) as well. In these three cases, the hysteresis band would look different:

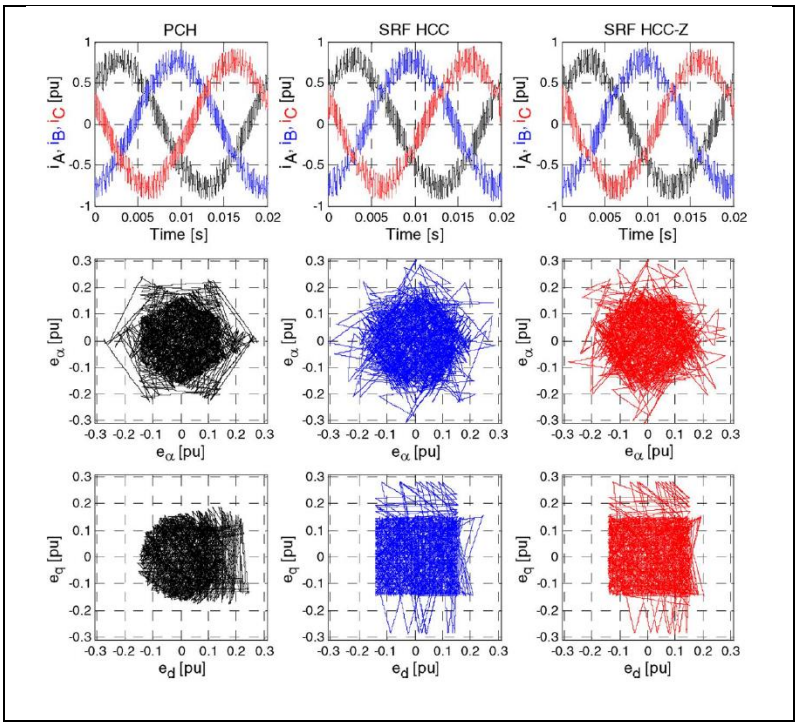

Figure 2.8: Simulation results showing phase currents and error trajectories in the stationary reference frame and synchronous reference frame. [10]

The idea behind an adaptative hysteresis band is to get a switching frequency as constant as possible. According to [11], the main advantages of adaptive hysteresis current controller are constant switching frequency of operation, better dc-bus voltage utilization,

simple filter design and low total harmonic distortion (THD) at the point of common coupling (PCC). In any case, the effort done on trying to get a switching frequency as constant as possible may negate the simplicity of the hysteresis controller as a concept.

However, some applications where the risk of resonance due to the variable switching frequency is an issue [12] may need an adaptative hysteresis controller.

When a fixed hysteresis band current controller is applied to a power inverter with an LCL filter, it should meet certain characteristics. The switching frequency of a power inverter should be as low as possible to limit the switching losses, improving the efficiency of the converter. The typical maximum standard limit for switching frequency for a power inverter is around 3 kHz [13]. In the case of a hysteresis controller, the design of the LCL filter should be such that the *average switching frequency* is about 3 kHz. For this case, a fixed hysteresis band of 0.1 p.u. is typically chosen.

2.5 Design Criteria of an LCL filter

The grid filter goal as part of a VSC is twofold; first, it gives the dominant inductive behavior necessary to the converter to operate properly when connected to the utility grid. Second, the inverter itself, independently of the modulation method used in the current and voltage controllers, generate harmonics that cannot be fed into the grid [6] and they must be filtered. Very strict requirements stated by international standards such as IEEE 519, [14, 15], IEEE 929 and IEEE 1547 [16] pose limits on the harmonic level that can be fed into the grid at the point of common coupling. In the case of power converters, to limit the switching losses caused by semiconductor devices, low switching frequencies are used [13]. In these cases, the low order harmonics with high currents demand large and bulky inductors for filtering, which has an impact on the cost and the space required for it. In addition to this, the dynamic response may become poorer [6].

Typically, the standard requirements mentioned above makes necessary to use low pass filters to remove high order harmonics. Instead of an L filter, and LC filter may work, although this may leave the converter capacitor, with very low impedance at high frequencies, with no defense against harmonic produced somewhere else in the grid. A more efficient solution is to consider an LCL filter, i.e. an inductor in series with the converter, a capacitor in shunt and an additional inductor towards the grid as shown in Figure 2.9.

According to [6], the LCL filter gives optimal sizes for inductor and capacitors. A representation of the Bode Plot of an LCL filter is shown in Figure 2.9:

Something also important of an LCL filter is that provides attenuation of 60dB after its resonant frequency, which is always selected lower than the switching frequency, so it can filter the sideband voltage harmonics as well [6].

Several considerations must be taken into account to select the LCL filter parameters [6, 14, 16], but a general guideline can be established considering all of them:

- Limit the upper and lower limit of the converter side inductor by limiting the inductor current ripple and fundamental voltage drop on the inductors
- Establish the upper limit of the capacitor value and voltage considering the necessary converter current to charge it for easy synchronization
- Obtain the grid side inductor value by considering the resonant frequency of the converter with some margin and the harmonic restrictions in the grid side.

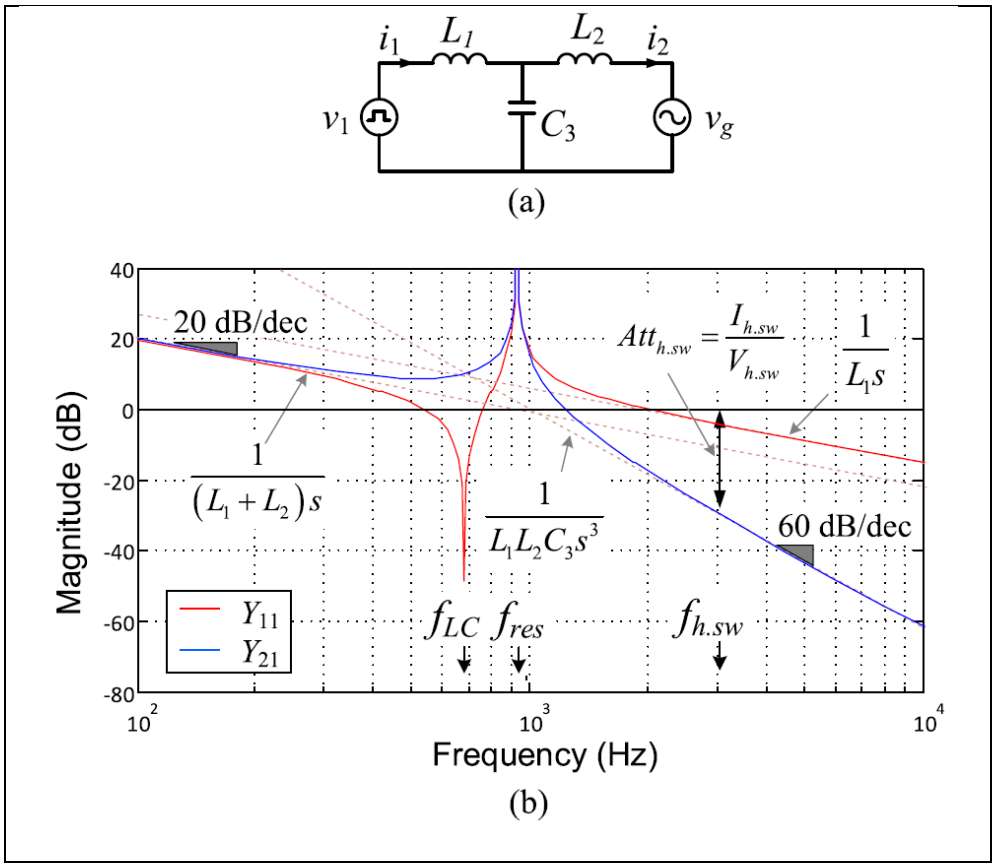

Figure 2.9: single phase representation of an LCL filter connected to the grid and its transfer functions $Y_{11} = {i_1}/{v_1}$ and $Y_{21} = {i_2}/{v_1}$ [17].

- Verify how the LCL will work with and without the active damping

More detailed requirements are necessary for a full design of the converter with an LCL filter, such as consider the optimization of the weight of the inductors and capacitor [17] and DC link voltage [18], however the first set of values can be obtained in the following way:

- Consider the magnitude of the capacitor impedance 10 times (10 p.u.) of the base impedance. This is to guarantee around 1.0 p.u. in the capacitor voltage when a 0.1 p.u. converter current is used to charge it before synchronization and connection to the grid. This means:

$$C = 0.1\frac{P_R}{\omega_1 {V_g}^2} \tag{12}$$

  P_R is the converter rated output, ω_1 is the grid fundamental frequency, and V_g is the grid voltage.

- Limit the inductance voltage drop to 10% in operation, preferably 5% on each inductor as a first step. Otherwise, it is necessary to have a higher DC link voltage to guarantee current controllability, which leads to higher losses. [14]. This means that the converter side inductance is:

$$L_1 = 0.05\frac{V_N}{\sqrt{3} I_N} \tag{13}$$

  Other formulations such as the one proposed in [17] provide similar results.

- Calculate the resonant frequency of the LCL filter considering both inductances equal and verify if there is enough margin. The resonant frequency calculation should also include the grid impedance, and an estimation of its variation should be considered to assess its impact in the resonant frequency [6]. The resonant frequency calculation should be done with the following formula:

$$f_{res} = \frac{1}{2\pi}\sqrt{\frac{L_1 + L_2}{L_1 L_2 C}} \tag{14}$$

  L_2 includes the grid side inductor value and the grid equivalent impedance. If, as a first approximation, the grid side inductance is considered equal to the converter side inductance, then L_2 will be:

$$L_2 = L_1 + L_g \tag{15}$$

- The resonance frequency can be assessed considering the factor K_{res}:

$$K_{res} = \frac{f_{res}}{f_s} \tag{16}$$

  According to [14], the resonant frequency should be in the range of $[10f_1, \frac{1}{2}f_s]$ to avoid resonance problems in the lower and upper parts of the harmonic spectrum. Another author [17], consider the K_{res} range of [0.2,0.4] for a power inverter.

- According to [17], a good target harmonic current is 0.3% to fulfill the current harmonic limits of IEEE 519 for grids with a low short circuit ratio, but this target changes according to the requirements of the grid codes. This seems a rather strict requirement, therefore in this thesis, a limiting THD of 5% is considered in the capacitor voltage.

When a hysteresis controller is considered, it should be checked that the average switching frequency does not exceed 3 kHz, the value considered a maximum value of a power converter to limit switching losses. The converter side inductor is the one that has more influence in the average switching frequency of a hysteresis controller.

Additional detailed criteria for the design of an LCL filter can be found in several references [6, 14, 16-18].

2.6 PI Controllers in the dq and $\alpha\beta$ frame

PI controllers are the most widely used controllers in the industry nowadays [19]. They are simple, and the rules to tune them are well understood. The general form of a PI Controller is:

$$K_P + \frac{K_I}{s} \tag{17}$$

Analyzing closely this transfer function, it is observed that the PI controllers have a pole at zero frequency, which means that they cannot eliminate the steady-state error at the fundamental frequency [19].

To eliminate this problem, a synchronously rotating dq transformation where the PI controller can be implemented is needed. A typical implementation of a PI controller as such is:

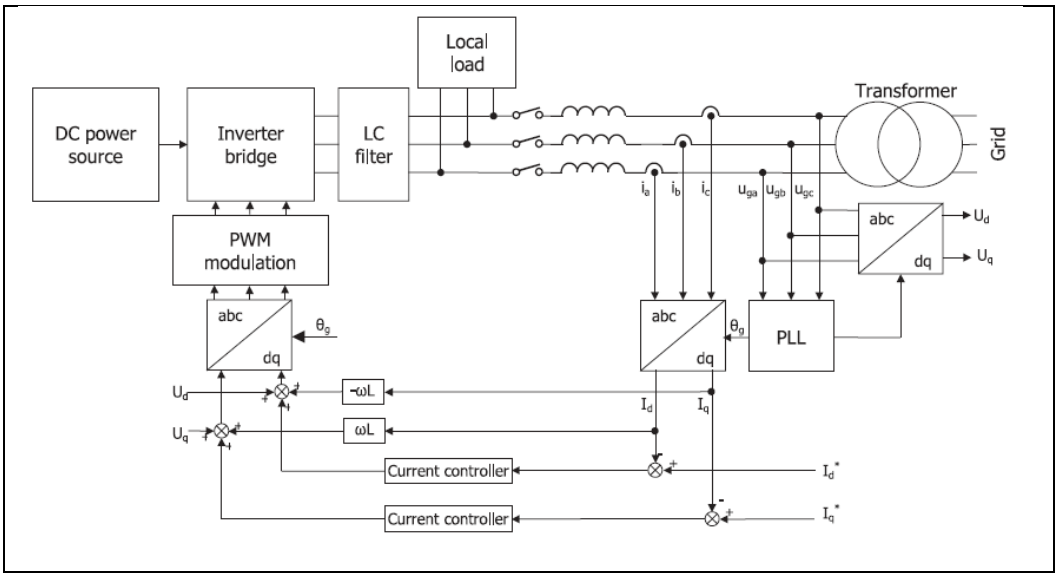

Figure 2.10: Typical block diagram of a current-controller VSI in the synchronously rotating (d-q) reference frame. [19]

Considering only the integral part of the PI controller, a resonant controller without damping is obtained in the $\alpha\beta$ frame. The proof can be seen in [6].

The resonant controller with damping in the $\alpha\beta$ can be obtained considering an approximation of the integral part of the PI controller considering the function:

$$G_{dq}(s) = \frac{K_I}{1 + \frac{s}{\omega_c}} \tag{18}$$

Note that $\omega_c \ll \omega$, therefore the integral transfer function in the $d-q$ frame can be obtained in this way:

$$G_{dq}(s) = \frac{K_I \omega_c}{\omega_c + s} \approx \frac{K_I \omega_c}{s} \tag{19}$$

This approximation makes easy to obtain the resonant controller in the $\alpha - \beta$ frame. Applying the transformation from dq to $\alpha\beta$ in the same way [6]:

$$G^{+}_{\alpha\beta}(s) = \frac{1}{2}\begin{bmatrix} G_{dq1} + G_{dq2} & jG_{dq1} - jG_{dq2} \\ -jG_{dq1} + jG_{dq2} & G_{dq1} + G_{dq2} \end{bmatrix} \tag{20}$$

$$G_{dq1} = G_{dq}(s + j\omega_h) \tag{21}$$

$$G_{dq2} = G_{dq}(s - j\omega_h) \tag{22}$$

$$G_{dq1} + G_{dq2} = \frac{K_I \omega_c}{\omega_c + (s + j\omega_h)} + \frac{K_I \omega_c}{\omega_c + (s - j\omega_h)} \tag{23}$$

$$G_{dq1} + G_{dq2} = \frac{K_I\omega_c(s - j\omega_h)}{(s+\omega_c)^2 + {\omega_h}^2} + \frac{K_I\omega_c(s + j\omega_h)}{(s+\omega_c)^2 + {\omega_h}^2} = \frac{2K_I\omega_c s}{(s+\omega_c)^2 + {\omega_h}^2} \approx \frac{2K_I\omega_c s}{s^2 + 2\omega_c s + {\omega_h}^2} \quad (24)$$

$$jG_{dq1} - jG_{dq2} = j\frac{K_I\omega_c(s - j\omega_h)}{(s+\omega_c)^2 + {\omega_h}^2} - j\frac{K_I\omega_c(s + j\omega_h)}{(s+\omega_c)^2 + {\omega_h}^2} = \frac{2K_I\omega_c\omega_h}{(s+\omega_c)^2 + {\omega_h}^2} \approx \frac{2K_I\omega_c\omega_h}{s^2 + 2\omega_c s + {\omega_h}^2} \quad (25)$$

$$-jG_{dq1} + jG_{dq2} = -(jG_{dq1} - jG_{dq2}) \approx -\frac{2K_I\omega_c\omega_h}{s^2 + 2\omega_c s + {\omega_h}^2} \quad (26)$$

The variable ω_h is the harmonic frequency $h\omega_1$. For the negative sequence, the expression is obtained by replacing ω_h by $-\omega_h$. Looking at the equations, only the non-diagonal terms are affected, they become the opposite for each sequence.

The complete $\alpha\beta$ transfer function is obtained by using the following expression:

$$G_{\alpha\beta}(s) = \frac{1}{2}\left[G^{+}_{\alpha\beta}(s) + G^{-}_{\alpha\beta}(s)\right] \quad (27)$$

$$G_{\alpha\beta}(s) = \frac{1}{2}\begin{bmatrix} \frac{2K_I\omega_c s}{s^2 + 2\omega_c s + {\omega_h}^2} & 0 \\ 0 & \frac{2K_I\omega_c s}{s^2 + 2\omega_c s + {\omega_h}^2} \end{bmatrix} \quad (28)$$

This is the integral part of the PI controller in the $\alpha\beta$ frame, which becomes a resonant controller with damping.

Several authors, such as [20] have listed the limitations that the PI controllers have to control harmonics, for instance, the distortion of line currents when there are distorted voltages caused by background harmonics introduced into the system through the feedforward path. This harmonic distortion may trigger an LC resonance, especially in an LCL filter. The formula 28 proves that the P+Resonant controller in the $\alpha\beta$ frame is the equivalent of the PI controller in the dq frame.

Several features are attributed to resonant controllers. [21] mentions that resonant controllers are capable of tracking sinusoidal references of arbitrary frequencies of both positive and negative sequences with zero steady-state error, being comparable to PI control in a synchronous reference frame.

Other important features mentioned are the important saving of computational resources because of their lack of Park transformations, less sensitiveness to noise and error in synchronization, compensation of unbalance with a smaller number of regulators because of the ability to track both sequences.

The amount of applications where resonant controllers have been applied successfully is long [21]: active power filters, photovoltaic systems, wind turbines, controlled rectifiers, permanent magnet synchronous motors, induction drives, and fuel cells, and others.

According to [19], the Proportional Resonant Controller (PR Controller) introduces an infinite gain at a selected resonant frequency, eliminating in this way the steady state error at that frequency. This means that the property of introducing an infinite gain at zero frequency of the PI controller in the dq frame is equivalent to introduce an infinite gain at the resonant frequency in a PR controller in the $\alpha\beta$ frame.

2.7 Resonant Controllers in the $\alpha\beta$ frame

The general form of a resonant controller without damping is given by:

$$G_{PR_h}(s) = K_{P_h} + K_{I_h}\frac{s}{s^2 + h^2\omega_1^2} \tag{29}$$

Where:

K_{P_h} is the proportional term and K_{I_h} is the resonant gain at frequency $h\omega_1$. This controller gives an infinite gain at the resonant frequency $h\omega_1$ when this is implemented in a closed loop.

The Bode plots for a typical resonant controller with and without a proportional term are shown below:

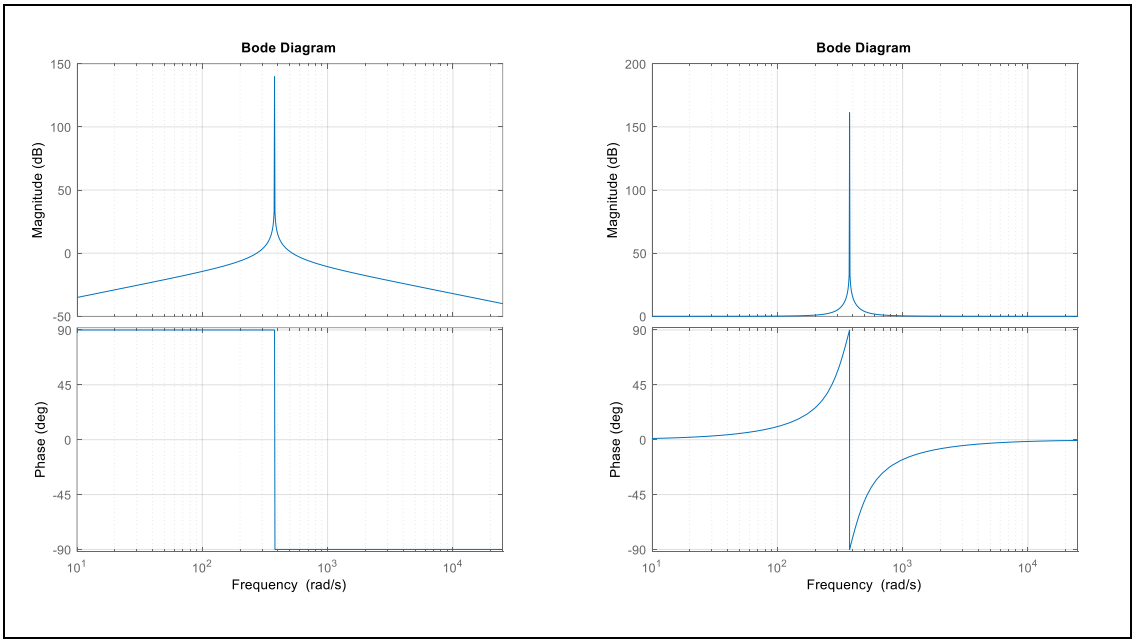

Figure 2.11: Bode Plot of R Controller and a P+R Controller for a gain $K_{P_h} = 1.0$ and $K_{I_h} = 250$, fundamental frequency 60 Hz

See, for instance, this case:

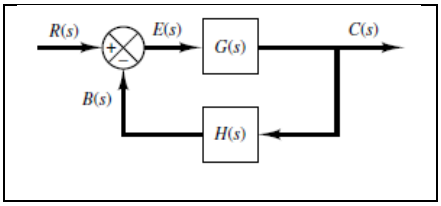

Figure 2.12: A closed-loop system. [22].

A closed loop system whose close loop transfer function is:

$$\frac{C(s)}{R(s)} = \frac{G(s)}{1 + G(s)H(s)} \tag{30}$$

If the resonant controller G(s), which is in the numerator and denominator, has a very high gain, will make that the output follows the input. This assures a good reference tracking.

When several harmonics need to be tracked, the transfer function will be:

$$G_{PR_h}(s) = K_{P_h} + K_{I_1}\frac{s}{s^2 + h^2\omega_1^2} + \sum_{h=5,7,11,\ldots,6p\pm1} \frac{K_{I_h}s}{s^2 + (\omega_1 h)^2} \tag{31}$$

A typical Bode Plot for a resonant controller is shown in Figure 2.13.

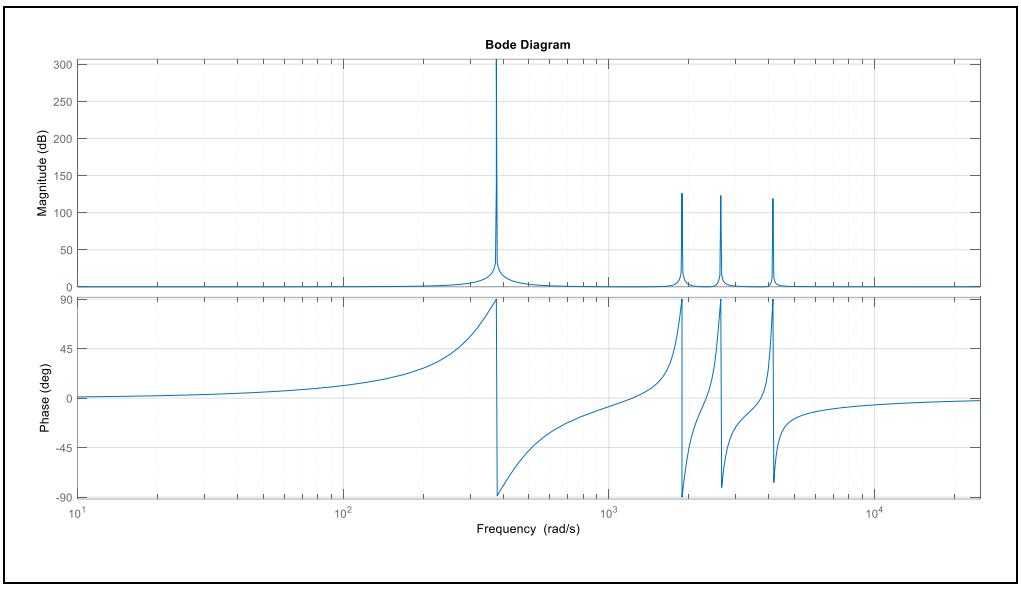

Figure 2.13: Bode Plot of R Controller and a P+Resonant Controller for a gain $K_{P_h} = 1.0$ and $K_{I_h} = 250$ for fundamental frequency, and harmonics 5,7,11

It is also possible to have a PI controller for the fundamental term and consider resonant controllers for the harmonic terms. In this case, the transfer function of the controller will be:

$$G_{PR_h}(s) = K_P + \frac{K_I}{s} + \sum_{h=5,7,11,\ldots,6p\pm1} \frac{K_{I_h}s}{s^2 + (\omega_1 h)^2} \tag{32}$$

The Bode plot would change in this case, having some infinite gain at DC, and this gain reduces when the frequency increases.

A typical Bode Plot for a resonant controller with these features is Figure 2.14:

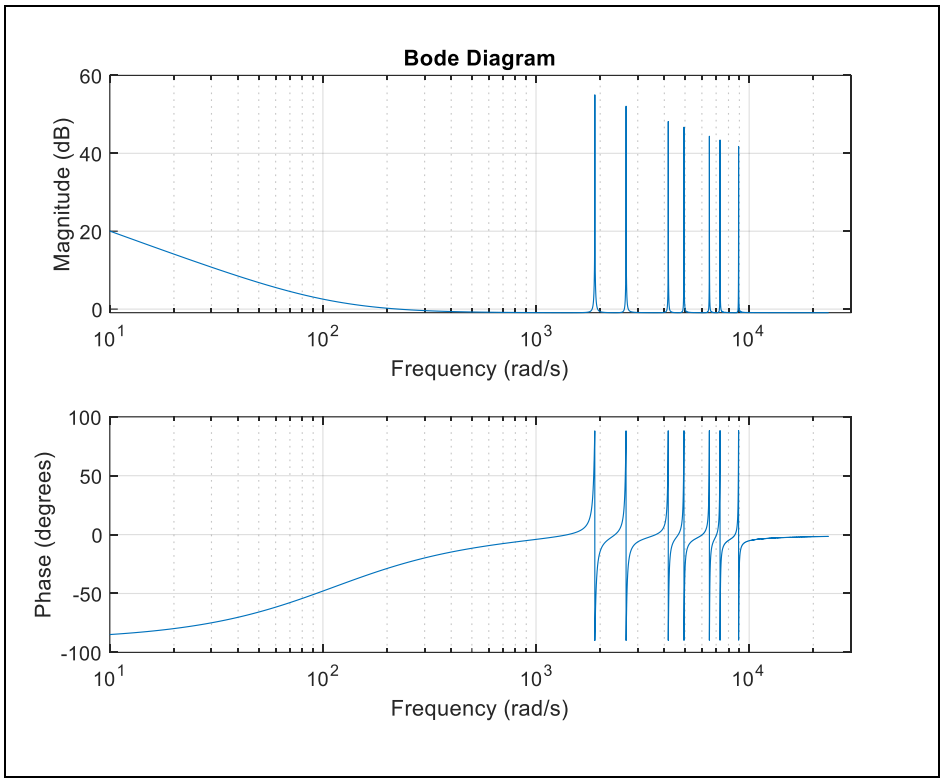

Figure 2.14: Bode Plot of PI + R Controller for a gain $K_P = 1.0$, $K_I = 100$ for fundamental frequency and $K_{I_h} = 250$, for harmonics 5,7,11

The damping term in the PR controller, such as the one presented in equation 36 helps to control the gain of the resonant term and avoid stability problems associated with the infinite gain.

$$G_{PR_h}(s) = K_{P_h} + K_{I_h}\frac{s}{s^2 + 2\zeta h\omega_1 s + h^2\omega_1^2} \tag{33}$$

In this case, the Bode Plot for a resonant controller damping is shown in Figure 2.16:

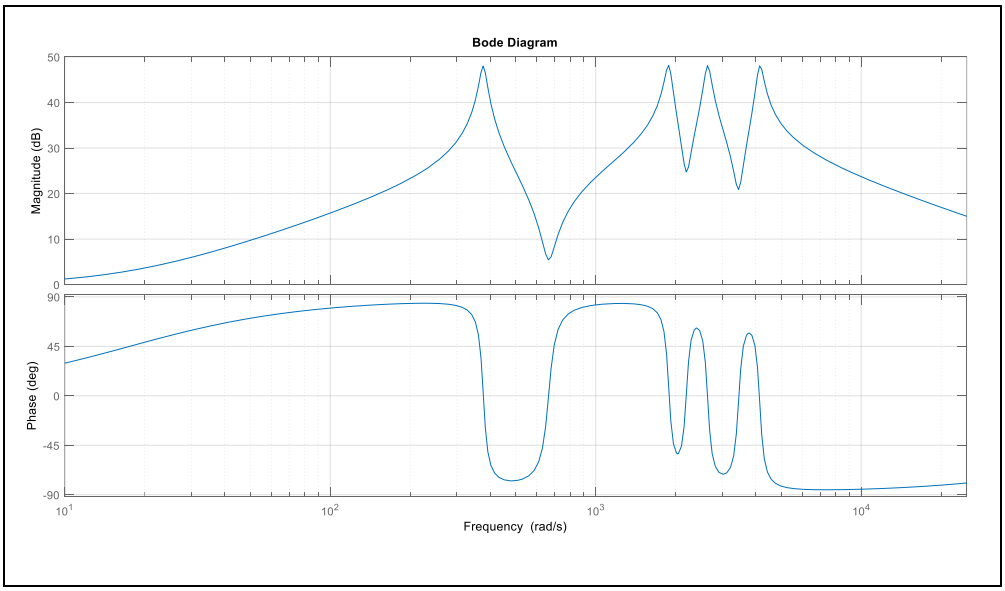

Figure 2.15: Bode Plot of a P+Resonant Controller for a gain $K_P = 1.0$, $K_I = 100$ for fundamental frequency and $K_{I_h} = 250$, for harmonics 5,7,11 and a damping term $\xi = 0.03$

When several harmonics need to be tracked and to control the fundamental with a PI controller, the transfer function will be:

$$G_{PR_h}(s) = K_{P_h} + \frac{K_I}{s} + \sum_{h=5,7,11,\ldots,6p\pm1} \frac{K_{Ih}s}{s^2 + 2\zeta h\omega_1 s + (\omega_1 h)^2} \tag{34}$$

In this case, the Bode Plot for a PI +R controller with damping is shown in Figure 2.16:

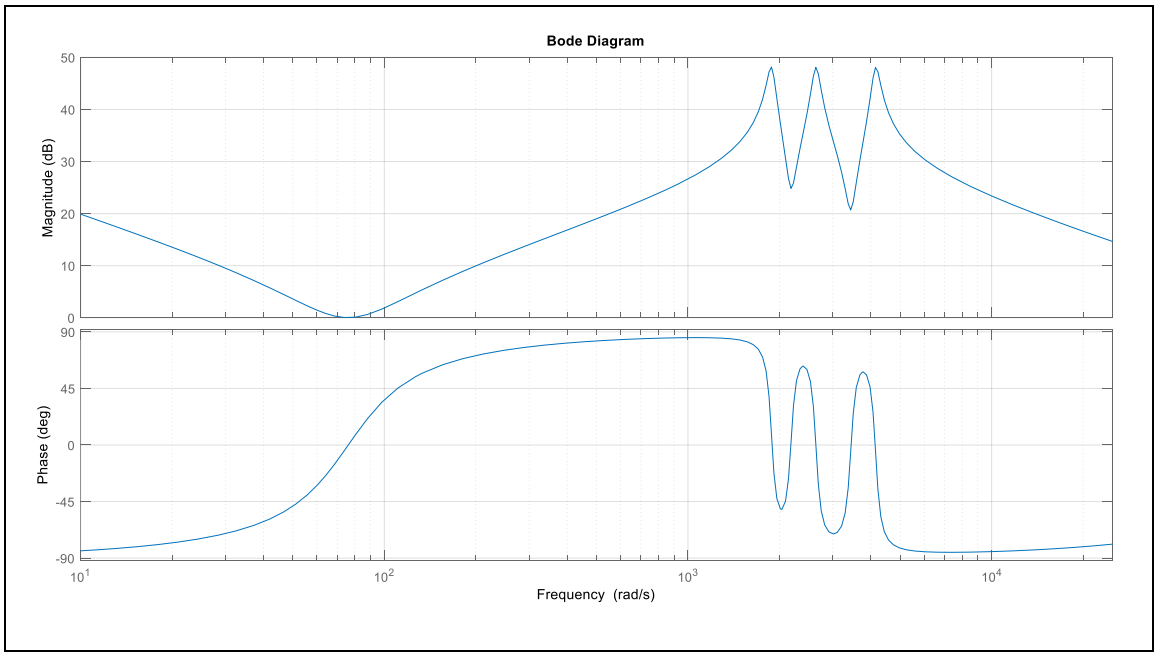

Figure 2.16: Bode Plot of PI + Controller for a gain $K_P = 1.0$, $K_I = 100$, and $K_{I_h} = 250$ for the fundamental frequency, and harmonics 5,7,11 and a damping term $\xi = 0.03$

From Figure 2.16, the damping term helps with the stability of the controller. The phase does not exceed 90°, which is well below the limit of 180°.

When the delay compensation is considered, the resonant transfer function will be:

$$G_{PR_h}(s) = \frac{K_{Ih}[scos(\phi_h) - h\omega_1 sin(\phi_h)]}{s^2 + 2\zeta h\omega_1 s + (\omega_1 h)^2} \tag{35}$$

The difference with the transfer function of the resonant controller is minimum and not much difference can be seen in the Bode diagram. However, something important happens with the phase angle. In the case of a transfer function without delay compensation, the Bode plot will be:

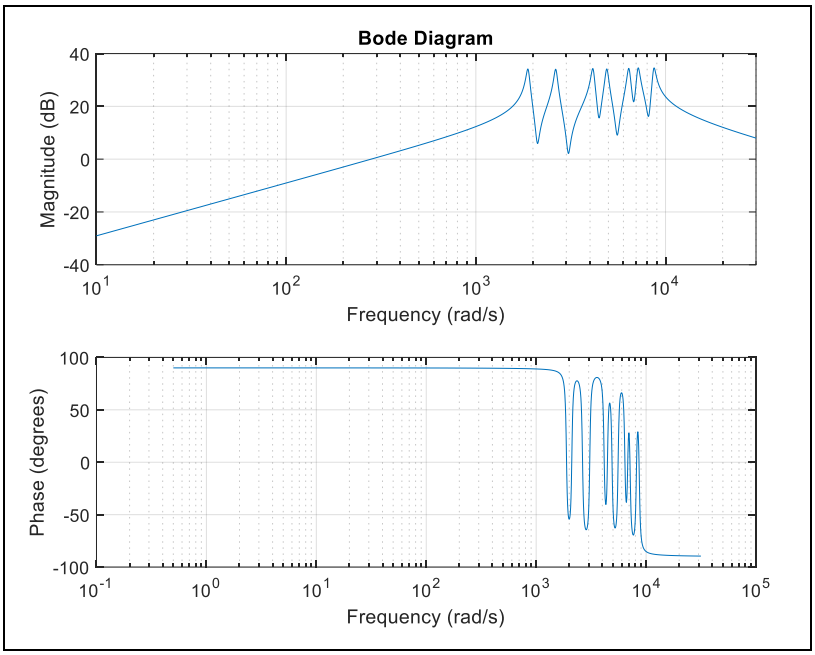

Figure 2.17: Bode plot of a resonant transfer function for several harmonics without compensation delay

The phase angle is limited within +/-90 degrees, with enough margin with respect to the limit 180 degrees. In the case of the Bode plot for the transfer function considering the compensation delay of 4 samples ($4\omega_1 T_s$), the Bode plot will look like:

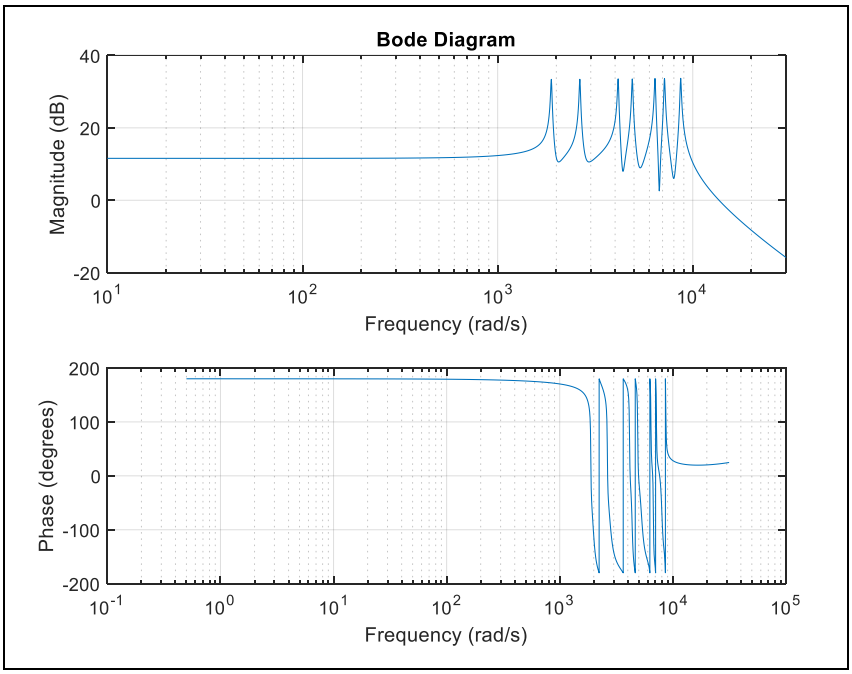

Figure 2.18: Bode plot of a resonant transfer function for several harmonics with compensation delay

A notable difference in the phase angle in the second case is that the phase angle reaches approximately +/-180 degrees. This is very close to the stability limit.

2.8 Low and high pass filters in the dq and $\alpha\beta$ frame

In the same way as the PI controllers, a low pass filter implemented in the dq frame can also be transferred into the $\alpha\beta$ frame. The low pass filter in the dq frame is:

$$LPF_{dq}(s) = \frac{1}{1 + T_{LP}s} \tag{36}$$

Applying the same expression (20), the equivalent dq low pass filter in the $\alpha\beta$ frame will be:

$$LPF_{\alpha\beta}(s) = \begin{bmatrix} \frac{1 + T_{LP}s}{(1 + T_{LP}s)^2 + (\omega_1 T_{LP})^2} & 0 \\ 0 & \frac{1 + T_{LP}s}{(1 + T_{LP}s)^2 + (\omega_1 T_{LP})^2} \end{bmatrix} \tag{37}$$

The high pass filter can be obtained by subtracting the low pass filter transfer function from 1, without considering the non-diagonal terms:

$$HPF_{\alpha\beta}(s) = 1 - LPF_{\alpha\beta}(s) = \begin{bmatrix} \frac{T_{LP}s(1 + T_{LP}s) + (\omega_1 T_{LP})^2}{(1 + T_{LP}s)^2 + (\omega_1 T_{LP})^2} & 0 \\ 0 & \frac{T_{LP}s(1 + T_{LP}s) + (\omega_1 T_{LP})^2}{(1 + T_{LP}s)^2 + (\omega_1 T_{LP})^2} \end{bmatrix} \tag{38}$$

This is important because when an equivalent control loop in the $\alpha\beta$ frame is needed, all components must be available in the same coordinate frame.

The loss pass filter and high pass filter in the dq frame are similar to a bandpass filter and stopband filter in the $\alpha\beta$ frame respectively, as seen in the picture below:

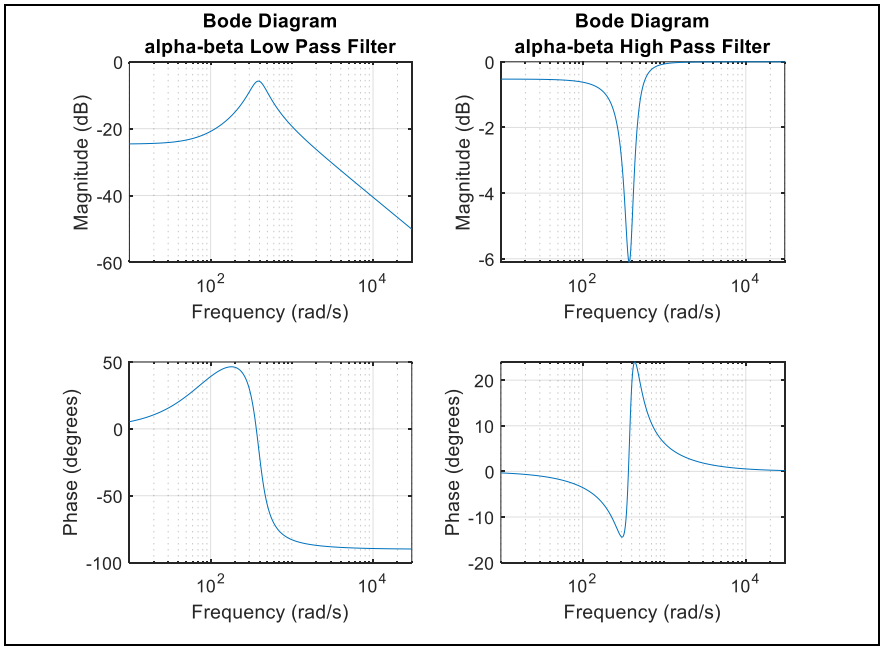

Figure 2.19: dq frame Low pass filter and high pass filter transferred to the $\alpha\beta$ frame.

2.9 Harmonics of positive, negative and zero sequence

If the system is balanced, no triplen or zero sequence harmonics should be present, because they are the zero sequence harmonics. However, a resonant controller for zero sequence harmonics could be also added to try to eliminate those harmonics.

The harmonics of interest are the $6p \pm 1$ also called $3h + 1, 3\mathrm{h} + 2$, as described in Table 2.1:

Sequence	Harmonic order					Rotation
+	1st	7th	13th	19th	… 3h+1	Forward
0	3rd	9th	15th	21st	… 3h	No rotation
-	5th	11th	17th	23rd	…3h+2	Reverse

Table 2.1: Harmonic Order and sequence (note: even orders not considered) [23].

Both positive and negative sequence harmonics need to be controlled. Fortunately, with only one resonant controller both types of harmonics can be handled at the same time.

2.10 Impact of PR Controllers without damping and with damping in the tracking of negative sequence components.

Resonant controllers with damping and without damping can track negative sequence components if there is a resonant controller for those negative sequence components. As described in equations 27 and 28, the coupling between negative and positive sequences are eliminated which means that if resonant controllers are implemented in both α and β frames, the resonant controller will track also steady state unbalanced voltages/currents. If it is also required that the controller eliminates unbalanced voltages, it should also contain a resonant controller for the fundamental frequency.

2.11 Nyquist stability criterion

Nyquist diagram is a polar plot of a transfer function $H(j\omega)$, which means that is a plot of the magnitude of $H(j\omega)$ versus the phase angle of $H(j\omega)$, when ω is varied from zero to infinite [22]. In this diagram, the angle is measured positive when it rotates counterclockwise and negative when it rotates clockwise from the positive real axis.

The Nyquist stability criterion determines the stability of a closed-loop system from its open-loop frequency response and open-loop poles. The Nyquist stability criterion relates the open loop frequency response $G(j\omega)H(j\omega)$ to the number of zeros and poles of $1 + G(s)H(s)$ that lie in the right half plane. The Nyquist stability criterion is based on the theory of complex variables.

Considering that a transfer function of $1 + G(s)H(s)$ has both zeros and poles and is a linear control system, three possibilities can occur [22]:

1. There is no encirclement of the $-1 + 0j$ point. This implies that the system is stable if there are no poles of $G(s)H(s)$ in the right-half s plane; otherwise, the system is unstable.

2. There are one or more counterclockwise encirclements of the $-1+0j$ point. In this case the system is stable if the number of counterclockwise encirclements is the same as the number of poles of $G(s)H(s)$ in the right-half s plane; otherwise, the system is unstable.

3. There are one or more clockwise encirclements of the $-1+0j$ point. In this case, the system is unstable.

2.12 Stability margins for a robust design

For the design of a control system, the plant model may have some uncertainties in its parameters or the system characteristics such as the frequency, may change, and the control system must continue operating. This is possible if the stability of the closed loop is maintained when the plant model uncertainties appear. A closed control loop will be termed ¨robust¨ if the stability is maintained when uncertainties in the model appear [24].

To evaluate how far is the critical point from the locus of the open loop transfer function, four elements help in the task and they are [24]:

- Gain margin
- Phase margin
- Delay margin
- Modulus margin

Their definitions can be better understood with the help of Figure 2.20:

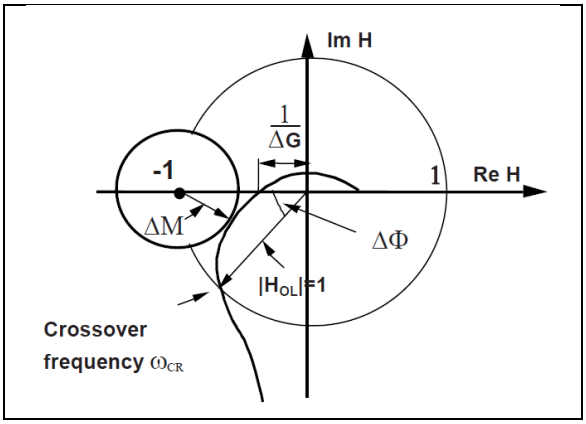

Figure 2.20: Gain, phase and modulus margins. [24]

2.12.1 Gain Margin

The gain margin ΔG is equal to the inverse of the open loop transfer function when the phase shift equals $\angle\phi(\omega) = -180°$. Then:

$$\Delta G = \frac{1}{|H_{OL}(e^{-j\omega_{180°}})|} \tag{39}$$

If the Nyquist plots cross the x-axis several times for the multiples of $-180°$, then the gain margin is given by the minimum value. This criterion is important in the case of resonant controllers because this type of controllers have circumferences as loci as will be explained in Section 3.

2.12.2 Phase margin

The phase margin $\Delta\phi$ is the phase difference between the phase of the OL at the crossover frequency and $-180°$. This means:

$$\Delta\phi = 180^{\circ} - \angle\phi(\omega_{\mathrm{cr}}) \tag{40}$$

ω_{cr} is called crossover frequency and is the frequency when the HOL crosses the unit circle. This is the same frequency that is seen in the Bode diagram when the HOL gain becomes 1.0 or 0dB in the Bode plot. In cases where the HOL crosses the unit circle at several frequencies ω_{cr}^{i} several phase margins will be obtained. In that case, the system phase margin [24] is defined as:

$$\Delta\phi = min_i \phi_i \tag{41}$$

2.12.3 Delay margin

This is an important margin since the time delay introduces a phase shift proportional to the frequency ω. For a frequency ω_0, the phase shift introduced by a time delay τ is:

$$\Delta\phi\ (\omega_0\ ) = -\omega_0\ \tau \tag{42}$$

This phase shift can be also expressed as ¨time delay margin¨, which can be interpreted as the maximum increase in the time delay in the open loop system before the closed-loop system becomes unstable. As the time delay margin, the phase shift is:

$$\Delta\tau = \frac{\Delta\phi}{\omega_{\mathrm{cr}}} \tag{43}$$

In the cases where the HOL crosses the unit circle at several frequencies, the delay margin is the minimum of the time delay obtained at those frequencies. Then:

$$\Delta\tau = \min \frac{\Delta\phi_i}{\omega_{cr}^{i}} \tag{44}$$

[24] points out that a good phase margin does not guarantee a good delay margin. This is the case when the delay margin is low even if the phase margin is enough.

2.12.4 Modulus margin

This is perhaps the most interesting of all margins and will be used in detail later in this thesis. As shown in Figure 2.15, the modulus margin is defined as the radius of the circle centered in the instability point (-1, 0j) and the open loop transfer function $H_{OL}(z^{-1})$ [24]. The radius is tangent to the $H_{OL}(z^{-1})$, this also means that is the minimum distance between the instability point and the $H_{OL}(z^{-1})$.

The typical values for stability margin in a robust design are [24]:

- gain margin: $\Delta G \geq 2$ (6 dB) [minimum:$1.6\ (4\ dB)$]
- phase margin: $30^{\circ} \leq \Delta\phi \leq 60^{\circ}$
- delay margin: $\Delta\tau = \frac{\Delta\phi}{\omega_{cr}} \geq T_s$ [minimum: $0.75T_s$]
- modulus margin: $\Delta M \geq 0.5$ (-6 dB) [minimum: $0.4\ (-8\ dB)$]

2.12.5 Sensitivity function, its meaning and its relationship with modulus margin

When a system has multiple inputs and multiple outputs (MIMO), multiple outputs and one single input, and the system is linear, it is possible to analyze the impact of one of the inputs independent of each other. Later, the outputs can be added, and the complete output is obtained [22].

For instance, in the case of a closed loop subjected to a disturbance, the disturbance can be treated as an input, as shown in Figure 2.21:

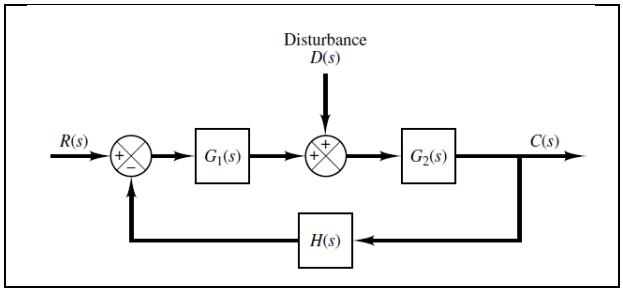

Figure 2.21: Close loop system with a disturbance as input. [22]

The transfer function between the output and the input R is:

$$\frac{C_R(s)}{R(s)} = \frac{G_1(s)G_2(s)}{1 + H(s)G_1(s)G_2(s)} \tag{45}$$

The transfer function between the output and the disturbance is:

$$\frac{C_D(s)}{D(s)} = \frac{G_2(s)}{1 + H(s)G_1(s)G_2(s)} \tag{46}$$

The added effect of both inputs is:

$$\frac{C_R(s) + C_D(s)}{D(s)} = \frac{G_1(s)G_2(s) + G_2(s)}{1 + H(s)G_1(s)G_2(s)} \tag{47}$$

If the disturbance is applied directly into the output, $G_2(s) = 1$ and the transfer function between the output and the disturbance becomes:

$$S_{yp} = \frac{C_D(s)}{D(s)} = \frac{1}{1 + H(s)G_1(s)} = \frac{1}{1 + H_{OL}} \tag{48}$$

This is the system's response only to the disturbance and this is called ¨output sensitivity function¨ [24].

If a perfect rejection of the disturbance is required, S_{yp} should be zero.

S_{yp} is also called error rejection [13] or disturbance rejection [24]

Looking at the equation 48, the relationship between the output sensitivity transfer function, open loop transfer function, and modulus margin is:

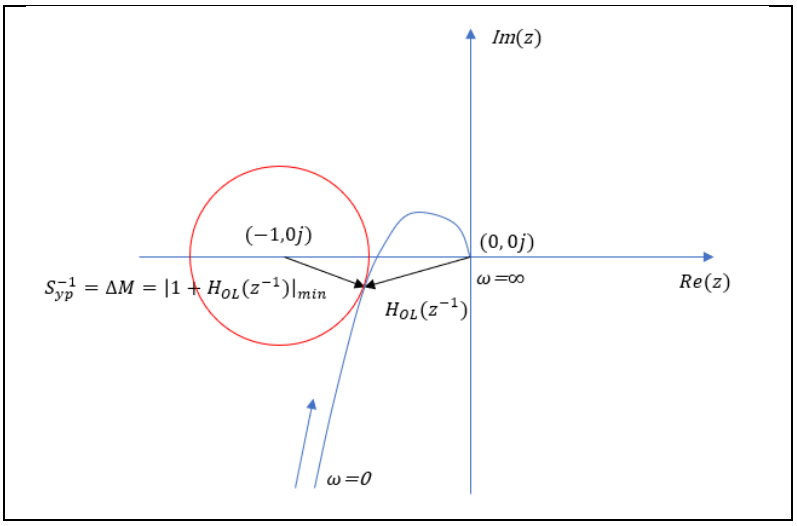

Figure 2.22: Relationship between S_{yp} ,ΔM, the H_{OL} in the z plane and the instability point

$$S_{yp} = \frac{1}{|1 + H_{OL}|} = \frac{1}{\Delta M} \tag{49}$$

2.13 Classical Tuning of PI Controllers

There are several ways to select the parameters K_P and K_I in a PI controller, being the most common [5]:

- Utilizing Bode-plots where a classic criterion is that the open loop transfer function will have a gain margin of at least 6 dB and a phase margin of 45 degrees.
- Pole location
- Use of criterion as Modulus optimum and Symmetric optimum for the synchronous reference frame.

The classic criteria to assess the stability of resonant controllers is to achieve a phase margin of 45° and gain margin of 6 dB, in the same way as any other controllers.

2.14 Discretization of transfer functions

When a control loop is implemented into a computer or similar automatic processing device for its use, the computer performs calculations according to the synchronization clock frequency. The computer receives the discrete signal $e(k)$ and produces the signal $u(k)$. This signal $u(k)$, which is a discrete series of pulses, is kept constant up to next pulse by means of a zero-order hold (ZOH) implementation. This modified signal is sent to the process. Another analog quantity measured from the process plant is discretized by means of the analog to digital converter (ADC), so the computer can understand and provides a command to the system. A graphical description is given in Figure 2.23.

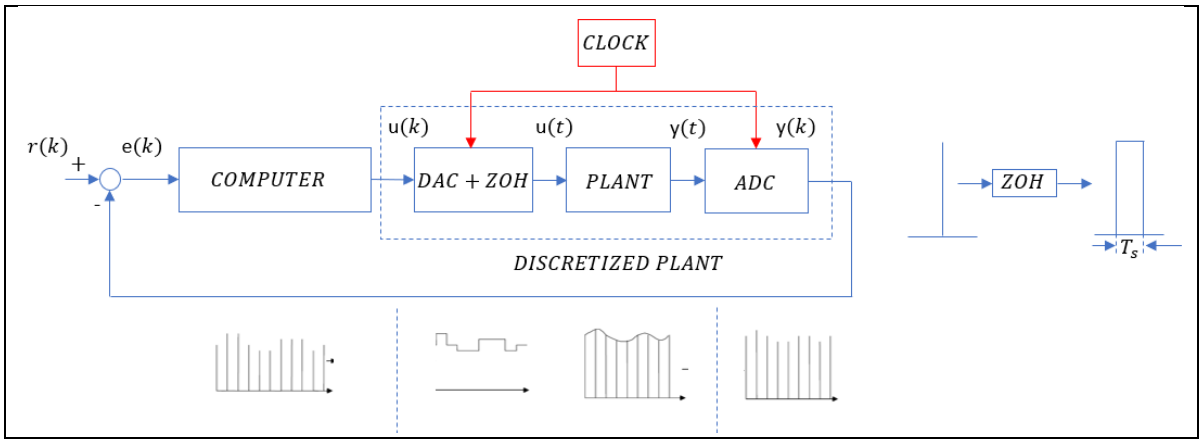

Figure 2.23: Digital control system and operation of the ADC, DAC and ZOH. Based on [24]

The ZOH implementation can be constructed by the difference of two unit steps shifted by one time sample, as shown in Figure 2.24.

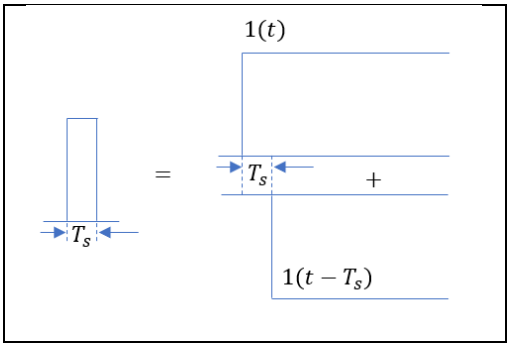

Figure 2.24: Construction of the zero-order hold. Based on [24]

The zero-order hold impact on how to handle the plant transfer function in the digital domain is essentially adding the expression in cascade with the original transfer function:

$$H_{ZOH}(s) = \frac{1 - e^{sT_s}}{s} \tag{50}$$

The global continuous transfer function will be:

$$H'(s) = \frac{1 - e^{sT_s}}{s} H(s) \tag{51}$$

To transfer the effect of the ZOH into the z transform, including the computational delay of one sample (T_s), it should be done in this way:

$$H(z) = z^{-1} Z\left\{ L^{-1}\left[\frac{1 - e^{-sT_s}}{s} H(s) \right] \right\} \tag{52}$$

2.14.1 Laplace transform, z transform, delta operator and w transform

The continuous transfer function in s domain cannot be directly applicable when a discrete implementation is necessary.

In order to study the continuous time models in the frequency domain, a periodic input of the complex exponential type has been used [24]:

$$e^{j\omega t} = \cos(\omega t) + jsin(\omega t) \tag{53}$$

Which corresponds to the relationship $s = j\omega$.

This is done considering only the steady-state periodic signals, such as the AC signals produced for electrical machines or electronic systems. If also the transitory states are to be studied, it is better to consider a more general and complex s variable of the form $s = \sigma + j\omega$. If a continuous time signal is to be measured for control purposes, this is done periodically as well at sampling intervals of $t = kT_s$, where T_s is the sampling time. These measured quantities are described as impulse sampling and, in this case, the z and s variables are related by the equation [24]:

$$z = e^{sT_s} \tag{54}$$

The variable sigma σ must be <0 (left half of the s plane) so the system is stable. Under this condition, the whole left s plane is transferred into the unit circle in the z plane.

$$z = e^{(\sigma + j\omega)T_s} \leq 1 \tag{55}$$

Sometimes, to get better numerical properties in the z plane, and more efficient implementation in controllers with limited process capacity an additional transformation is necessary and is called single-sided delta transform [25]:

$$z = 1 + \gamma\Delta \tag{56}$$

The value of Δ is adjustable depending on the specific case of digital implementation and is considered as a first estimation $\Delta = T_s$.

In order to use the well-developed frequency response methods to the analysis and design of control systems based on Bode plots, an additional transformation is necessary. This is called a bilinear transformation, and is defined in the following way [26]:

$$z = \frac{1 + \frac{T_s}{2}w}{1 - \frac{T_s}{2}w} \tag{57}$$

$$w = \frac{2}{T_s}\frac{z-1}{z+1} \tag{58}$$

The frequency in the w plane is distorted in relation with the real frequency ω and is called ν such that $w = j\nu$. Therefore, a transformation must be done once the design of the control discrete system is done in the w plane, to get the desired frequency in the s domain [26]:

$$\nu = \frac{2}{T_s}\tan(\frac{\omega T_s}{2}) \tag{59}$$

This distortion is not severe for small values of ωT_s, where the approximation

$$\nu \approx \omega \tag{60}$$

Is valid. A graphical description of the stability regions of the continuous Laplace plane, z plane, shift plane γ, and w plane is given in Figure 2.24.

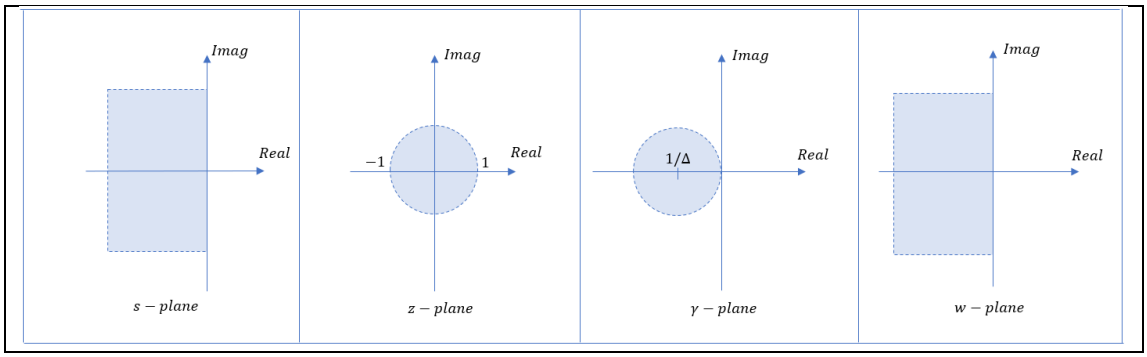

Figure 2.25: Stability regions/mapping of continuous Laplace plane, z plane, discrete delta and w planes. Based on [24, 25]

A full description of z and w transformations and their applications can be found in [24] and [26].

2.14.1 Prewarped Tustin Method

In order to avoid degradation of the operation of the resonant controller because of the resonant frequency shifting, the appropriate discretization method should be chosen. Several references recommend the use of the Tustin pre-warped method, such one of the methods that have the desired mapping and frequency properties. It consists of the substitution of s variable with the following expression:

$$s = \frac{h\omega_1}{tan\left(\frac{h\omega_1 T_s}{2}\right)}\frac{z+1}{z-1} \tag{61}$$

Or

$$s = \frac{\omega}{\tan\left(\frac{\omega T_s}{2}\right)}\frac{z+1}{z-1} \tag{62}$$

In a more general way.

The use of this transformation has the advantage that the frequency in the continuous and discrete planes are the same and therefore no additional transformations are necessary.

A good summary of the diverse discretization methods and their impact in the stability of the digital resonant controllers without damping is available in [27].

2.15 Frequency adaptation of digital resonant controllers

The final implementation of a controller of any type in a microprocessor is done by obtaining the discrete version (digital version) of this, which will be programmed into the processor´s memory. The discretization is essentially an approximation of the continuous solution that can be implemented sequentially in a microprocessor. This approximation is done mathematically by converting the transfer function from the Laplace domain to the Z domain.

There are different ways of doing this transformation, and the suitability of them depends on the intended use of the discrete version. The discretization involves sampling time, the accuracy of tracking, modification of the pole and zero placements, time delays, as well as the computational burden required to process the signals in a reasonable time. The modification of the location of zeros and poles because of the transformation, as well as the stability properties of the system changes once the discrete transformation is

performed. To mitigate the negative effects that these changes may have in the controller, error compensation strategies or delay compensation strategies are used.

These effects require some treatment, otherwise, the perfect tracking expected is not achieved and, the stability of the implementation may be compromised. It might happen that the system is inherently stable, but an inappropriate discrete implementation produces an unstable performance. [28].

As it can be seen in Figure 2.26, a small displacement of the resonant frequency away from the desired point changes severely the gain desired, compromising the tracking of the resonant frequency.

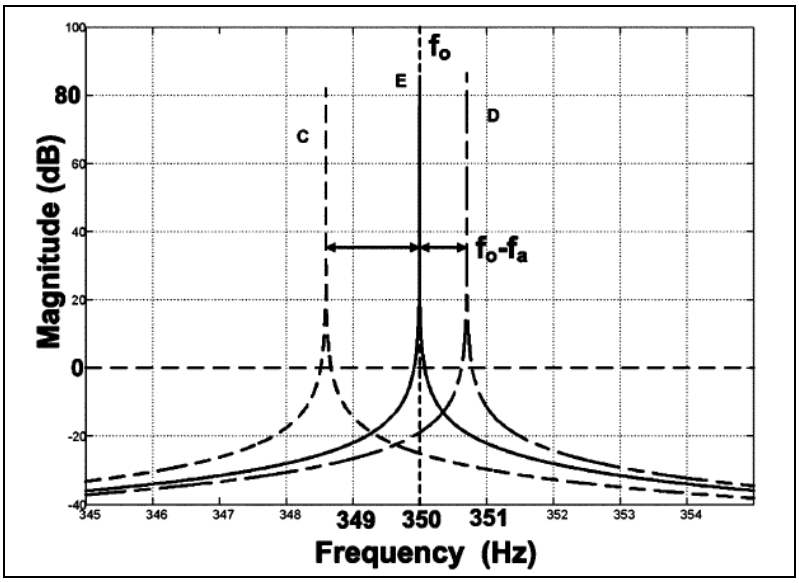

Figure 2.26: Effect of displacement of the resonant frequency. [27]

Several discretization methods have been proposed, such as the ones summarized in [27]. Besides the accuracy, the computational burden is also a consideration, because of its impact on the speed of the controller.

Despite the interesting development of numerical methods for an ideal resonant controller, as mentioned by Teodorescu [20], the ideal resonant controllers have problems with stability, due to infinite gains at resonant points. That instability can be corrected with a damping term. With damping, the gain is finite but still high enough to enforce small steady state error [20].

The question of how large the damping factor of the resonant controller could be answered thinking how large the frequency variation should be such that the controller can operate without significant deterioration of its high gain features. Reference [19] recommends a damping factor of $\zeta = 0.01$ whereas [29] recommends a range for $\omega_c = 2\zeta\omega_1$ of [5-15] rad/s. This means, for 5 rad/s:

$$\zeta = \frac{\omega_c}{2\omega_1} = \frac{5}{2 * 377} = 0.0066$$

For ω_c=15 rad/s, the damping factor is $\zeta \approx 0.02$.

2.16 Discretization Methods for Resonant Controllers without damping

Two integrator discretization methods seem to be the most popular among the available discretization methods because of their suitability for frequency adaptation with low requirement of computational capability [27].

One of the discretization methods evaluated in this thesis is proposed in [27]. This discretization method has already been applied in a previous master thesis as well [15]. It will be explained in Section 2.18 that the delay compensation strategy is dependent on the parameters of the plant model which means that the discretized version of the plant should be obtained.

The inaccuracies caused by the discretization methods can be evaluated based on the following criteria:

- Effect on the location of resonant poles
- Effect on zeros location or system delay
- Computational burden

The block diagram of the continuous resonant controller transfer function (equation 29) of order h is shown in Figure 2.27:

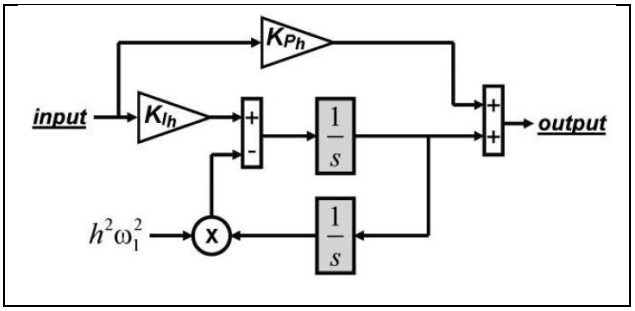

Figure 2.27: Block diagram of a continuous resonant controller based on two integrators. [21]

Being ω_1 the fundamental frequency. To consider the delay compensation due to computation, modulation, and passive filters, a phase lead should be introduced in the vicinity of the resonant frequency $h\omega_1$ of the resonant controller ([21] and previous authors) with the following expression:

$$G_{PR_h}^d(s) = K_{P_h} + K_{I_h}\frac{scos(\phi_h^*) - h\omega_1 \sin(\phi_h^*)}{s^2 + h^2\omega_1^2} \tag{63}$$

(ϕ_h^*) is the target leading angle, i.e. the angle needed to compensate the system delay. In the continuous domain, $G_{PR_h}^d(s)$ satisfies $\phi_h = \phi_h^*$. This correction in the transfer function of the resonant controller allows an improvement in the stability of the system. The block diagram for this corrected scheme is shown in Figure 2.28:

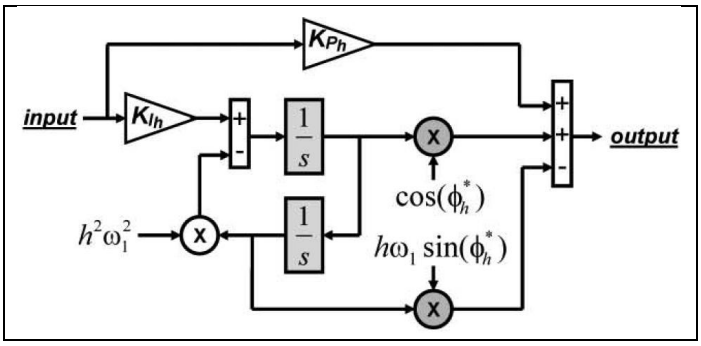

Figure 2.28: Block diagram of a continuous resonant controller based on two integrators with system delay compensation. [21]

A good discretization that implements the best features of the forward/backward Euler method for accurate pole location and impulse invariant method for less phase lag in a single expression has been proposed in [21]. The proposed discrete version of the resonant controller is:

$$G_{PR_h}^{cd}(z) = K_{P_h} + K_{I_h} T_s \frac{z^{-1} cos(h\omega_1 T_s + \phi_h^*) - z^{-2} cos(\phi_h^*)}{1 - 2z^{-1}\left(1 - \frac{C_h T_s^2}{2}\right) + z^{-2}} \tag{64}$$

Being C_h an expression derivated from the Taylor expansion of $cos(h\omega_1 T_s)$:

$$C_h = \sum_{n=1}^{k/2} \frac{(-1)^{n+1}}{(2n)!} (h\omega_1 T_s)^{2n} T_s^{-2} \tag{65}$$

Being k even values. The larger the terms included in h, the higher the accuracy of the method.

The block diagram for the corrected expression is shown in Figure 2.29:

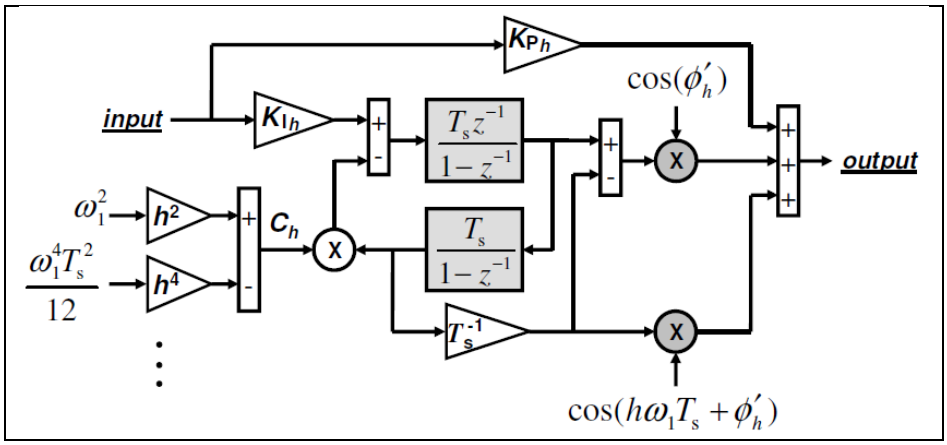

Figure 2.29: High performance proposed implementation of PR controllers based on two integrators, included resonant pole correction and accurate frequency adaptation. [13]

2.17 Discretization Methods for Resonant Controllers with damping

The resonant controller is, in fact, a band-pass filter of second-degree. Therefore, a realization structure suitable for filters is the most convenient way to represent digitally the resonant controller. Of all available filter realization structures, according to several references [25, 30, 31] the filter type IIR, Direct Form II transposed (DFIIt) is recommended as the most appropriate structure.

The digital version of the resonant controller with damping and no delay compensation using the pre-warped Tustin bilinear transform, considering the DFIIt version of the digital filter is given as [32]:

$$G_{PR_h}(z) = \frac{b_0 + b_1 z^{-1} + b_2 z^{-2}}{1 + a_1 z^{-1} + a_2 z^{-2}} \tag{66}$$

Where the coefficients are given by:

$$g = \frac{K_{Ih}}{2h\omega_{res}}\left[\frac{\sin(h\omega_{res}T_s)}{1 + \zeta\sin(h\omega_{res}T_s)}\right] \tag{67}$$

$$a_1 = -\frac{2\cos(h\omega_{res}T_s)}{1 + \zeta\sin(h\omega_{res}T_s)} \tag{68}$$

$$a_2 = -\frac{1 - \zeta\sin(h\omega_{res}T_s)}{1 + \zeta\sin(h\omega_{res}T_s)} \tag{69}$$

$$b_0 = K_P + g \tag{70}$$

$$b_1 = \mathrm{K}_P a_1 \tag{71}$$

$$b_2 = \mathrm{K}_P a_2 - g \tag{72}$$

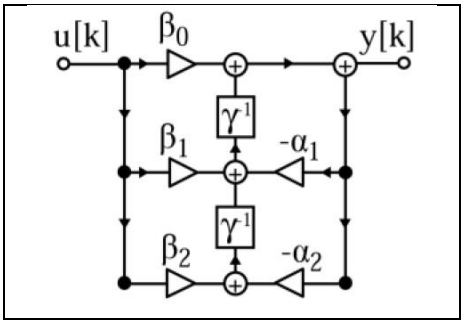

Figure 2.30: Block diagram for a Direct Form transposed digital structure DFIIt [25]

When better numerical properties are required to minimize the computational power and to get a faster operation, a low word length is required. A word length or machine word length in digital processing is the normal or preferred size number of bits used in a particular computer architecture, i.e. the number of bits that the processor or computer can process at a time. In this case, the delta operator is used and is defined as [33]:

$$\delta = \frac{z - 1}{\Delta} \tag{73}$$

In this case, Δ is an optimization parameter and $\Delta \leq 1$. It is important to mention that the discretization has a consequence of a deterioration of the signal, which can be observed in the Bode diagram as a deviation of the gain and phase deviation as in the Figure 2.26.

In this case, the delta operator gives a better precision which is observed as a digital implementation closer to the continuous transfer function.

The discretized transfer function considering the delta operator is:

$$G_{PR_h}(s) = \frac{\beta_0 \delta^2 + \beta_1 \delta + \beta_2}{\delta^2 + \alpha_1 \delta + \alpha_2} \tag{74}$$

Where the coefficients are:

$$\beta_0 = b_0 \tag{75}$$

$$\beta_1 = \frac{2b_0 + b_1}{\Delta} \tag{76}$$

$$\beta_2 = \frac{b_0 + b_1 + b_2}{\Delta^2} \tag{77}$$

$$\alpha_0 = 1 \tag{78}$$

$$\alpha_1 = \frac{2 + a_1}{\Delta} \tag{79}$$

$$\alpha_2 = \frac{1 + a_1 + a_2}{\Delta^2} \tag{80}$$

If a discrete model with delay compensation is necessary, [30] provides a discrete implementation with a delta operator considering $\Delta = 1$ and a transfer function as shown below:

$$G_{PR_h}(s) = \frac{b_0 \delta^2 + b_1 \delta + b_2}{\delta^2 + a_1 \delta + a_2}$$

Where the coefficients are:

$$r_h = \frac{1}{1 + \frac{\zeta}{2h\omega_1} \sin(h\omega_1 T_s)} \tag{81}$$

$$K_h' = \frac{K_h}{2h\omega_1} \tag{82}$$

$$b_0 = K_h'[sin(h\omega_1 T_s + \phi_h) - sin(\phi_h)] \tag{83}$$

$$b_1 = K_h'[3sin(h\omega_1 T_s + \phi_h) - 4sin(\phi_h) - sin(h\omega_1 T_s - \phi_h)] \tag{84}$$

$$b_2 = K_h'[2sin(h\omega_1 T_s + \phi_h) - 4sin(\phi_h) - 2sin(h\omega_1 T_s - \phi_h)] \tag{85}$$

$$a_1 = 2[1 - r_h \cos(h\omega_1 T_s)] \tag{86}$$

$$a_2 = 2r_h[1 - r_h \cos(h\omega_1 T_s)] \tag{87}$$

2.18 Tuning Methods for resonant controllers

Different methods to tune a resonant controller have been proposed for several authors, and they are based on different criteria. A small summary of the ones reviewed during the development of this thesis is given below:

- [13] proposed to evaluate and optimize the proximity to instability using Nyquist diagrams, and the sensitivity function.
- [30] proposed maximum values of K_{P_T} and K_{ih} for a P+R controller in a current control closed loop with a plant model of an inductance.
- [34] presented a method to avoid destabilization of a poorly damped grid and/or input filter resonances, particularly when the converter time delay is not negligible. The proposal is to make the converter´s input admittance passive.
- [35] proposed a controller parameter design method, based on the system error transfer function to extend the stable region of the controller.
- [36] proposed to use the weighted average value of the currents flowing through the two inductors of the LCL filter as feedback to the current PR regulator.
- [37] proposed the use of a direct discrete-time pole placement strategy from the classical control theory using transfer functions and involving two extra filters to enhance the performance of the resonant controller.
- [42] mentioned that it could be desirable to tune the harmonic gains proportionally to its percentage of THD to minimize the total error convergence rate.

One general idea that can be traced across all references is the presence of a plant model that is approximated as an inductance. Also, most of the references propose solutions based on current control loops.

2.19 Tuning criteria for PR Controllers without damping

The authors in [13] proposed a tuning criterion for current controllers using the Nyquist diagram and the output sensitivity function. It is based in maximization of the distance of the open loop transfer function to the instability point $D(z)$ and the minimization of the sensitivity peak $1/\eta$ at each frequency in the Nyquist diagram. It also combines this criterion with the maximum K_{P_T} that can be obtained to limit the interference of the commutation harmonics with the current control.

The voltage source converter analyzed in [13] is shown below:

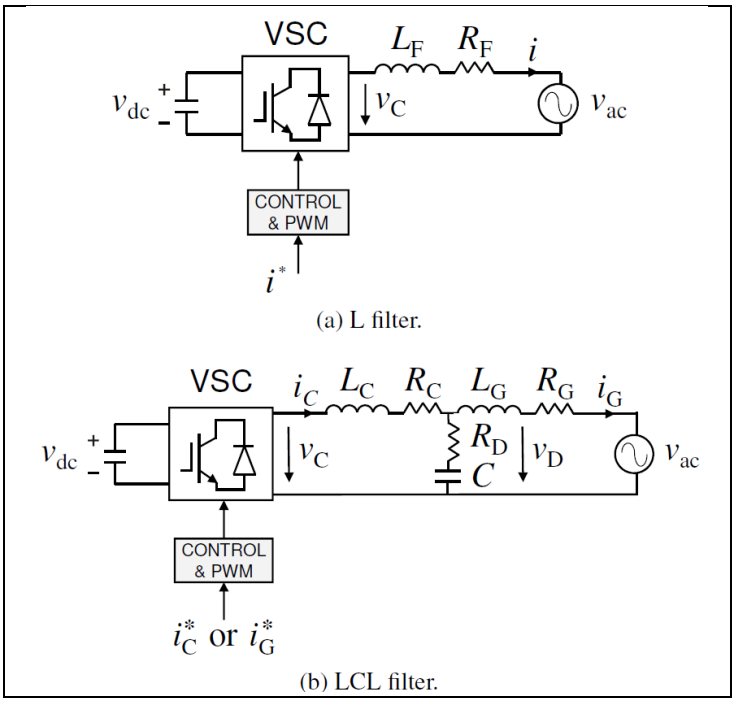

Figure 2.31: Current-controlled VSC supplying a voltage source (or equivalent) through a low-pass filter. Other control inputs are omitted for clarity. [13]

The authors in [13] analyzed the LCL filter, considering it as L filter for a range of frequencies below the resonant frequency f_{res}. In this case, the block diagram of the LCL filter, when modeled as an L filter is shown below:

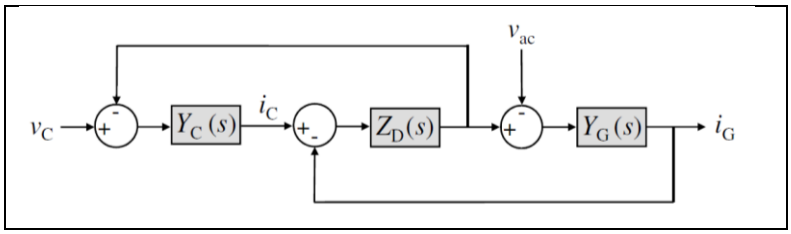

Figure 2.32: Block diagram of an LCL filter. [13]

The plant transfer function of the simplified system is:

$$G_L(s) = \frac{I(s)}{V_c(s)} = \frac{1}{sL_F + R_F} \tag{88}$$

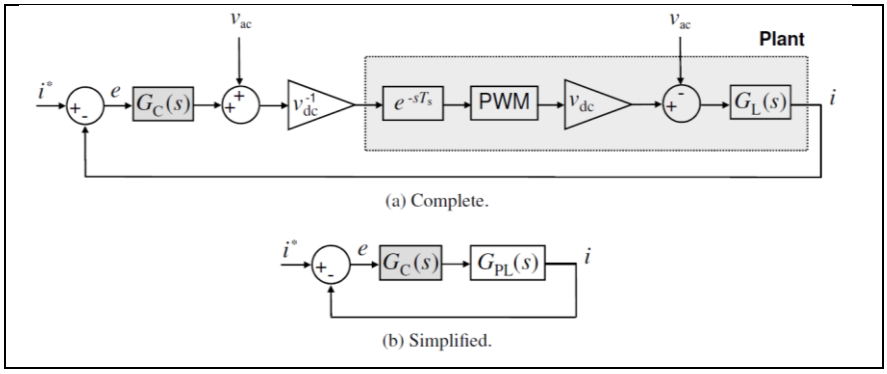

Figure 2.33: Block diagram of current control close-loop in stationary frame. [13]

The discrete-time transfer function equivalent to the plant in Figure 2.33 without neglecting the delays, the computational delay e^{-sT_S} is substituted by z^{-1} and the PWM block was substituted by a zero-order hold (ZOH) is:

$$G_{PL}(z) = z^{-1}Z\left\{L^{-1}\left[\frac{1-e^{-sT_S}}{s}G_L(s)\right]\right\} = \frac{z^{-2}}{R_F}\frac{1-\rho^{-1}}{1-z^{-1}\rho^{-1}} \tag{89}$$

Where $\rho = e^{\frac{R_F T_S}{L_F}}$.

The ZOH is claimed to be a very good approximation in the case of a triangular carrier waveform [13].

The whole method is based on the fact that the transfer function of the resonant controller without damping for each harmonic has a similar shape, with an asymptote at the resonant frequency $h\omega_1$.

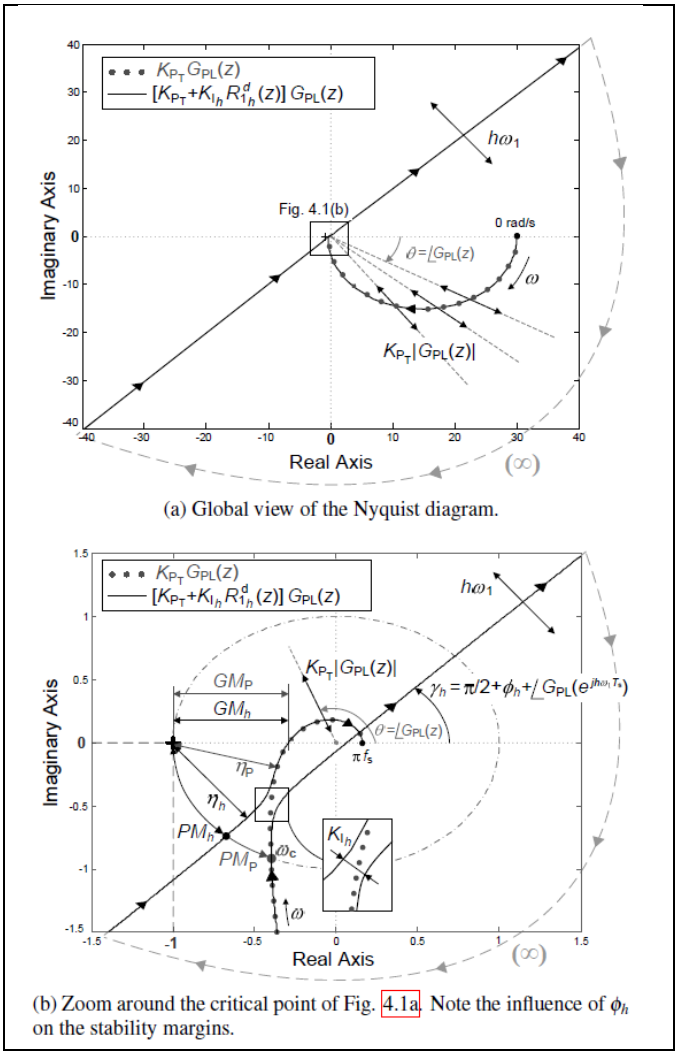

(a) Global view of the Nyquist diagram.

(b) Zoom around the critical point of Fig. 4.1a. Note the influence of ϕ_h on the stability margins.

Figure 2.34: Nyquist diagram of a generic $[K_{P_T} + K_{I_h}R^d_{I_h}(z)]G_{PL}(z)$, for positive frequencies . [13]

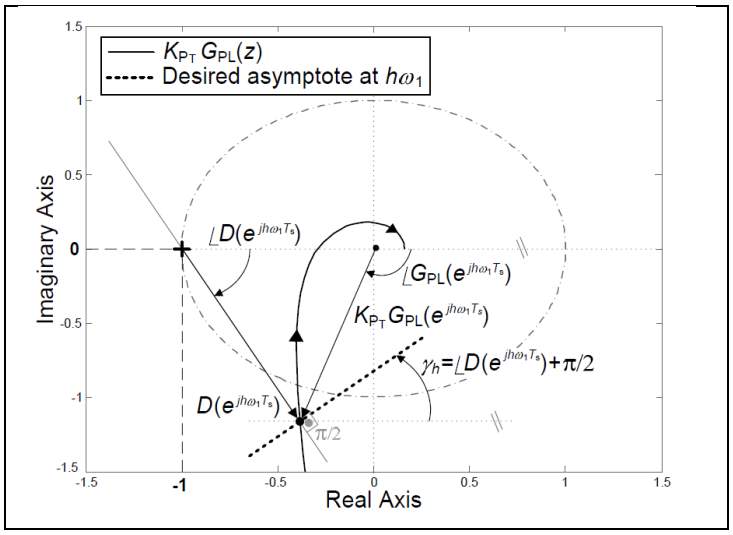

Figure 2.35: Optimum asymptote at $h\omega_1$ in order to maximize $D(z)$ at frequencies around $h\omega_1$, in $G^d_{PR_h}(z)$ controllers.[13]

The Figure 2.34.b shows that a good approximation of K_{P_T} can be obtained by recognizing that the consideration of the resonant controllers in the H_{OL} only affected the plot in a small range around $h\omega_1$ and in that way, K_{P_T} could be obtained by analyzing the system considering only K_{P_T} and the plant model without adding the resonant controllers. Note that the Nyquist plot of the H_{OL} does not enclose the instability point.

The way of obtaining this K_{P_T} value is by setting a desired sensitivity peak $1/\eta_P$, and finding the global minimum of $D(z)$ in this way:

$$G_{PL}(z) = z^{-1}Z\left\{L^{-1}\left[\frac{1-e^{-sT_s}}{s}G_L(s)\right]\right\} = \frac{z^{-2}}{R_F}\frac{1-\rho^{-1}}{1-z^{-1}\rho^{-1}} \tag{90}$$

$$D(e^{j\omega T_s}) = 1 + K_{P_T}G_{PL}(e^{jh\omega_1 T_s}) \tag{91}$$

$$g(\omega_\eta) = \frac{\partial\left|D(e^{j\omega T_s})\right|}{\partial\omega}(\omega_\eta) = 0 \tag{92}$$

$$\frac{\partial^2\left|D(e^{j\omega T_s})\right|}{\partial\omega^2}(\omega_\eta) > 0 \tag{93}$$

The value of ω_η is then used to obtain η_P by using the following relationship:

$$\left|D\left(e^{j\omega_\eta T_s}\right)\right| = \eta_P \tag{94}$$

Then, an expression of K_{P_T} as a function of η_P, T_s, R_F, L_F is obtained:

$$K_{P_T} = F_1(\eta_P, T_s, R_F, L_F) \tag{95}$$

The exact formulation is rather complex for such a small system, but it expresses appropriately the concept of minimization. The exact formula can be obtained in Appendix C.1 of [13].

The authors in [13] identified that in the resonant controllers without damping, the asymptote for each resonant frequency has a clear tendency and that by setting K_{P_T}, it was straightforward to fix $\eta_P = \eta_h$. The asymptote angle $\gamma_h = \frac{\pi}{2} + \phi_h + \angle G_{PL}(e^{jh\omega_1 T_s})$ in the Nyquist

diagram was set equal to the angle of the tangential line to the H_{OL} locus with the x-axis at the point where the distance to instability point $D(z)$ was the minimum. This is the way the delay compensation ϕ_h was minimized, assuring the optimum selection of K_{P_T} and the delay compensation angle together. This means that, comparing the asymptotic angle in Figure 2.34 and Figure 2.35:

$$\gamma_h = \frac{\pi}{2} + \phi_h + \angle G_{PL}(e^{jh\omega_1 T_s}) = \angle \mathrm{D}(e^{jh\omega_1 T_s}) + \frac{\pi}{2} \tag{96}$$

From this relationship, an expression for the delay compensation angle was obtained:

$$\phi_h' = -\angle G_{PL}(e^{jh\omega_1 T_s}) + \angle \mathrm{D}(e^{jh\omega_1 T_s}) \tag{97}$$

The terms of ϕ_h' are developed and an expression was obtained:

$$\phi_h' = F_2(h\omega_1, T_s, R_F, L_F) \tag{98}$$

The complete expression is available in Appendix C.2 of [13].

The limit of K_{P_T} established by the criterion of avoiding the interference of the commutation harmonics with the current control assuring that the crossover frequency is lower than a decade below the switching frequency (i.e., $\omega_c < \frac{\omega_{sw}}{10}$, $\omega_s = 2\pi f_{sw}$), so the attenuation at f_{sw} is at least 20 dB. Therefore, a relationship between K_{P_T} and ω_c was established:

$$\left|K_{P_T} H_{OL}(\omega_c)\right| = \left|K_{P_T} G_{PL}(\omega_c)\right| = \left|K_{P_T} G_{PL}\left(e^{j\frac{\pi}{5}}\right)\right| = 1 \tag{99}$$

This relationship is used to obtain the maximum acceptable K_{P_T} that satisfies $\omega_c = \frac{2\pi f_{sw}}{10}$.

Under this condition, a K_{P_T} value was proposed for a plant model that can be modeled as an inductance:

$$K_{P_T} = \frac{R_F}{(1-\rho^{-1})\sqrt{2}} \sqrt{2 + 2\rho^{-2} - (1+\sqrt{5})\rho^{-1}} \tag{100}$$

Being R_F the resistance of the inductance that represents the plant model and ρ is the term $e^{\frac{R_F T_s}{L_F}}$.

In this manner, the value of K_{P_T} obtained to minimize the interference of commutation control and the K_{P_T} required to minimize the distance of the open loop transfer function to the instability point for a desired sensitivity peak $1/\eta_P$ can be assessed. The most restrictive of the two values was used to tune the controller.

2.20 Active Damping

There are several methods to implement the active damping capability. Two of them, extracted from [1] and [10] will be explained. When there is an LC or LCL circuit, there is always a possibility of oscillations because the resonance frequency associated is activated by a transitory state, such as the startup, disconnection of a load, or a fault in the electric system. These temporary oscillations eventually disappear. Fortunately, it is possible that

these high oscillating frequencies can be attenuated if a control loop is added for that specific purpose.

One intuitive way of explaining the active damping is to remember that, when there is a resistance in an LC circuit, the resistance eventually attenuates the current. The implementation of this resistance in this LC circuit could be done in two ways; either adding a real resistance or adding an additional current reference that acts as a resistance. The first way is not the best way, because it consumes power and is also called passive damping [1]. The second one is to add an additional current reference that emulates a resistance R_p and carry a current i_p. This method is called active damping. The difference between active and passive damping can be appreciated in Figure 2.36:

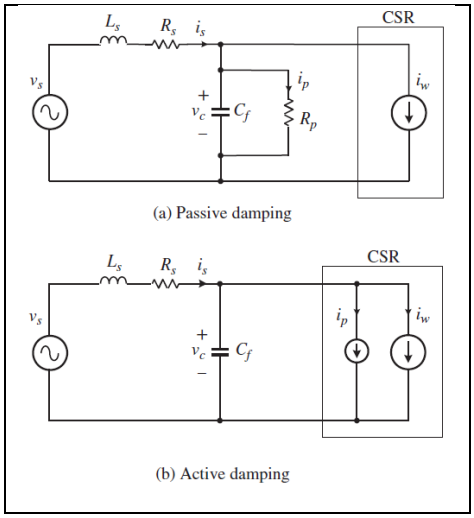

Figure 2.36: Realization of passive and active damping for a current source rectifier. [1]

In the case of a PWM rectifier (could be also an inverter), i_p can be generated following the next sequence:

- Detect the instantaneous capacitor voltage v_c;
- Calculate the damping current by $i_p = v_c/R_p$ and
- Adjust the modulation index m_a dynamically based on the calculated i_p.

Only the non-fundamental components of the voltage oscillations need to be removed. To achieve that, what can be done is identify the non-fundamental components of the capacitor voltage obtained through an abc/dq transformation using a PLL, incorporating a high pass filter to the voltage value in the dq frame. This is possible because the fundamental component of the ac capacitor voltage becomes DC when the transformation from abc to dq is done, then filtering all alternating components in the dq frame effectively eliminates the non-fundamental components. This can be understood looking at Figure 2.37:

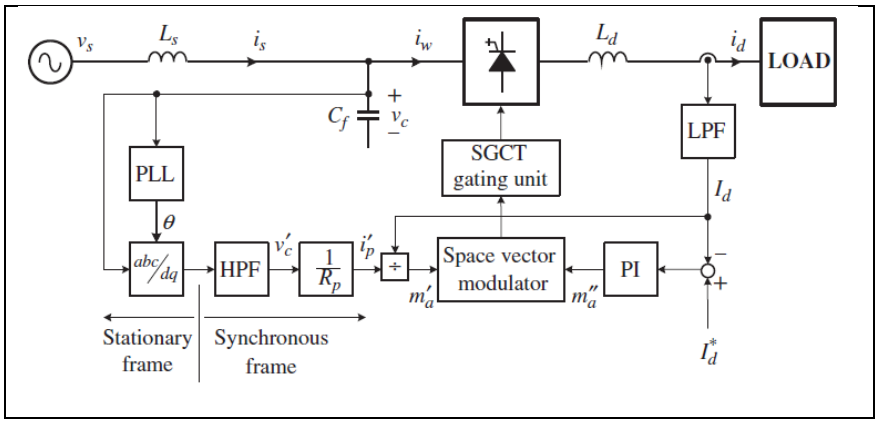

Figure 2.37: Block diagram of a vector-controller CSR with active damping control (HPF=High Pass Filter).[1]

The second way of obtaining the non-fundamental voltage oscillations is as proposed by [10], which includes close-loop feedback that reduces oscillations in the capacitor voltage to zero by adding damping currents to the current references.

One great advantage is that the higher oscillating frequency components can be controlled independently from others that comes from the converter itself or non-linear loads connected at the entrance of the converter. The additional inductance that converts the LC filter in an LCL filter blocks some harmonics as well.

The basic principle can be summarized as follows, according to [1]:

- The oscillating component of the capacitor voltage is extracted (the non-fundamental component)
- The error in the capacitor voltage is found by subtracting the oscillating component from its reference, which is equal to zero
- The error is amplified and added to the reference signal for the current controller.

The block diagram of the active damping loop is shown in the following figure:

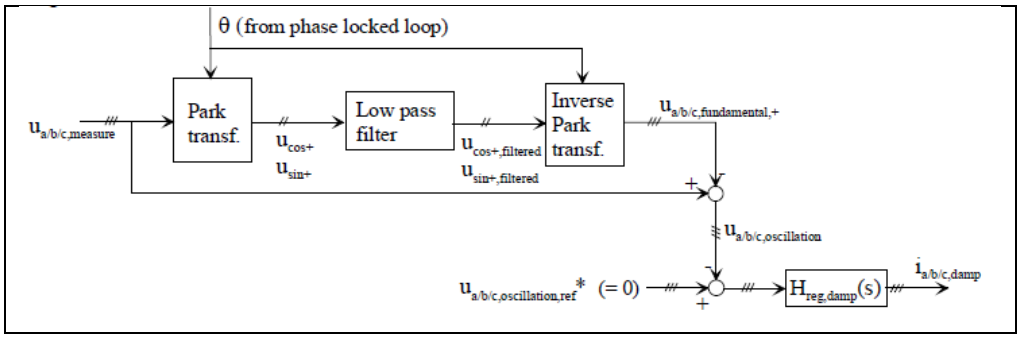

Figure 2.38: Block diagram of the active damping block.[38]

Also, according to [38], the time constant of the low pass filter has an influence in the performance of the active damping during slow transients and, also the performance when negative sequence components are present. For this reason, the filter should be selected according to the desired behavior.

Another benefit of the active damping is the minimization of the DC offset in the converter. However, there is always a tradeoff between minimization of oscillations and the minimization of DC offset.

In this thesis, the second version has been implemented.

2.21 Other Control Features of VSIs

2.21.1 Synchronization

A synchronization system is a system that verifies that the conditions to close a circuit breaker are met. This synchronization system allows the connection of one main equipment such as generators, electric drives, to the electric power systems or the interconnection of two systems.

To do this, it is necessary that three conditions are fulfilled, with different criteria according to the application:

- The Voltage difference is within a certain range
- The Frequency difference is within a certain range
- The Phase angle difference is within a certain range

When all these conditions are met, the circuit breaker can close the circuit and connect the equipment with the electric power system.

Depending on the voltage level, the synchronization system features vary, being common the following:

- Low and medium voltage level: three pole closing
- High voltage level: monopole closing and three pole closing

Sometimes, to minimize the overvoltage transients caused by the connection of the equipment, the closing of the three phases are done sequentially, which is called point-on-wave switching. This is a special feature that it is normally used to connect the extremes of long high voltage transmission lines, reactors or power transformers. In the case of the medium voltage and low voltages, this is not normally used, due to its high cost and complexity.

One of the great advantages of Voltage Source Converter or Voltage Source Inverters is that there is no need of a grid voltage to operate the switches (self-commutation). This feature is essential for grids with HVDC links in case of blackouts, where a VSC can help to restart the grid after a blackout (black start) [39]. The possibility of the inverter of creating its own voltage such as a conventional generator allows synchronization.

To achieve this, in the case of an AFE, normally the breaker is installed next to the filter capacitor, as shown in the figure below:

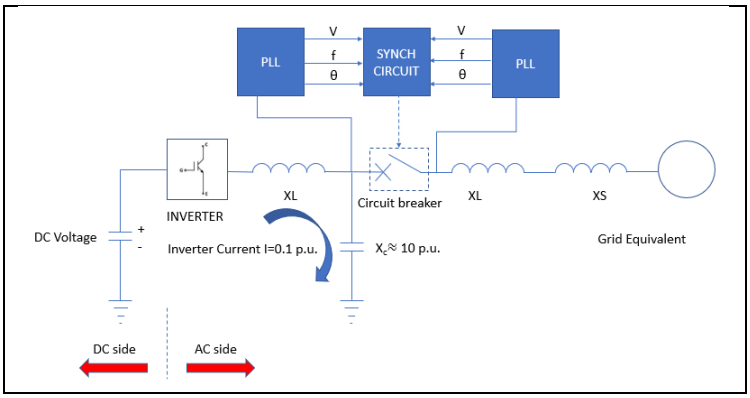

Figure 2.39: Single phase schematic of the Synchronization Circuit

The voltage needed in the capacitor can be obtained charging the capacitor with current, using the voltage in DC side of the inverter. The DC side voltage can be either a battery or a machine side converter which connects the drive with a motor or generator. In the case of a solar panel, since the power is generated directly in DC, this additional converter is not needed.

Voltage transformers are needed to measure the voltages in both sides of the breaker and two phase locked loop systems to obtain the angle reference and frequency on both sides.

Once the capacitor is charged with the voltage necessary and the frequency and angle is within the correct limits, the circuit breaker can close.

2.21.2 Normal Operation

Once the circuit breaker is closed, the voltage controller raises the voltage up to the reference value (1.0 p.u.) and increases the converter current up to the rated value. It is expected that the time the controller uses to take the current and voltage to their rated values be the minimum possible.

During normal operation, the inverter should be able to handle the load and voltage variations without losing stability, as well as handle reasonably the non-linear loads, reducing the total harmonic distortion (THD) up to an acceptable limit.

3 Proposed Delay Compensation Method of Resonant Controllers with Damping

Despite the fact that the authors in [13] have proposed a promising delay compensation method, other authors claim that it is inaccurate for an LCL filter [35]. However, conceptually, the method is simple and could be extended for a general system. It is necessary to mention that for applications where adaptative frequency is necessary, damping is a must. Another important aspect is that in real control applications, low pass filtering, uncertainty in the obtention of plant models, active damping, hysteresis controllers and other control features must be incorporated into the system. Therefore, in those cases, the direct formula proposed in [13] is no longer valid.

It would be desirable as well that the open loop transfer function can be obtained for any control implementation and use it as the general description of the model to obtain the delay compensation necessary and K_{P_T}.

Two other important aspects highlighted in the method proposed in [13] is the combination of the ZOH method for the z model of the plant, while using the pre-warped Tustin method for the discretization of the controller. The first important aspect to assess stability in the z plane is how the resonant controller with damping should be represented in that plane.

The resonant controller transfer function is repeated below:

$$RC(s) = \sum_{h=5,7,11,\ldots,6p\pm1} \frac{K_{Ih}s}{s^2 + 2\zeta h\omega_1 s + (\omega_1 h)^2} \tag{101}$$

Its Bode diagram in the z plane is shown below:

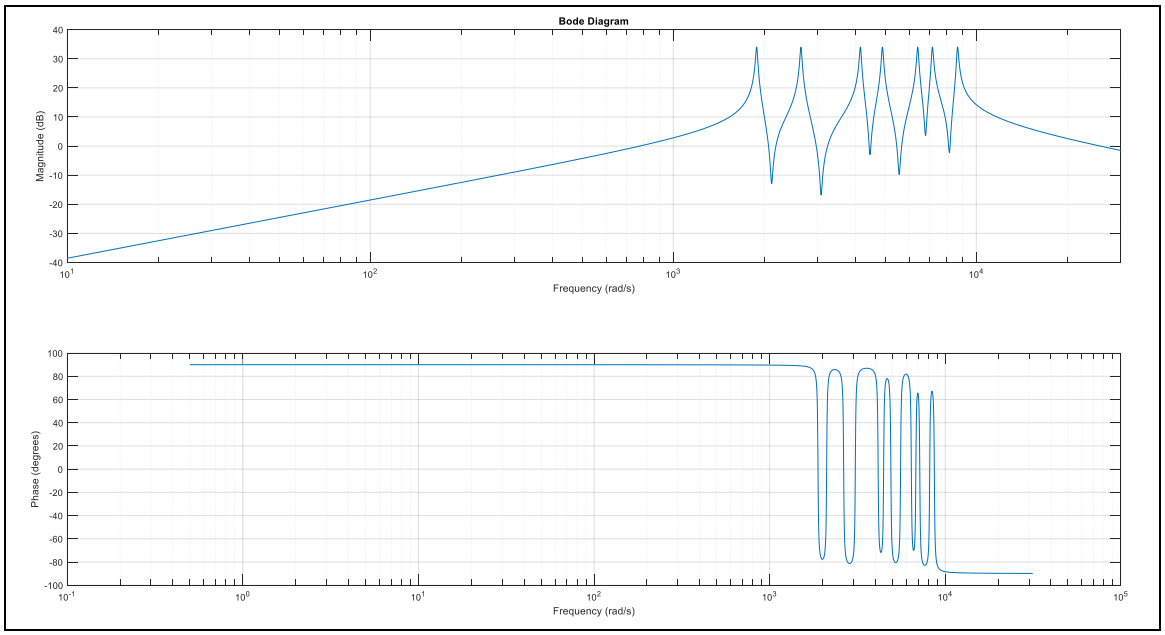

Figure 3.1: Bode diagram of a set of resonant controllers implemented in digital domain w.

Given the structure of the resonant controller transfer function in the s plane, the value of the transfer function is zero at the origin ($s \to 0$) and when $s \to \infty$.

When a resonant controller with or without delay compensation is converted into the z plane, the locus of it becomes a circumference. In this case, the locus of a resonant controller is a circumference centered in ($K_{Vh}/2$, $0j$), as shown in Figure 3.2:

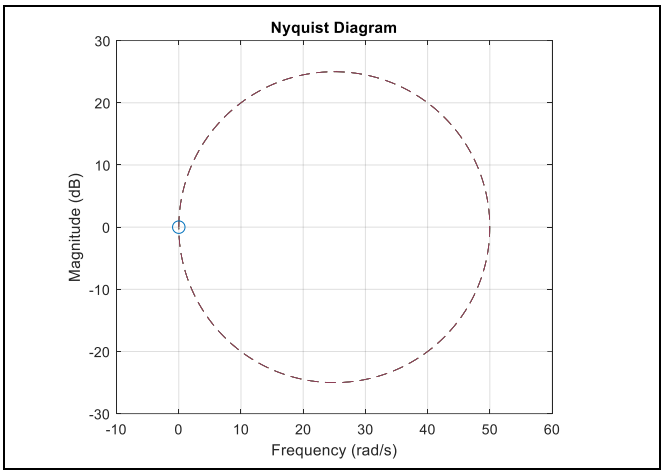

Figure 3.2: Nyquist plot of resonant controllers 6p+/-1 for p=1…4 without delay. The small light blue circle is the unit circle. $K_{Vh} = 50$.

Since the resonant gains K_{Vh} for all harmonics have the same value, the loci of the resonant transfer functions are the same circumference. As the point in the s plane moves from $\omega \to 0$ to $\omega \to \infty$, its corresponding value in the z plane travels along the circumference starting from the origin in the s and z plane and ends in the origin as well. The circumference is traveled several times, one time for each resonant frequency. It is worth mentioning that the resonant controller is the type of functions called proper functions [40], which means that the denominator of the transfer function has one order greater than the denominator, which implies that the locus of the Nyquist plot of the transfer function will end up in the origin when $\omega \to \infty$ always.

If the delay compensation is included, the center of the circumference is different for each resonant controller when they are plotted independently, however, the radius is the same. This can be seen in Figure 3.3:

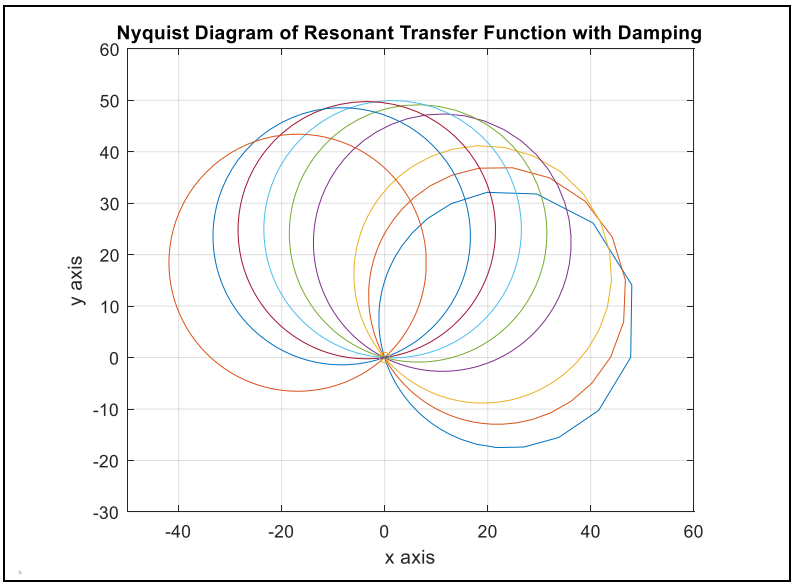

Figure 3.3: Nyquist plot of resonant controllers 6p+/-1 for p=1…4 with delay compensation included, same harmonic gains

With different gains, the resonant controllers will become circumferences of different radius and they would look like Figure 3.4.

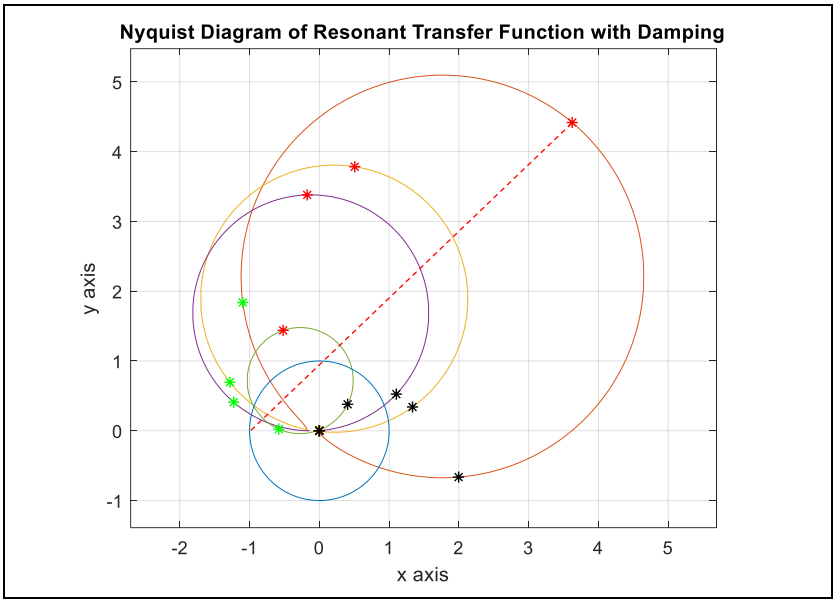

Figure 3.4: Nyquist plot of resonant controllers 6p+/-1 with delay compensation included and different harmonic gains

The asterisks that are included in Figure 3.4 represent the harmonic resonant frequency $h\omega_1$ (red) and their upper and lower typical limits $0.95h\omega_1$ (green) and $1.05h\omega_1$ (black). The blue circle is the unit circle. This is mentioned to show that most of the circumference of the resonant controller is formed essentially by the frequencies around the harmonic frequency. This is an interesting property that can be exploited.

In the case of the voltage controller of an inverter with an LCL filter, with a hysteresis current controller approximated as a first-order filter when a resonant controller with delay compensation is used, the locus of the open loop transfer function is shown in Figure 3.5, In this case the orange circle is the unit circle.

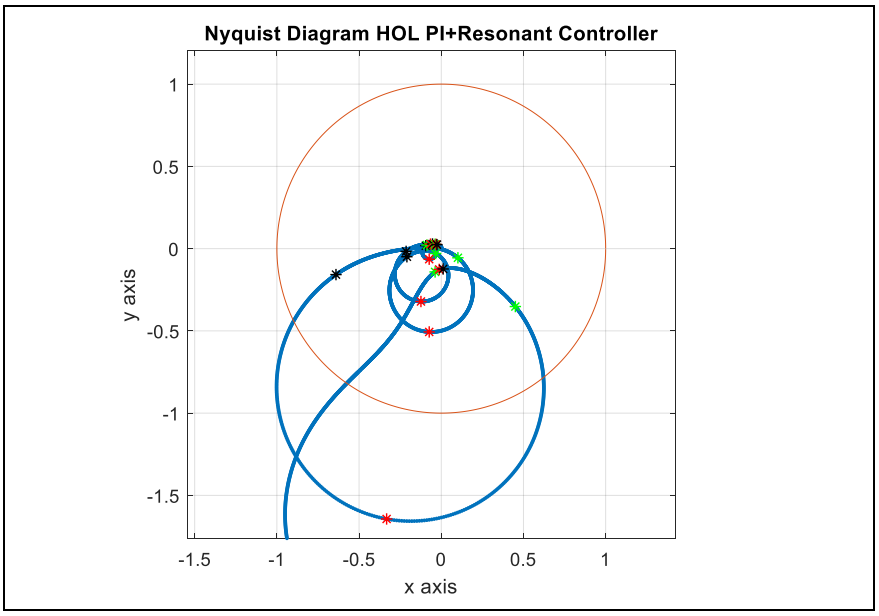

Figure 3.5: Nyquist plot of open loop transfer function of a voltage controller of an LCL filter, with resonant controllers for several harmonics

Something that can be concluded comparing Figures 3.3, 3.4 and 3.5 is that the resonant controllers dominate other terms in the open loop transfer function. As already mentioned, this is an important feature that can be exploited to find a suitable delay compensation angle.

Another interesting aspect is that the resonant controller locus of lowest order harmonic frequency, 5th harmonic in this case, encircles the part of the open loop transfer function locus influenced by the higher order resonant controllers. In this sense, the radii formed by H_{OL} at frequencies close to the higher order harmonic frequencies become smaller when frequency increases. This situation might be the result of adding all resonant controllers. This is a new characteristic that appears here, and it can be used. This means that the H_{OL} approaches the instability point at frequencies close to the lowest harmonic frequency.

Since the resonant controllers seem to influence each other, the gain of each of them contributes to the overall stability. This cannot be concluded looking at Bode plots. Typically, the most practical way of tuning resonant controllers has been to set the same gain to all of them. But the truth is that not all harmonic currents or voltages have the same contribution to the overall THD, and the harmonic values are normally a fraction of the fundamental value.

If all the gains are considered the same, the relative gain of each resonant controller with respect to the current that this is trying to control or to eliminate would be very high for the harmonic terms. This reasoning coincides with the one mentioned in [42] mentioned that it could be a good idea to tune the harmonic gains proportionally to its percentage of THD to minimize the total error convergence rate or inverse proportional to the corresponding harmonic frequency.

Therefore, to reach absolute stability of the open loop it is a good idea to focus in the resonant controller of lower harmonic frequency first and then in the higher order ones, reducing their harmonic gains, to get a stable solution.

As in the case of the analysis done by [13] and summarized in Section 2.19, it is necessary to identify the minimum distance between the instability point and the open transfer function including the resonant controller. The gain margin is not analyzed at this moment, it will be done in Section 4.

Thus, a generalization of the open loop transfer with one resonant controller, the lowest order one, could be done for an open loop transfer function as shown in Figure 3.6:

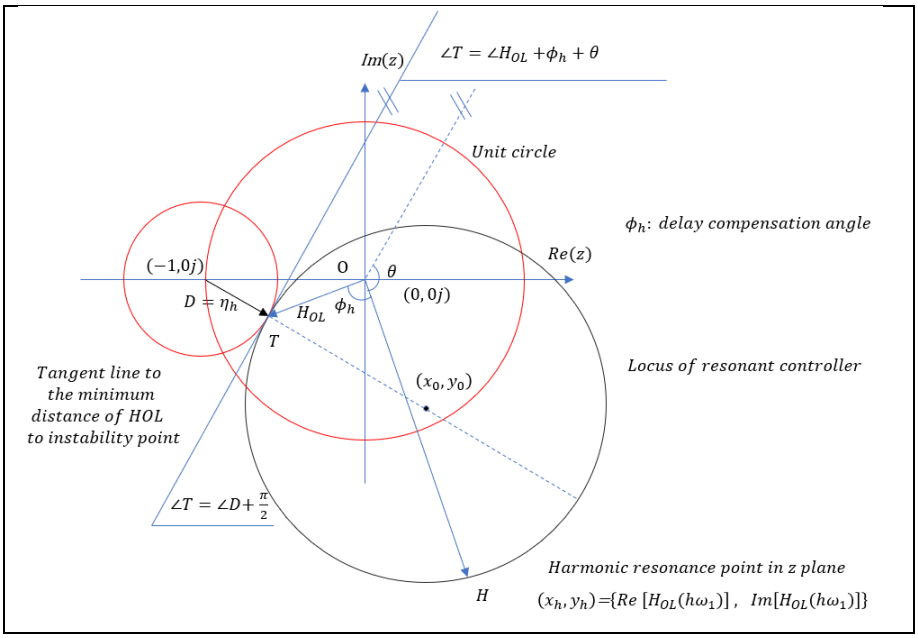

Figure 3.6: Optimum asymptote to maximize $D(z)$ for one generic harmonic h in the z plane at frequencies around $h\omega_1$ for resonant controllers with damping term

The tangent point T is an excellent place to find a suitable relationship that can relate the delay compensation angle ϕ_h, $\angle H_{OL}$, and $\angle$D angle.

The angle of the tangent line with the x-axis $\angle$T at the resonant controller locus can be obtained by using trigonometry in several ways. The first way is to identify the angle of the vector D, i.e. $\angle$D, as seen in the picture and its relationship with $\angle$T.

The tangent point T is at a frequency that it is at the vicinity of $h\omega_1$ and the harmonic resonant frequency is at H. ϕ_h could be the delay compensation necessary to reach the resonant frequency point H. θ is the angle necessary to shift the open loop vector H to become parallel to the tangent line T.

In a similar way as proposed for the resonant controllers without damping in [13], in this case, the angle of the tangent line is, as shown in Figures 2.35 and 3.7, the following:

$$\angle \mathrm{T} = \angle \mathrm{D} + \frac{\pi}{2} = \angle H_{OL} + \phi_h + \theta \tag{102}$$

With these relationships, a value for the delay compensation can be obtained:

$$\phi_h = -\angle H_{OL} + \angle \mathrm{D} + \frac{\pi}{2} - \theta \tag{103}$$

The variable θ is dependent on all the other factors involved in the open loop transfer function. However, it should not be as large as π .This will vary among the resonant controllers when used together. The delay compensation proposed with a value of $\theta = \frac{3\pi}{4}$ is given by equation 104:

$$\phi_h = -\angle H_{OL} + \angle \mathrm{D} - \frac{\pi}{4} \tag{104}$$

When the relative damping factor ζ is very small, the angle θ may become zero, the radius of the resonant controller locus becomes very large and the delay compensation angle becomes very similar to the angle proposed in [13]. The radius continues increasing and

when $\zeta = 0$ there is an asymptote at $h\omega_1$ that jumps from one extreme of the plot to the other at the resonant frequency, as in the Figure 2.34.

An approximation to that case is provided in Figure 3.7.

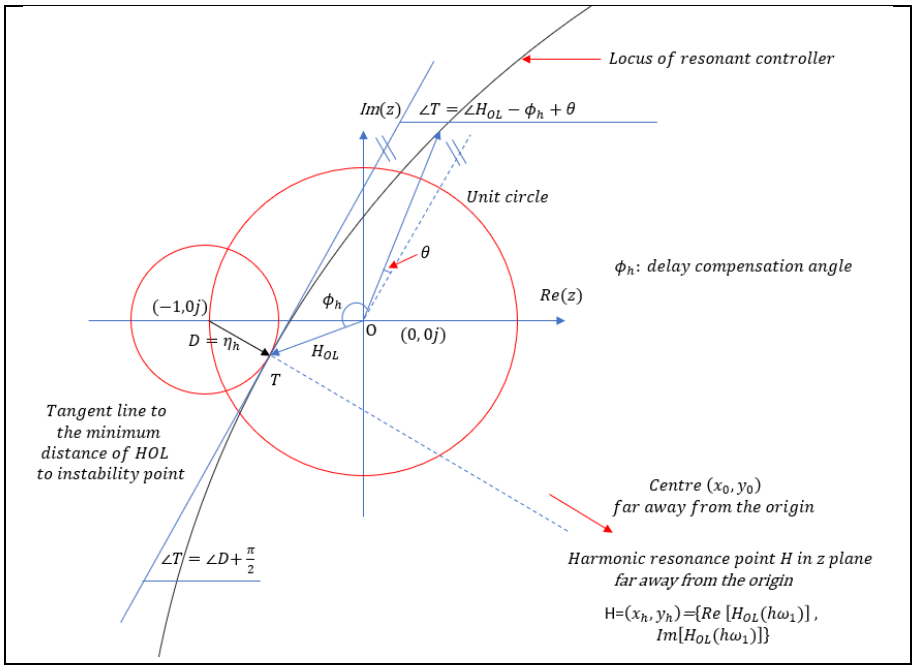

Figure 3.7: Resonant controller locus when the damping factor ζ becomes very small

In that case, the delay compensation would be:

$$\phi_h = -\angle H_{OL} + \angle \mathrm{D} + \frac{\pi}{2} \tag{105}$$

There is no need to propose an exact formula for ϕ_h since this can be obtained using the actual open loop transfer function with any commercial software such as Matlab for any specific case, and also the z transfer function of the open loop transfer function with any discretization method is too complex even for small control loop systems. It is also not necessary to set $\eta_P = \eta_h$ as proposed in [13], since the loci of the resonant transfer function of each harmonic interact among them when damping is included and only locus of the open loop transfer function around the lowest harmonic frequency considered is prevalent. Thus, analysing the lowest order harmonic, a relationship can be established for the rest of controllers.

Considering that θ could vary between 0 and a value less than π, in some cases ϕ_h could become equal to the one proposed in [13]. In that sense, the delay compensation proposed could be regarded as a generalization of the formula provided in [13].

4 Active Front End Converter Control System Design

4.1 Typical Design

The cascade control system of an AFE can contain controllers of different types depending on the performance desired on each specific stage. An example of the inner control loops of an AFE is shown below:

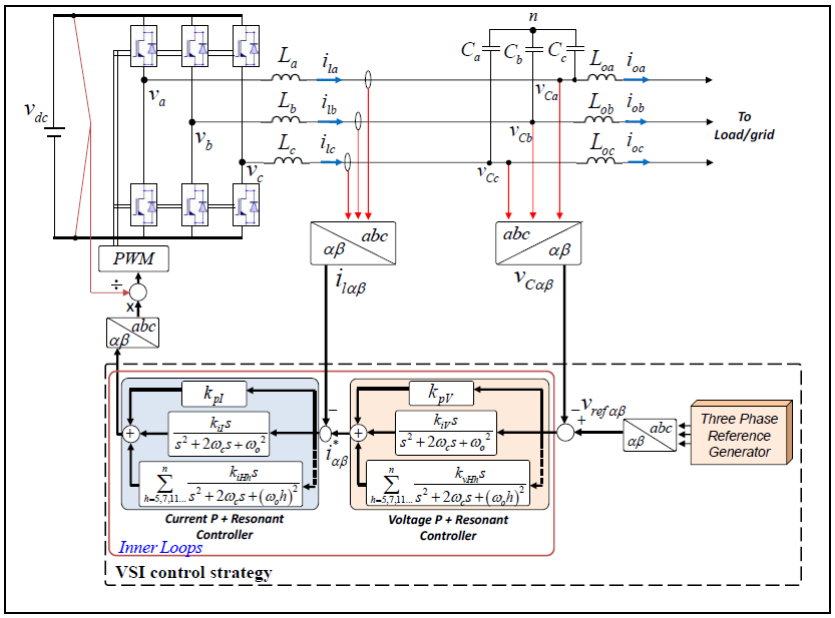

Figure 4.1: Current and voltage control loops of a VSI.[41]

In an AFE is possible to implement several functionalities, such as unbalanced compensation, droop control of active and reactive power, harmonic compensation, virtual impedance control, synthetic inertia, etc. A proposal of control implementation [41] is shown below:

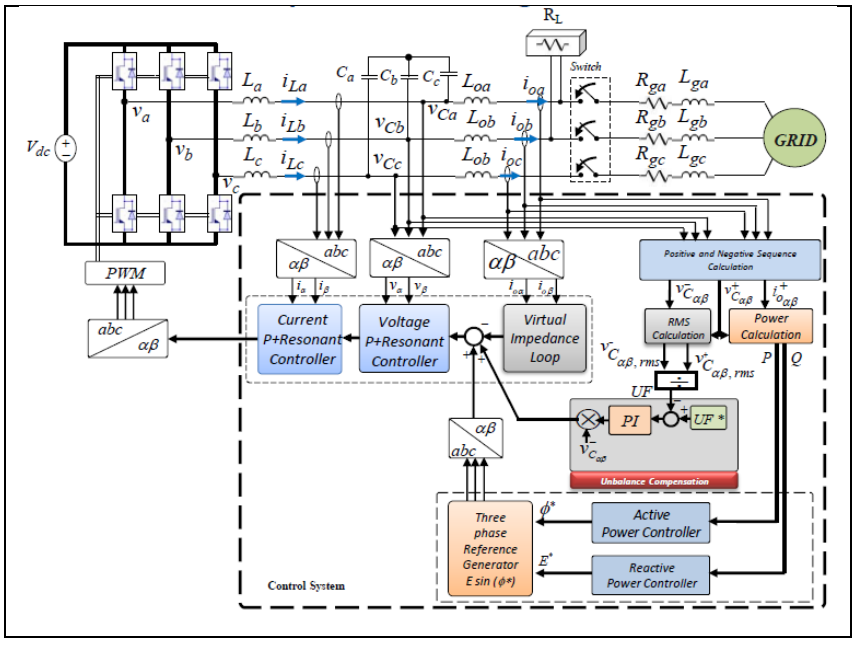

Figure 4.2: Block diagram of the closed control loop of a voltage source inverter. [41]

4.2 LCL dimensioning

Considering the criteria explained in Chapter 2.5 regarding the design of the filter, the capacitor and inductor components of the LCL filter has been selected.

$$C = 0.1\frac{P_N}{\omega_1 {V_g}^2} = 0.1\frac{1.79}{377 * 690^2} = 998.76 * 10^{-6} = 998.76\ \mu F$$

The power in MW, the angular frequency in rad/s and the voltage in V. A value of $990\ \mu F$ was chosen.

$$L_1 = 0.05\frac{V_N}{\sqrt{3}I_N} = 0.05\frac{690}{\sqrt{3} * 1500} = 13.2\ mH$$

The voltage in V, the angular current in A.

The resonance frequency with these values would be:

$$f_{res} = \frac{1}{2\pi}\sqrt{\frac{L_1 + L_2}{L_1 L_2 C}} = \frac{1}{2\pi}\sqrt{\frac{2L_1 + L_g}{L_1(L_1 + L_g)C}} = \frac{1}{2\pi}\sqrt{\frac{2 * 13.2 + 53}{13.2(13.2 + 53)990}} = 897\ Hz$$

$$K_{res} = \frac{f_{res}}{f_s} = \frac{1503.5}{3000} \approx 0.5$$

This value is not the recommended range [0.2, 0.4]. A value of $L_1 = 41.5\ mH$ meet the requirements of average switching frequency of 3 kHz in the inverter, obtaining a $K_{res} = 897/3000 \approx 0.3$, in the expected range.

The variation of the grid impedance has an impact in the resonance frequency, although in this case is not critical. Doubling the grid impedance, which means that the grid has become weaker, only varies the resonant frequency from 897 to 888 Hz. This is not a critical situation. The design seems reasonable and other detailed studies can be conducted to optimize the solution.

4.3 General description of the control loops implemented

The simplified inner current control loop and voltage control loop developed is shown in Figure 4.3:

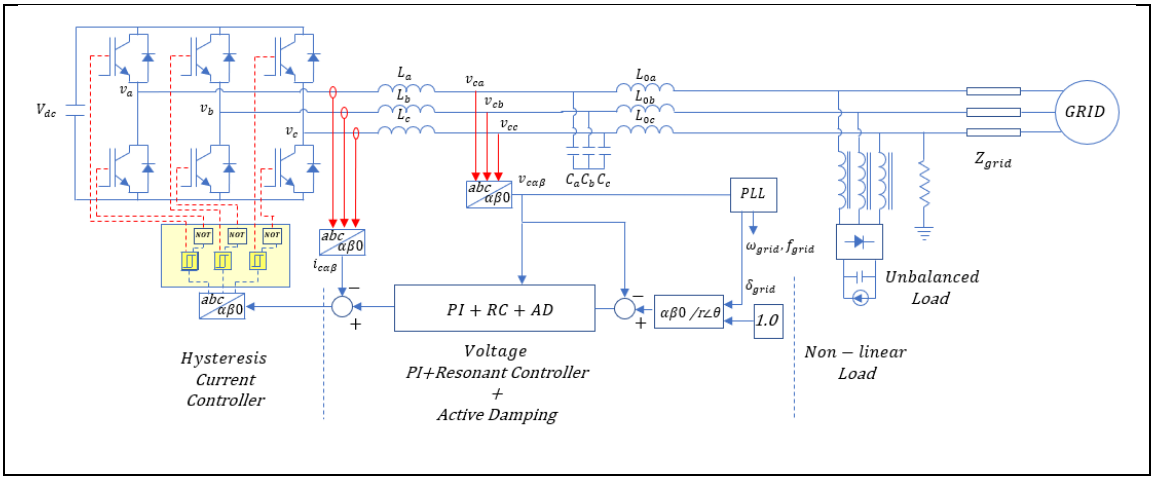

Figure 4.3: General Power and Control Circuit of the closed-loop voltage source inverter

The voltage closed-loop control system has the main goal of control the capacitor voltage. This is done taking the grid voltage angle δ_{grid} with a voltage reference of 1.0 p.u. The inner control loop is a hysteresis controller and uses the output of the voltage controller as reference current. The feedback in this case is the inverter current. The hysteresis controller provides as output, gates signals to the inverter switches.

As part of the voltage controller, a PI controller, resonant controllers and active damping control has been implemented. A connection to the grid with a non-linear load and an unbalanced load has been considered.

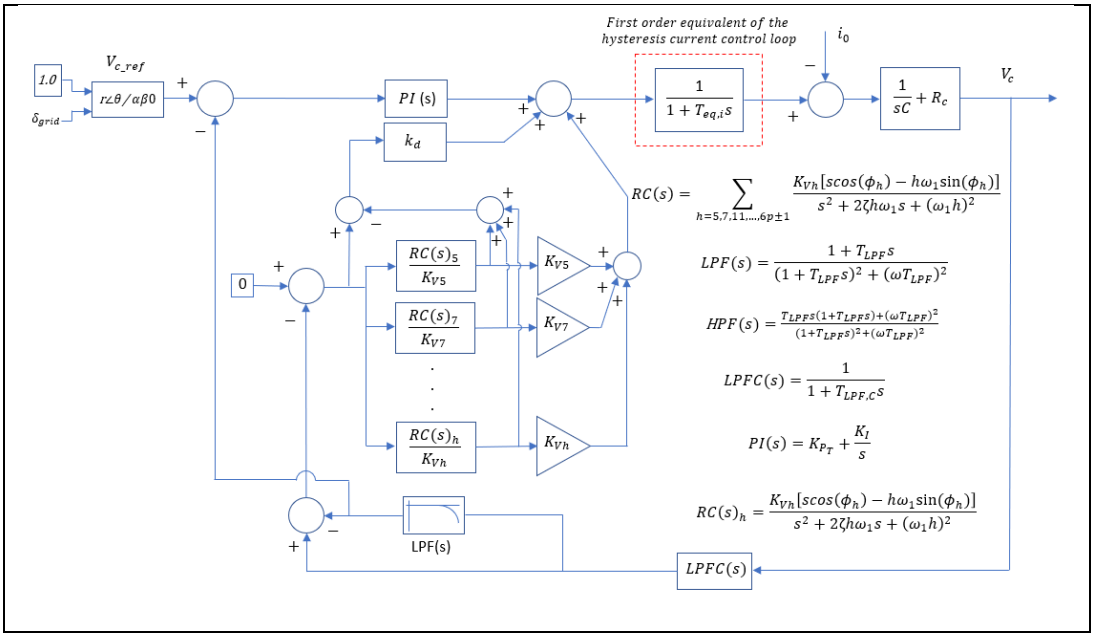

Figure 4.4: Voltage control loop with PI controller, Resonant Controller including delay compensation, active damping, voltage capacitor filter and first order equivalent current control loop

As shown in Figure 4.4, in order to do an analysis of the voltage control loop considering the impact of the current control loop as well, a first-order equivalent transfer function of the hysteresis current control loop has been done. Since the hysteresis controller itself is a non-linear controller, the equivalent first order transfer function is just an approximation.

The plant model of the first order equivalent control loop in this case is:

$$G_{PL}(z) = Z\left\{L^{-1}\left[\frac{1-e^{-sT_s}}{s}G_{PL}(s)\right]\right\}$$

$$G_{PL}(z) = Z\left\{L^{-1}\left[\frac{1-e^{-sT_s}}{s}\frac{1}{1+T_{eq,i}s}\right]\right\}$$

$$AB(z) = (1-z^{-1})Z\left\{L^{-1}\left[\frac{1}{s}-\frac{1}{(1/T_{eq,i}+s)}\right]\right\}$$

$$AB(z) = (1-z^{-1})Z\left\{L^{-1}\left[\frac{1}{s}-\frac{1}{\left(\frac{1}{T_{eq,i}}+s\right)}\right]\right\}$$

$$AB(z) = (1 - z^{-1})\left(\frac{1}{1 - z^{-1}} - \frac{1}{1 - e^{-\frac{T_s}{T_{eq,i}}}z^{-1}}\right)$$

The sample and hold circuit is applied to the capacitor model as well. In this case:

$$G_{PL}(z) = Z\left\{L^{-1}\left[\frac{1 - e^{-sT_s}}{s}G_{PL}(s)\right]\right\}$$

$$G_{PL}(z) = Z\left\{L^{-1}\left[\frac{1 - e^{-sT_s}}{s}\frac{1}{sC}\right]\right\}$$

$$G_{PL}(z) = \frac{(1 - z^{-1})}{C}Z\left\{L^{-1}\left(\frac{1}{s^2}\right)\right\}$$

$$G_{PL}(z) = \frac{(1 - z^{-1})}{C}\frac{T_s z^{-1}}{(1 - z^{-1})^2}$$

$$G_{PL}(z) = \frac{1}{C}\frac{T_s z^{-1}}{(1 - z^{-1})}$$

As mentioned in [21], the resonant controllers appear as a solution to track sinusoidal references with zero error. However, resonant controllers implemented in the stationary reference frame cannot eliminate the DC offset. To solve this problem, a combination of the best attributes of the PI controller and resonant controllers have been used. It is expected some steady state error because the fundamental frequency is not controlled with a resonant controller, but the error obtained can be adjusted modifying slightly the K_{P_T} value.

Another possibility is to include an integral controller (I) and a P+R controller for fundamental frequency and harmonics frequencies.

A zero-voltage reference has been included for the resonant controllers and active damping, such that the control system can force the harmonic voltages and high frequency voltages to become zero up to the extent possible. To minimize the interference of the active damping with the resonant controller and to facilitate the tuning of both controllers, the harmonic currents before the resonant gain are subtracted from the error signal, before to be applied to the active damping gain k_d. In this way the active damping only works with the high frequency harmonics and the resonant controllers work with the low-order harmonics.

The low pass filter implemented in the capacitor feedback loop is necessary to avoid feeding the controller with very high frequency signals that can be regarded as noise and that can be amplified, affecting the performance of the controller. A time constant of $50\,\mu s$ has been used for this purpose.

The separation of the fundamental frequency voltage and the harmonic frequency voltages is done using a low pass filter in the dq frame. The details are shown in Figure 4.11 and it will be explained later.

A simplification of the voltage control loop is necessary to analyze its open loop transfer function. Using the classical block diagram reduction properties [22], the simplified equivalent model is shown in Figure 4.5.

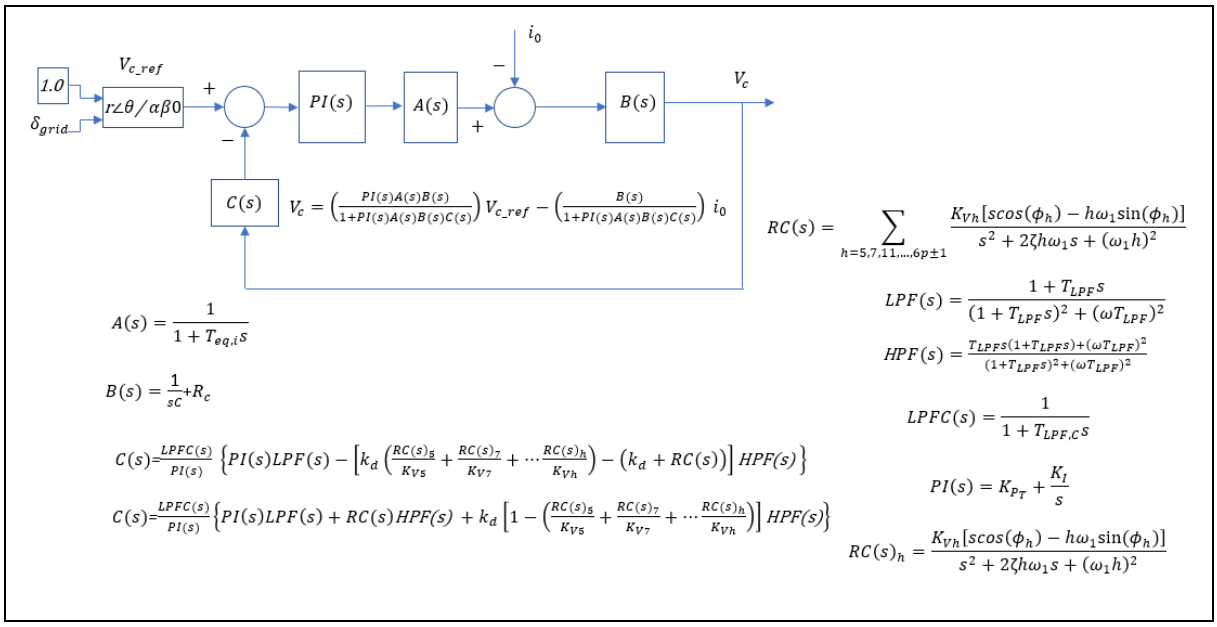

Figure 4.5: Simplified equivalent model of the voltage control loop.

Looking at the $C(s)$ expression, the PI controller is restricted to act for low frequencies by the direct multiplication $PI(s)LPF(s)$ and the resonant controllers and active damping are restricted to act only for high and very high frequencies. A small reorganization of the $C(s)$ term is shown in equation 106:

$$C(s)=\frac{LPFC(s)}{PI(s)}\left\{PI(s)LPF(s) + RC(s)HPF(s) + k_d\left[1 - \left(\frac{RC(s)_5}{K_{V5}} + \frac{RC(s)_7}{K_{V7}} + \cdots\frac{RC(s)_h}{K_{Vh}}\right)\right]HPF(s)\right\} \quad (106)$$

The PI controller and the resonant controller are added, and the active damping is an additional term that is working only for high frequencies. In this sense, with the exception of the active damping term and the low and high pass filters, the control loop is equivalent of control loop shown in the Figure 4.1 and proposed in [41]

The resonant controller normally is accompanied by a proportional gain. However, in this implementation, the proportional gain related to the PI controller and the resonant controllers have been grouped as one single K_{P_T} value to facilitate the tuning process, which will be explained in detail in Section 4.5.

4.4 Detailed implementation in Simulink

4.4.1 Synchronization Circuit

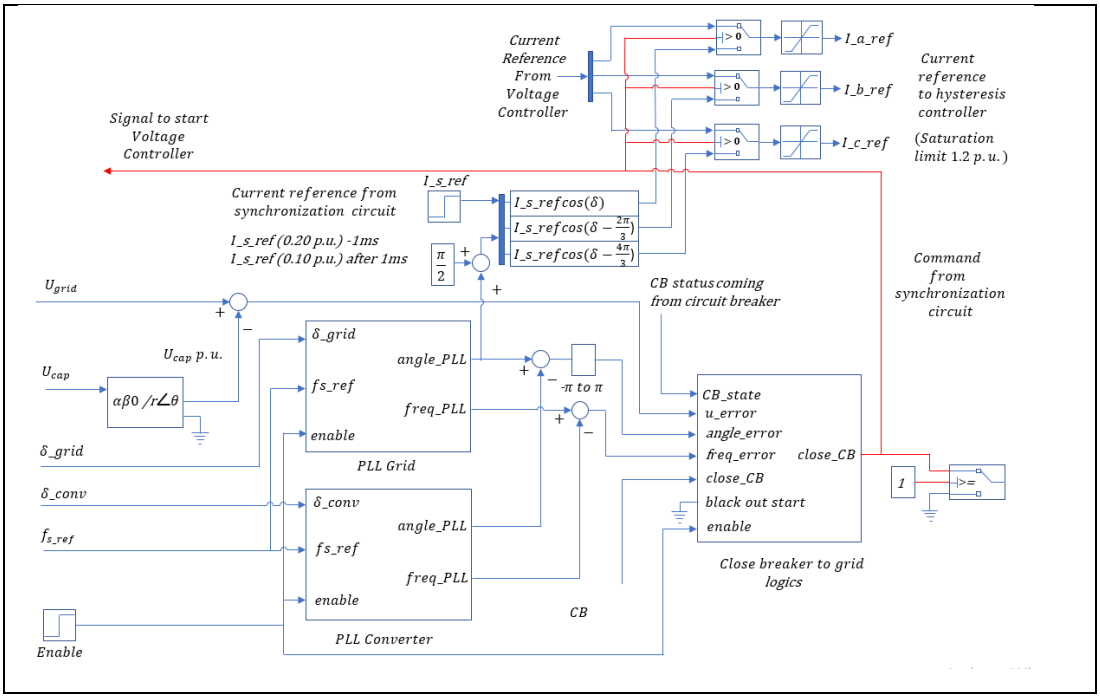

Figure 4.6: Implementation of the synchronization scheme in Simulink.

The synchronization circuit implementation is shown in Figure 4.6. Two PLLs are necessary to measure the grid angle (δ_grid_PLL) and the converter angle (δ_conv_PLL). A logic implemented helps to decide when to generate the signal to close the breaker.

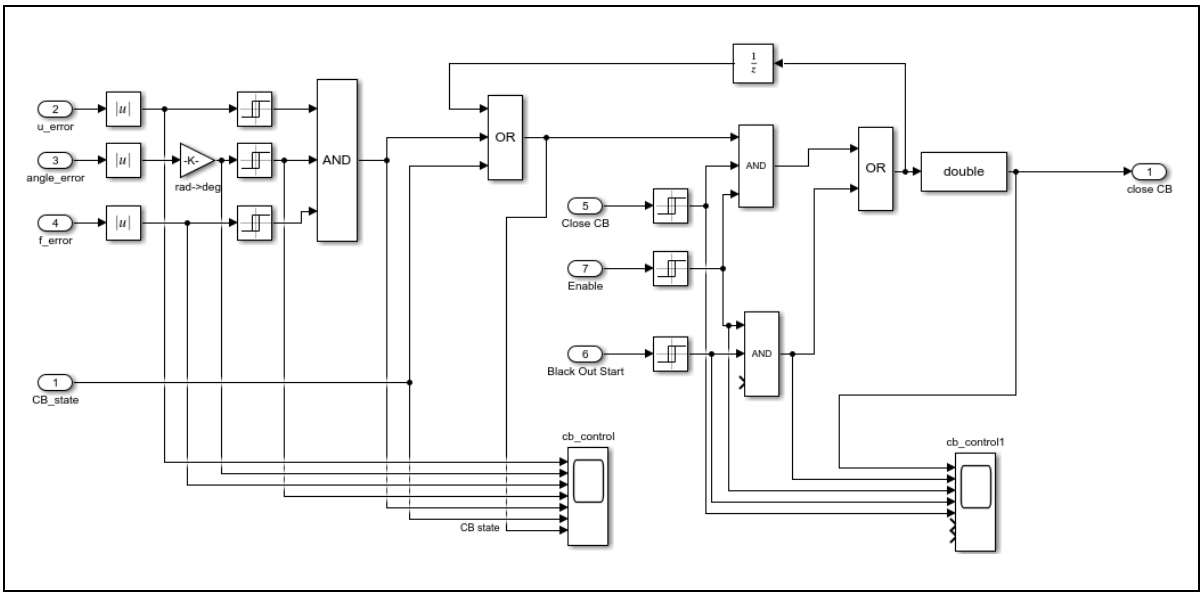

Figure 4.7: Implementation of the synchronization logic in Simulink. It uses voltage, angle and frequency difference.

4.4.2 Non-linear and unbalanced load

The non-linear load was a truster drive of 800 kW, whose nonlinear currents have the following waveform at the start of its operation as shown in Figure 4.8.

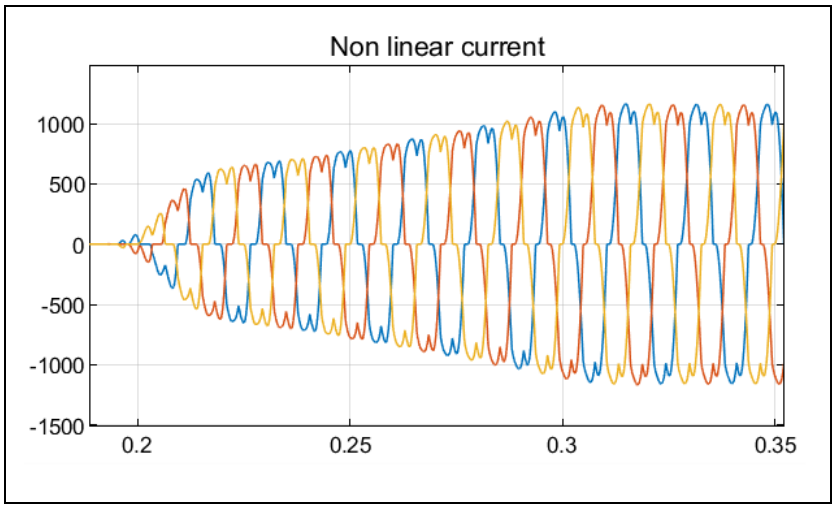

Figure 4.8: Three-phase non-linear load waveform (time in s and current in A)

4.4.3 Hysteresis controller

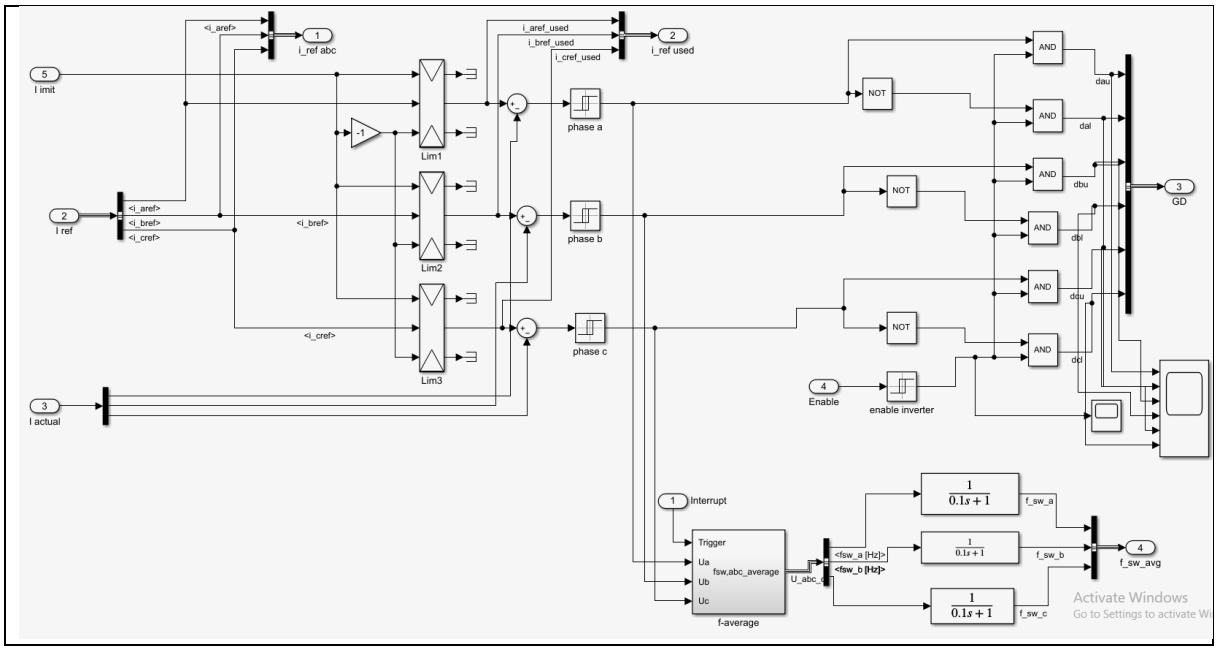

Figure 4.9: Hysteresis controller for stationary frame implemented in Simulink

The hysteresis controller takes the current references provided by the voltage controller and convert them into gate signals. An additional routine has been implemented to obtain the average switching frequency of the hysteresis controller. A 0.10 p.u. hysteresis bandwidth represents an average switching frequency of 3 kHz.

4.4.4 Resonant Controller with and without Active Damping

Four different implementations of the resonant controllers considering the same control strategy have been simulated and evaluated to assess the impact of damping, delay compensation, z transform and delta operator. They are:

1. Resonant Controller without damping but including delay compensation
2. Resonant Controller with damping and without delay compensation, with z transform
3. Resonant Controller with damping and without delay compensation, implemented using a delta operator

4. Resonant Controller with damping and delay compensation, implemented using a delta operator

The detailed implementations are explained below:

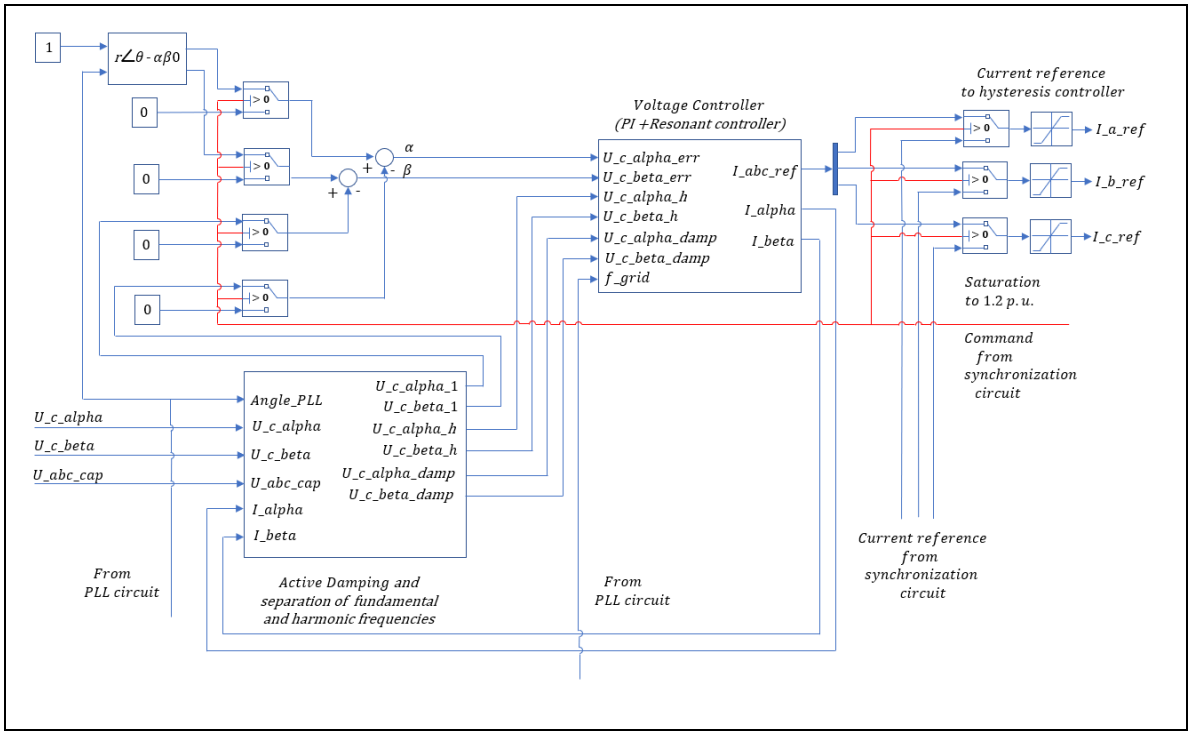

Figure 4.10: Discrete implementation of PI+R voltage controller and active damping.

The current reference sent to the hysteresis controller has a saturation limit of 1.2 p.u. to protect the equipment of unexpected current peaks. The frequency of the grid and the capacitor voltage angle are necessary signals for theses controllers. In the case of the separation of the fundamental and harmonic components of the capacitor voltage, a low pass filter in the dq frame is necessary and to do that transformation, the capacitor voltage angle is needed, while in the case of the PI and resonant controllers that use the Tustin prewarped transformation ω (and therefore f_{grid}) is necessary.

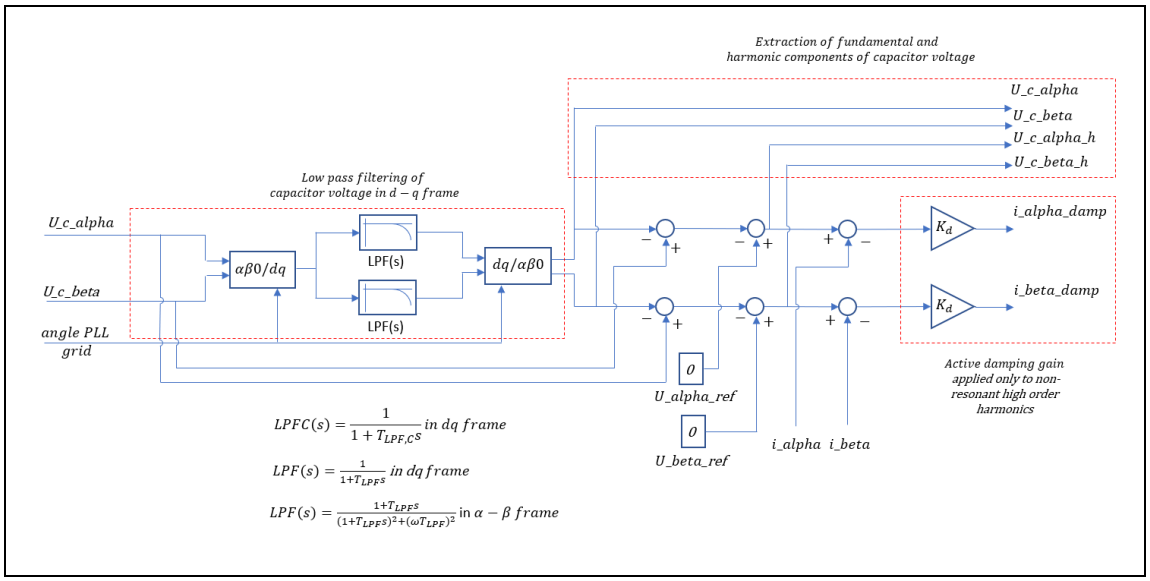

Figure 4.11: Active damping modelling and harmonic separation implemented based on [38].

The active damping implementation and the separation of fundamental and harmonic voltages has been done as shown in Figure 4.11. The low pass filtering is done in the dq frame and then transformed into the $\alpha\beta$ frame as explained in Chapter 2.8. The extraction of the higher order harmonics that are not handled by the resonant controllers and the high frequency noise is done before the active damping gain k_d is applied.

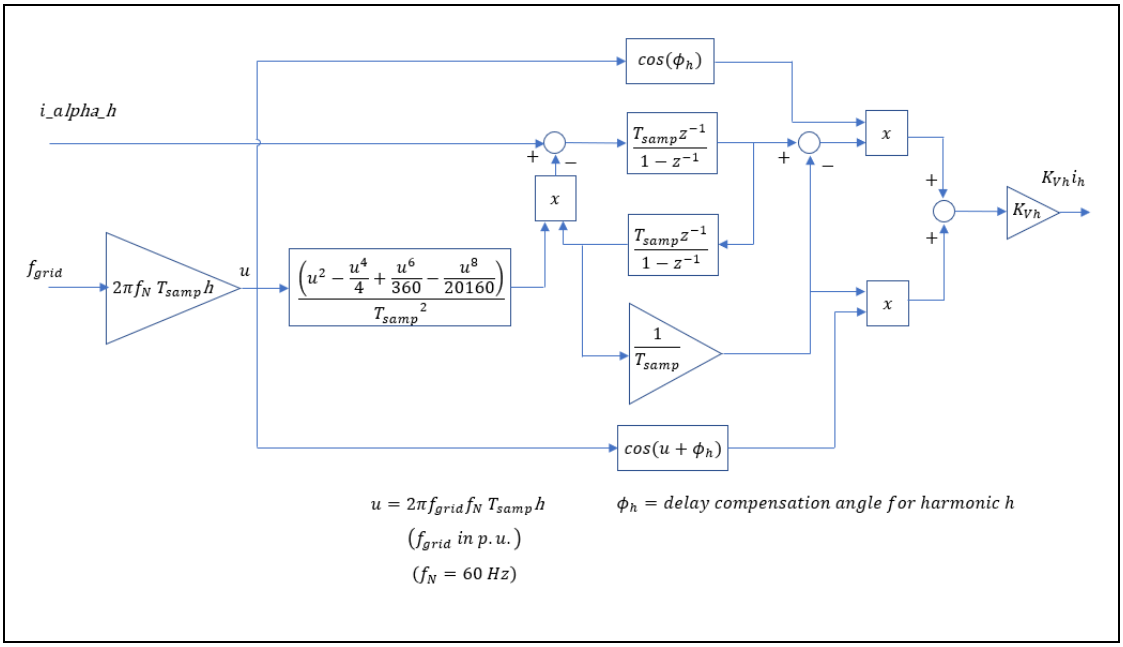

Figure 4.12: Resonant controller without damping and considering delay compensation implemented with two integrators modelled in Simulink, according to [21].

The discrete version of the resonant controller without damping and with delay compensation for a one specific harmonic is shown in Figure 4.12, as suggested in [21]. Four terms of the Taylor expansion of $\cos(h\omega_1 T_{samp}) = \cos(2\pi f_{grid} f_N T_{samp} h)$ were included to reduce the error by the Taylor approximation.

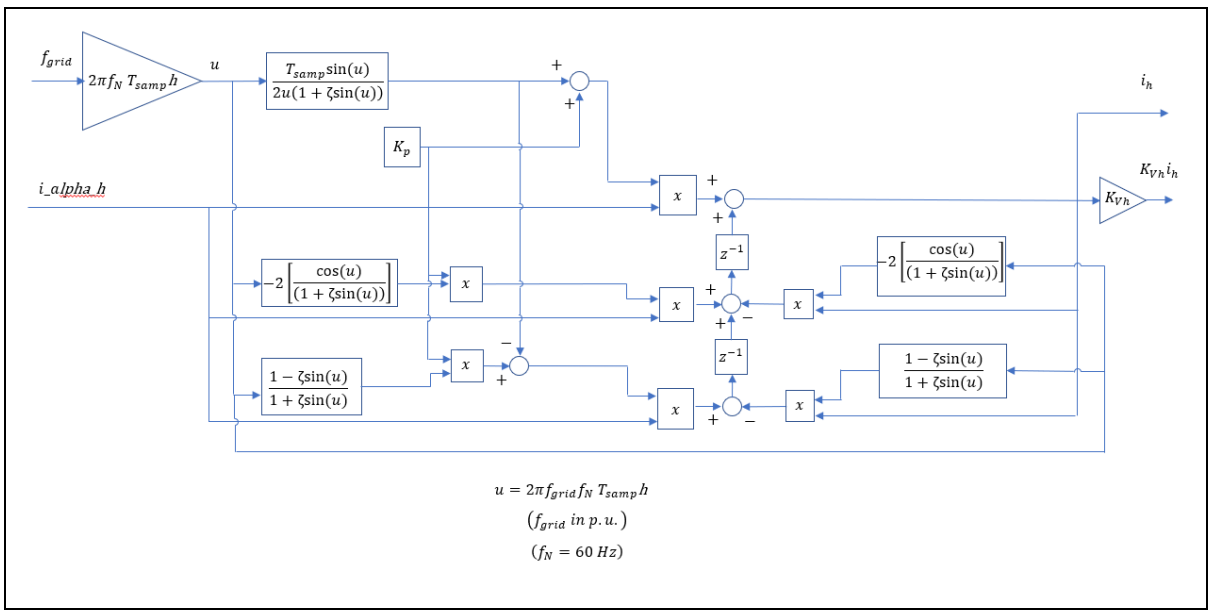

Figure 4.13: Resonant controller with damping discretized in a zeta realization implemented in Simulink, according to [32]

The discrete version of the resonant controller with damping without delay compensation represented as an IIR-DFIIt, is shown in Figure 4.12 and the same resonant controller

but using a delta realization is shown in Figure 4.13. For this last implementation, a value of $\Delta = T_{samp}$ has been used for the simulation. The harmonic current i_h is extracted before the gain K_{Vh} is applied to be used in the active damping scheme is shown in the right upper side of the Figure 4.14.

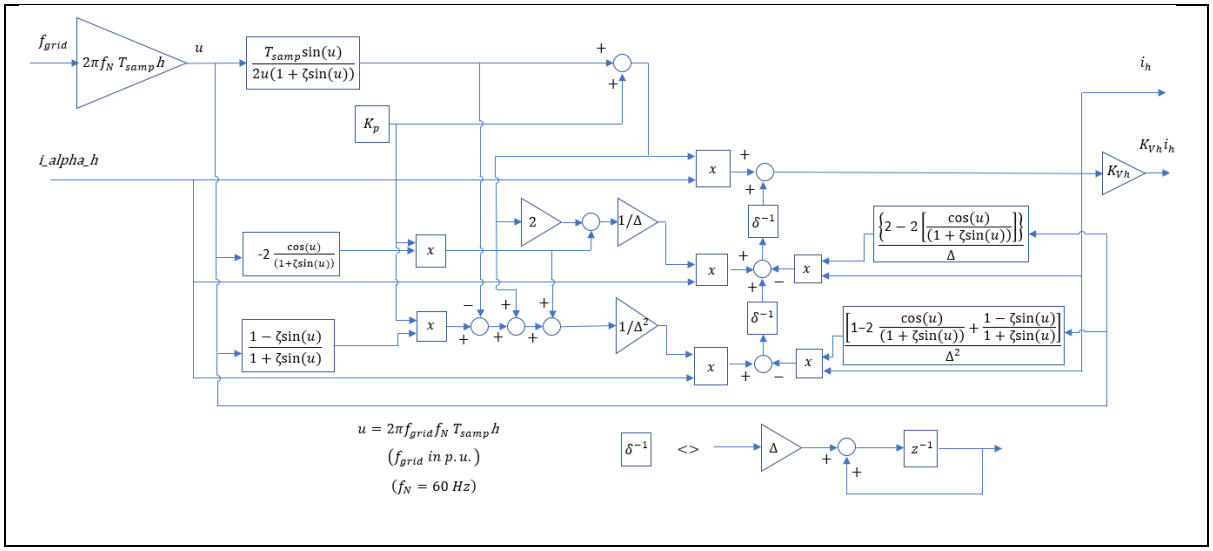

Figure 4.14: Resonant controller with damping discretized in a delta realization implemented in Simulink, according to [31] and [32].

The most complete implementation of the resonant controller with damping, with delay compensation implemented in a delta realization is shown in Figure 4.15.

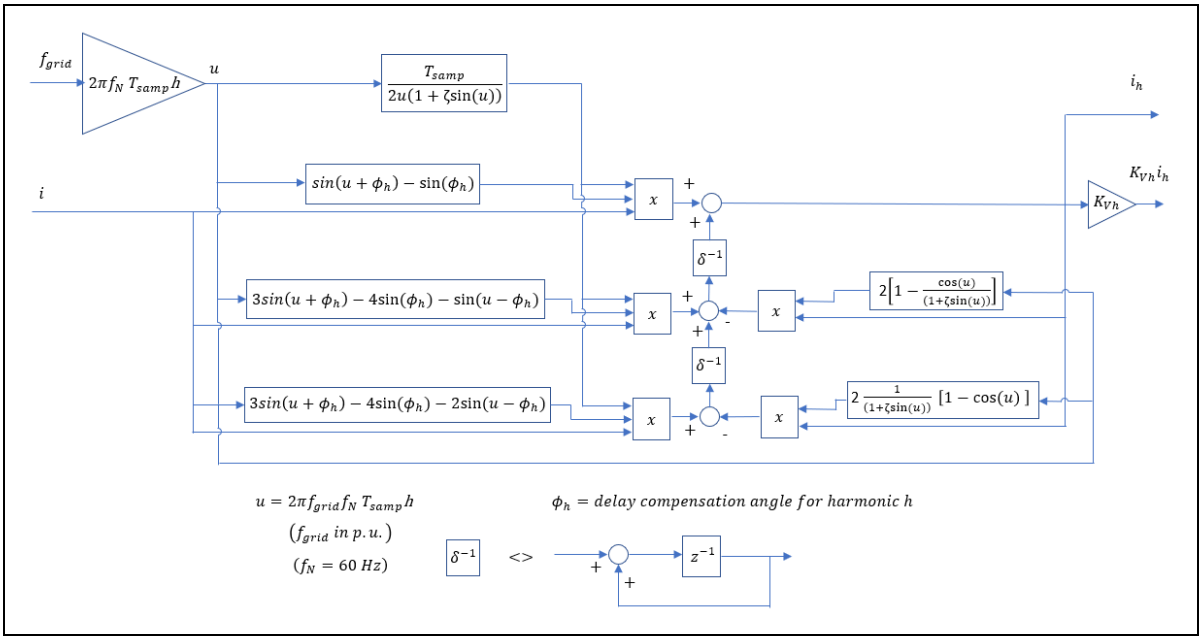

Figure 4.15: Resonant controller with damping and with delay compensation discretized in a delta realization implemented in Simulink, according to [30].

4.5 Voltage Controller Tuning for stable operation

4.5.1 Tuning methodology proposed

Several variables are involved in the stability of the control loop. These are:

- Integral gain K_I

- Active damping gain k_d
- Damping factor in resonant controller ζ
- Harmonic gain in resonant controller K_{V_h}
- Proportional gain K_{P_T}
- Crossover frequency ω_{cr}
- Switching frequency f_{sw} or average switching frequency f_{sw_avg} in the case of a hysteresis controller

Each variable is possible to be changed in a limited range.

Therefore, an iterative process must be applied to obtain the proper tuning. Some of the variables such as the damping factor and the crossover frequency can be somewhat pre-stablished, but the rest of variables must be obtained checking whether the control loop is stable or not. A tuning methodology is proposed and translated into a chart, which is shown in Figure 4.16 below:

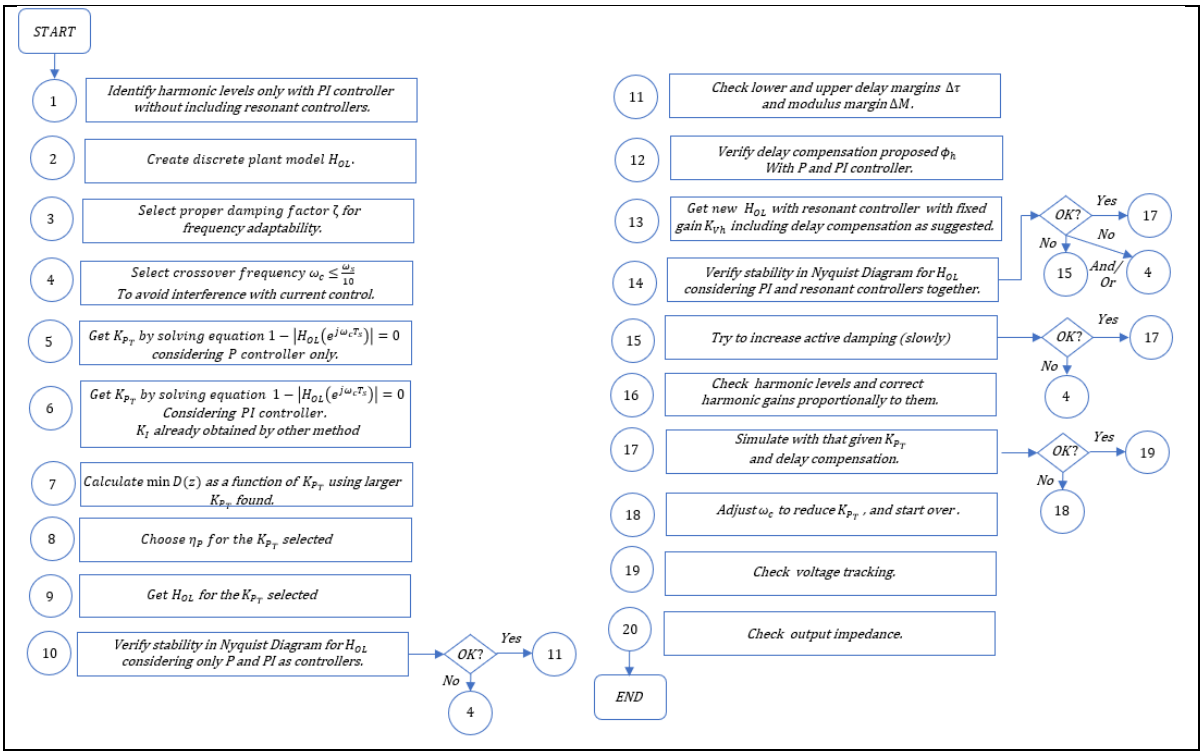

Figure 4.16: Proposed tuning methodology flow chart for a voltage controller with PI+R controllers and active damping.

Therefore, to start this discussion, a pre-analysis has been done to find a suitable stable solution that can help explain the main characteristics of the methodology and later in Section 6 the influence of the variation of the most important parameters is assessed to understand how this affect stability.

Some of the variables have already been pre-defined as design criteria, and they are the starting point of the tuning process. In this case:

- Following the established practices, a resonant damping factor of $\zeta = 0.02$ is considered, to allow frequency adaptability of the resonant controller in a range of $\Delta f = \frac{2\zeta\omega_0}{2\pi} = 2.4\ Hz$
- The integral gain has been obtained by other methods and is not discussed here. For all the cases, $K_I = 85$ has been used.

- The active damping gain has been chosen $k_d = 1$. This is a usual choice according to several references [1, 10].
- Arbitrary harmonic gain K_{Vh} in the resonant controller are chosen, but just at a starting point. They will be adjusted to make the system stable if necessary. Only requisite is that it should be high enough to have good dynamic performance and low enough to keep the system stable.
- The crossover frequency ω_{cr} has an initial value of $\omega_{cr} = \frac{\omega_{sw}}{100} = \frac{2\pi f_{sw}}{100}$. It will be adjusted to get a K_{P_T} high enough to make the current controller follow the reference properly.

Therefore, the only variable that will be adjusted at the beginning will be the crossover frequency ω_{cr}. A value of K_{P_T} is obtained, as well as the recommended delay compensation angle ϕ_h for each harmonic frequency. Later, if no stable solution is found, the gains K_{Vh} are adjusted proportionally to THD in the load that is the harmonics source in this case. The converter itself also creates harmonics, but a starting point is necessary.

The K_{P_T} values obtained considering a P and PI controller are different in each case. However, the difference becomes less significant for larger values of K_{P_T}. The delay compensation angles obtained in each case are similar for both cases. The integral gain of the PI controller handles the fundamental frequency and for that reason the K_{P_T} value obtained considering the PI controller is the most reliable. For low K_{P_T} values calculated considering only the P controller, K_{P_T} becomes zero. Therefore, using the complete PI controller is the most accurate way for small values of K_{P_T}.

4.5.2 Controller tuning results considering damping and delay compensation

The key results of the tuning procedure for the design chosen are shown in Table 4.1.

k_d	K_{V_h}	K_{P_T}	ω_c (rad/s)	$\Delta\phi$ (degrees)	ΔG	ΔM	Delay compensation angle ϕ_h (rad)						
							5	7	11	13	17	19	23
1.0	9.5	1.1	189.82	33.14	5.36	0.46	1.09	1.55	2.06	2.22	2.47	2.57	2.75

Table 4.1: Tuning results following proposed methodology.

The graphical selection of all the parameters can be explained looking at Figures 4.17 and 4.18 shown below:

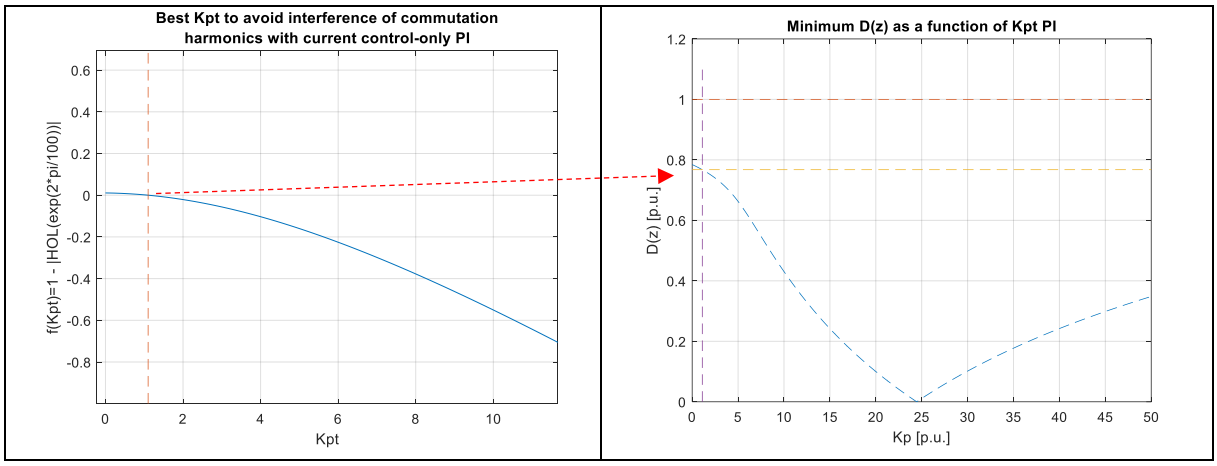

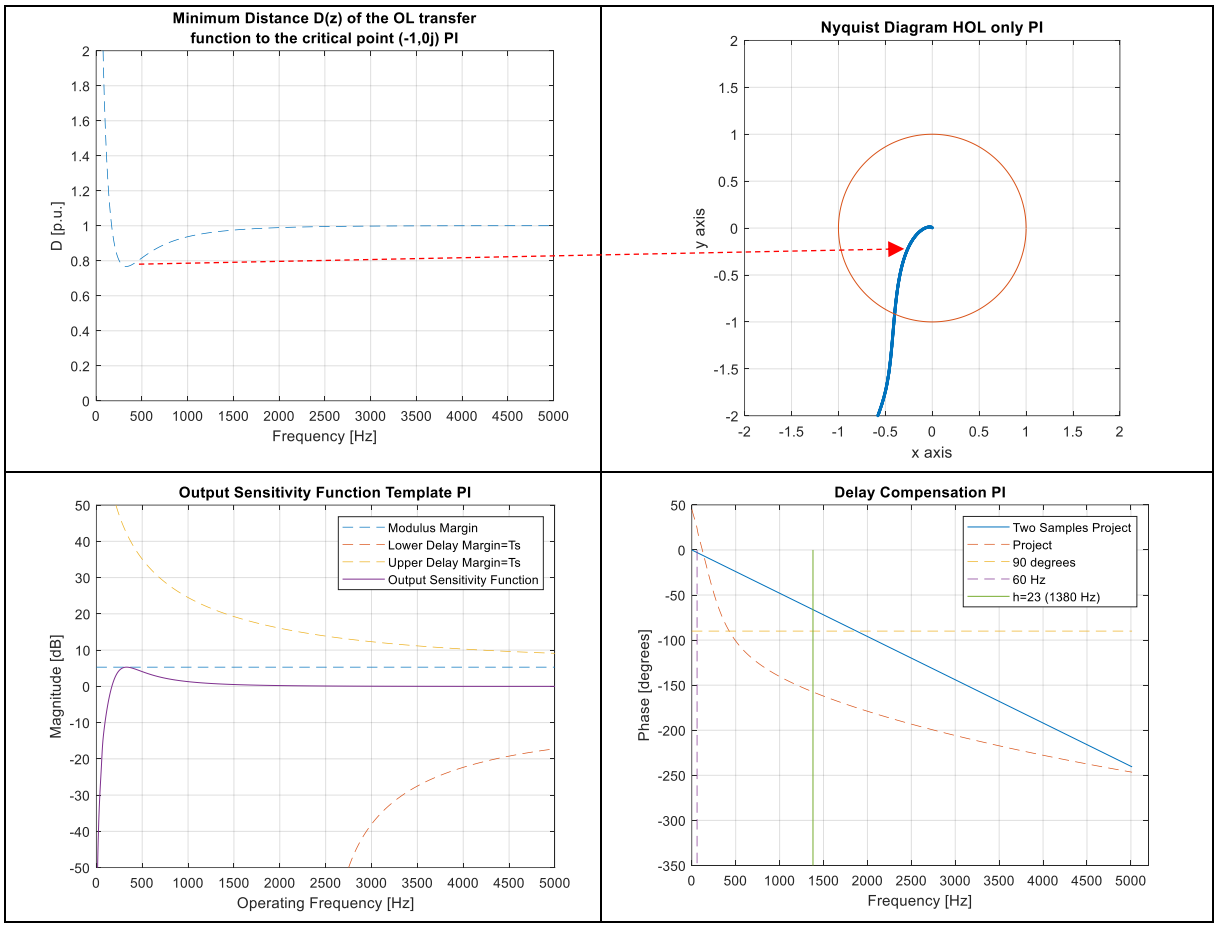

Figure 4.17: Graphical selection of key results of the tuning procedure only PI controller

Considering PI controller and resonant controllers, the basic change with respect to the previous case without resonant controllers is that with the resonant controllers the distance from the H_{OL} to the instability point becomes smaller. This makes sense, considering to what it was explained in Section 3.

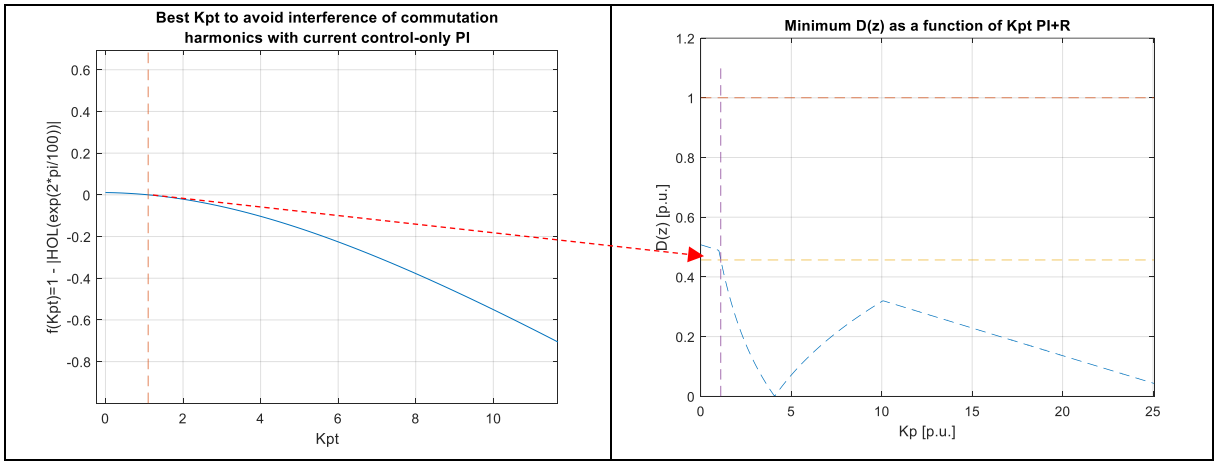

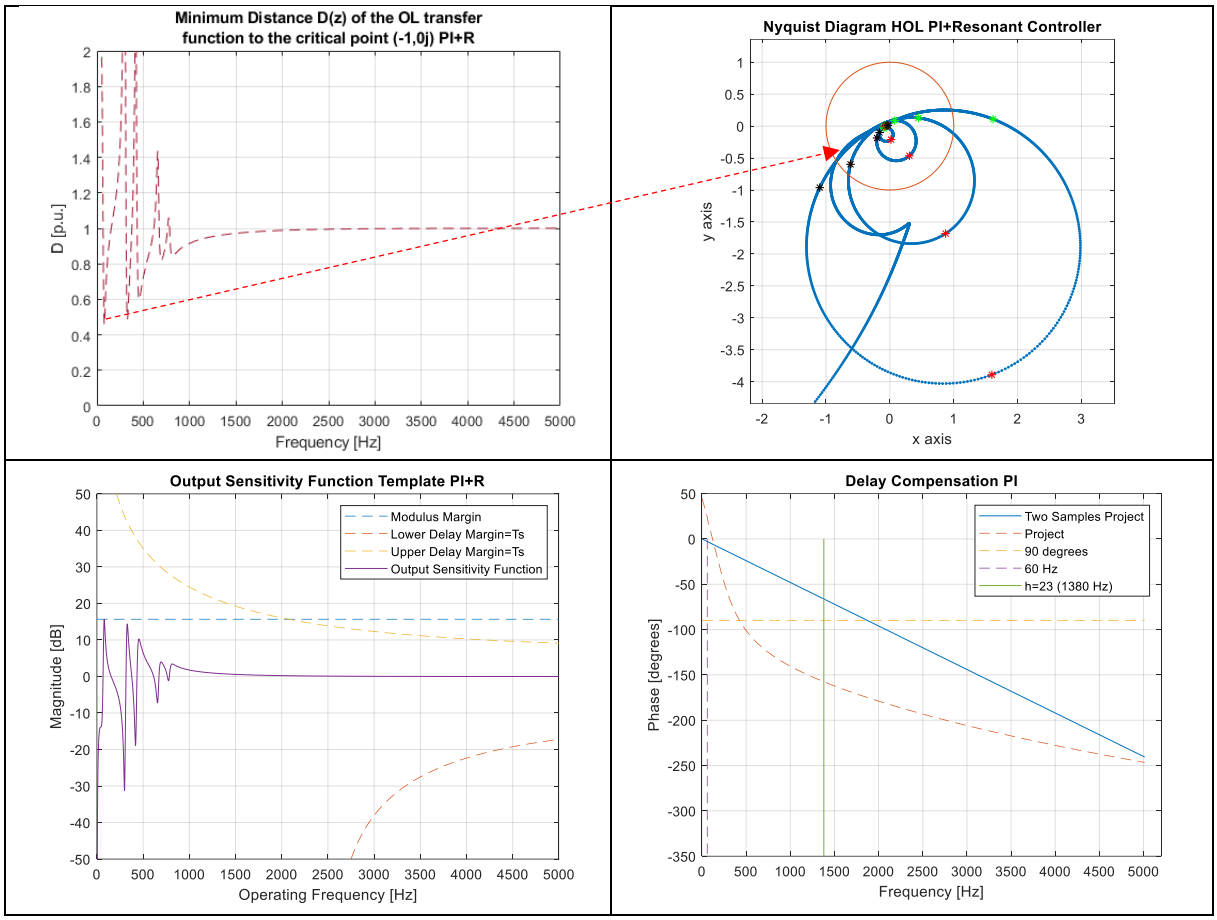

Figure 4.18: Graphical selection of key results of the tuning procedure with a PI +R controller

As mentioned previously, in the z plane, in contrast to what it was seen in the Bode plots, resonant controllers interact each other. The locus of the open loop transfer function including PI+R controllers behaves as expected. To improve the overall stability of the system, it could be accepted that the harmonics frequencies with minimum or no presence in the harmonic spectrum should have a minimum or zero gain. This help to the overall stability; the smaller the large circle is, the more probable is to reach stability.

The output sensitivity template shown in Figure 4.18 demonstrates that the tuning proposed has good margins. The delay compensation angle if not affected by the resonant controllers because by definition the delay compensation is necessary to compensate the effect of the plant model only. At lower frequencies it seems that the delay compensation angle is positive (the reference is negative). The reason is that the θ angle has been assumed fixed for all frequencies and this is indeed variable.

4.5.1 Controller tuning results without considering damping and with delay compensation

If a very low damping is used (almost zero), the plots would change in this way:

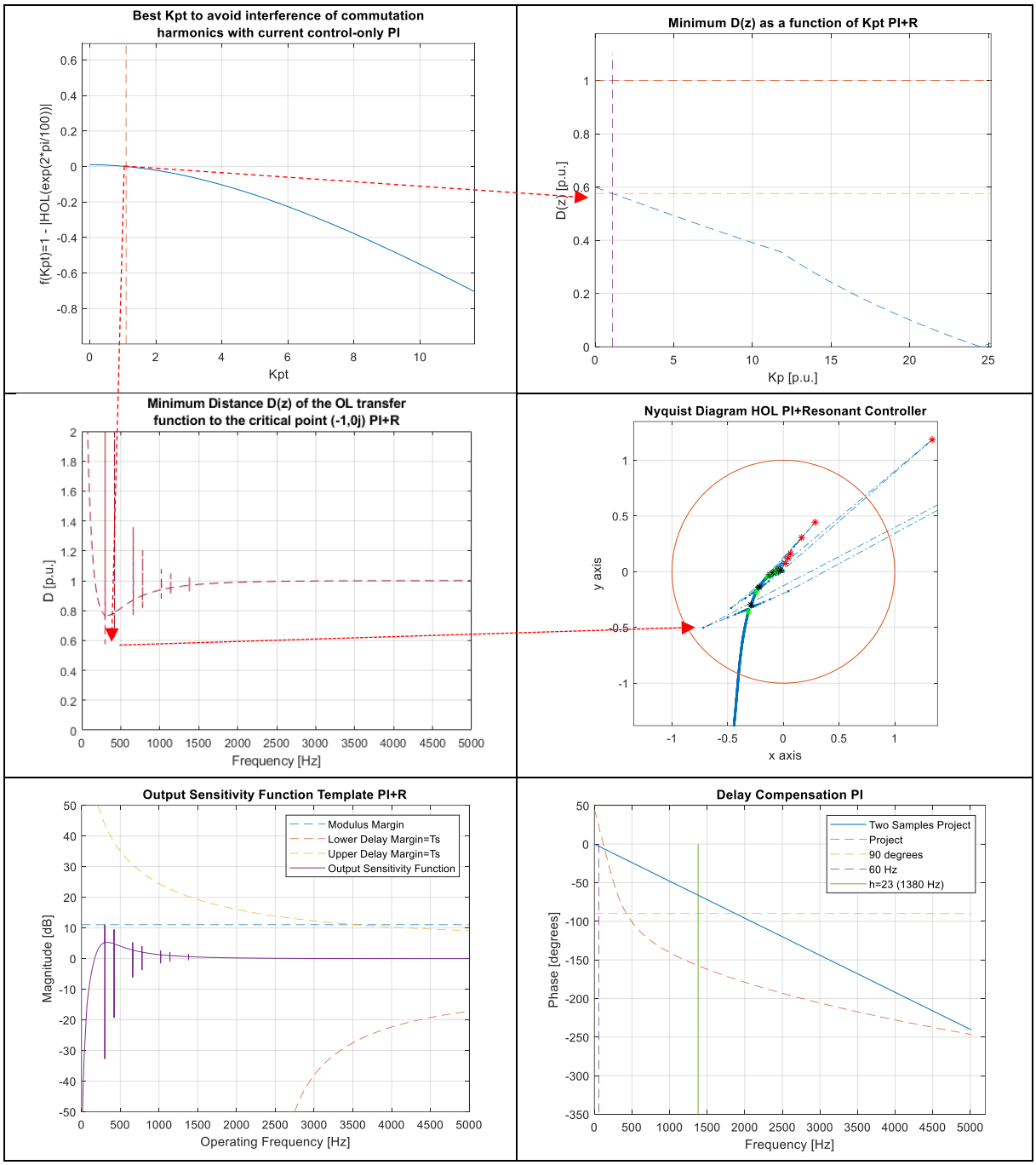

Figure 4.19: Graphical selection of key results of the tuning procedure PI +R controller without damping

The Nyquist plot shown in Figure 4.19 becomes very similar to the one seen in Section 2.34. A zoom of the Nyquist plot close to the origin is available in Figure 4.20. It can be seen that there is an asymptotic behavior close to the harmonic frequencies, something expected for a resonant controller without damping.

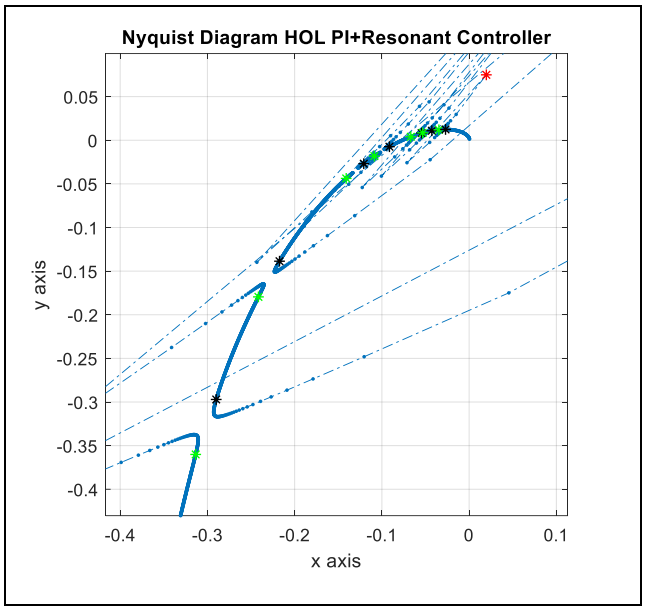

Figure 4.20: Zoom close to the origin in the Nyquist diagram of HOL using PI+R without damping

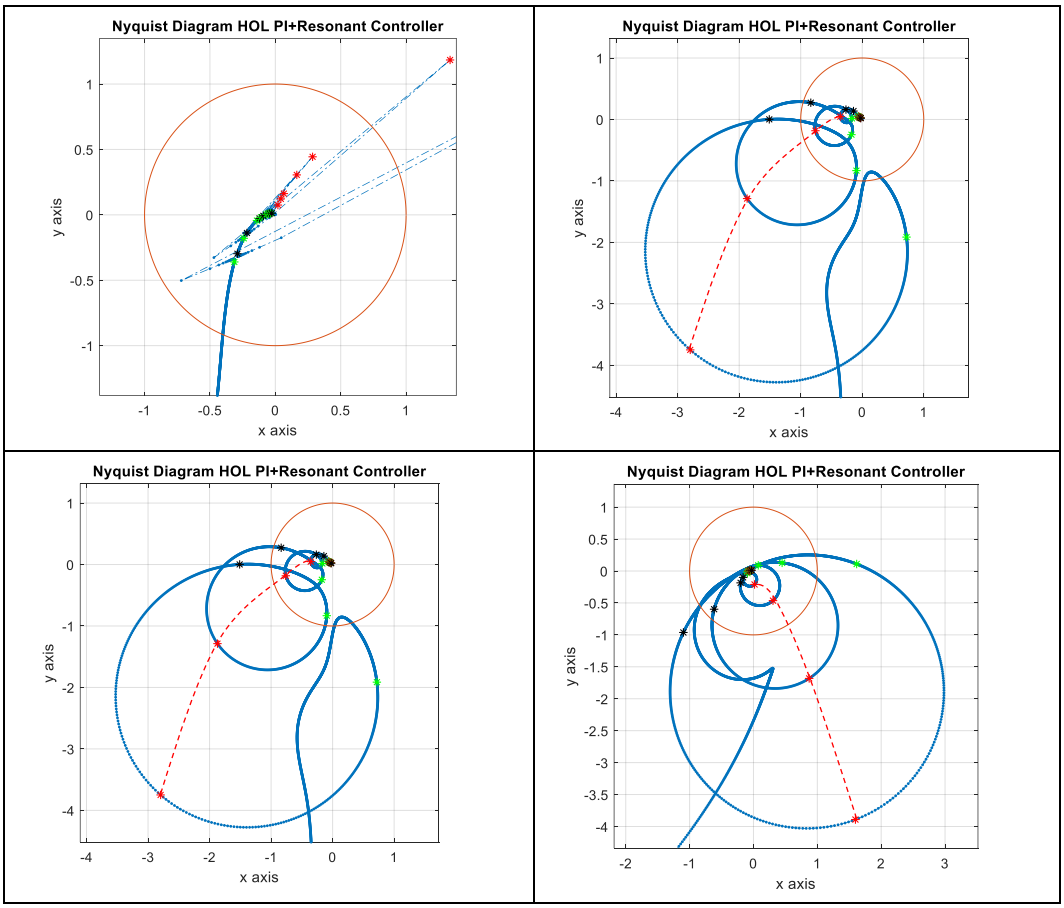

Figure 4.21: Comparing of Nyquist diagrams for PI+R controllers with and without damping and with and without delay compensation

Looking at Figure 4.22, the upper left and right Nyquist diagrams are from cases 1 and 2 respectively whereas the lower left and right Nyquist diagrams are from cases 3 and 4 respectively. All damping factors and delay compensation angles have been considered equal for comparison purposes. It seems that the consideration of the delay compensation makes system stable. Cases 2 and 3 does not consider delay compensation and the Nyquist

plots predicts unstable behavior in those cases. However, something interesting to mention is that, at rated frequency, which is represented by the dashed red lines joining the points in the plot at rated frequency, the system could be still stable. Only the cases 1 and 4 would be stable for all frequency conditions.

4.6 Bode Plots for the Voltage Control loop

4.6.1 Resonant Controller

Once a stable solution is found, the Bode plot is obtained directly. The Bodes plot obtained for resonant controllers with delay compensation and with/without damping are shown in Figures 4.23 and 4.24 respectively. The harmonic gains K_{Vh} have been chosen 9.5, $9.5 * 0.75$, $9.5 * 0.5$, $9.5 * 0.25$ for harmonics 5,7,11 and 13 respectively. The rest of higher order harmonics have been chosen equal to zero. Notice that the sequence 1.00, 0.75, 0.5 and 0.25 is close to the sequence $5/5$, $5/7$, $5/11$ and $5/13$. To choose the harmonic gains proportional to the harmonic frequency was also possible, but it was chosen this sequence for easy manipulation. 9.5 is approximately 11.1% of the gain used for the K_I used in the PI controller of 85, which is in line with the idea of having the harmonic gains proportional to its percentage of the THD.

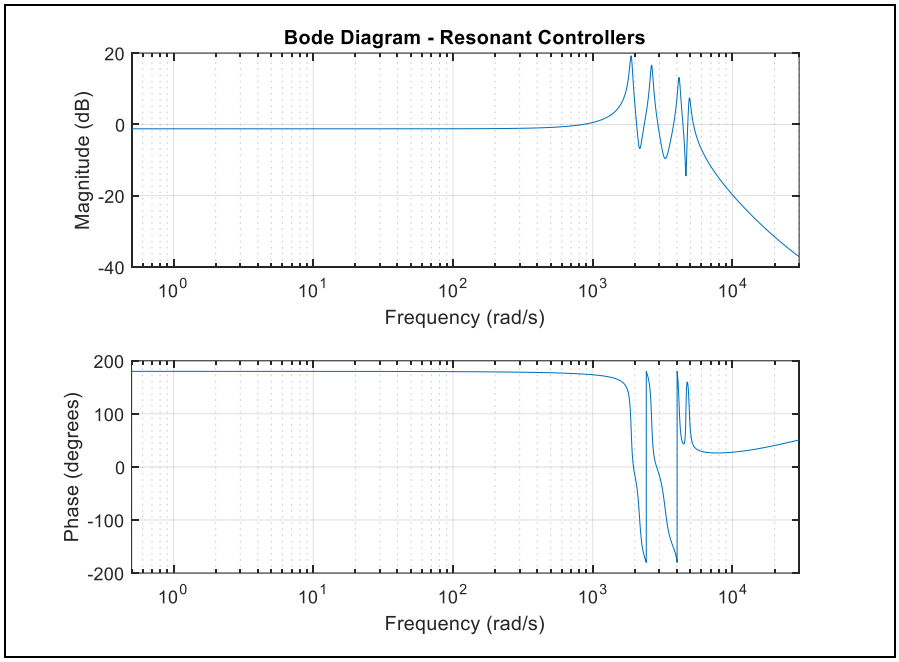

Figure 4.22: Bode Plot of Resonant controller implemented with damping.

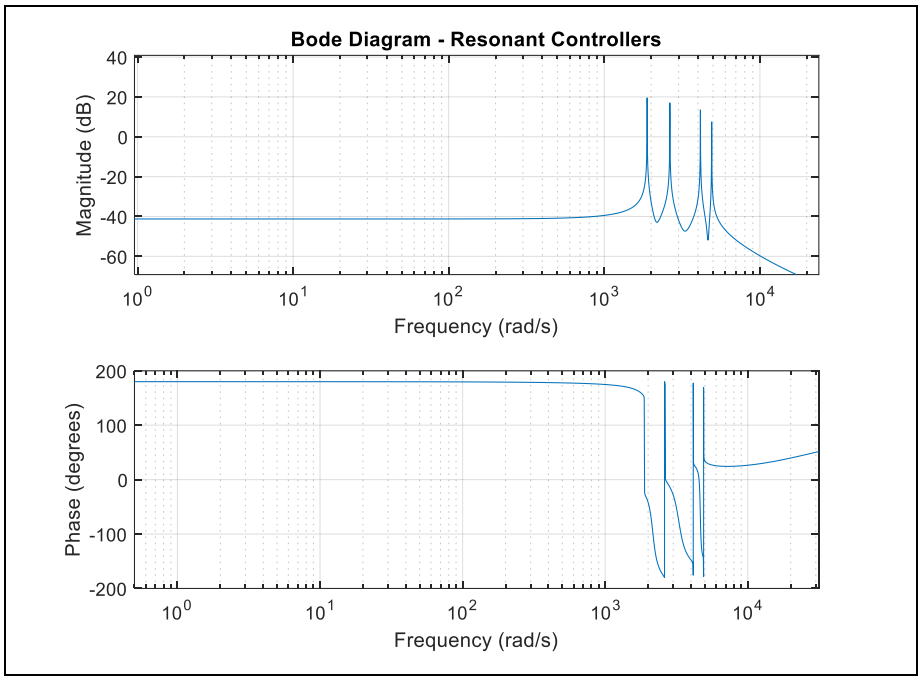

Figure 4.23: Bode Plot of Resonant controller implemented without damping.

The resonant controller implemented using Tusting prewarped transformation seems correct. The resonant gains were not chosen equal, has been already explained in Chapter 4.5. Notice that the gain in the resonant controller is not infinite, the discretization process makes the gain finite and it has a very sharp form in the Bode plot.

4.6.2 Open Loop Transfer Function

The results obtained for the open loop transfer function are shown in Figures 4.25 and 4.26 for the cases of resonant controller with and without damping respectively.

The open loop transfer function crosses 0 dB several times, and it is hard to see which phase margin is the most critical. In this case, the Nyquist plot does a good job showing the absolute phase margin directly.

Something worthy of mention is that there is an anomalous peak at a frequency very close to the fundamental frequency. The reason is that the low pass filter used in the capacitor voltage loop to separate the fundamental frequency voltage and the harmonic frequency voltages in the dq frame becomes a bandpass filter in the $\alpha\beta$ domain. And it turns out that the resonant frequency of that low pass filter is close to the fundamental frequency.

This is the reason of the additional unexpected loop found in the Nyquist diagram as seen in Figure 4.25 as well.

Other than that, the open loop transfer function has a form which is in line with the expected requirement.

In the case of the resonant controller without damping the effect of the resonant controller is high in a very narrow band of frequency which is a weakness when frequency adaptation is necessary.

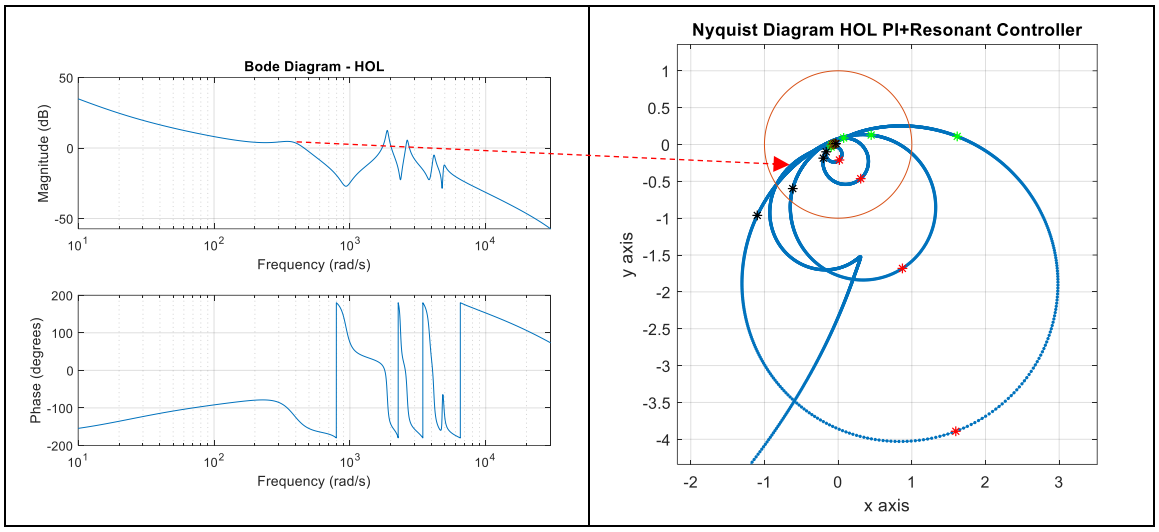

Figure 4.24: Impact of the low pass filter into the Nyquist plot of the H_{OL} transfer function with damping.

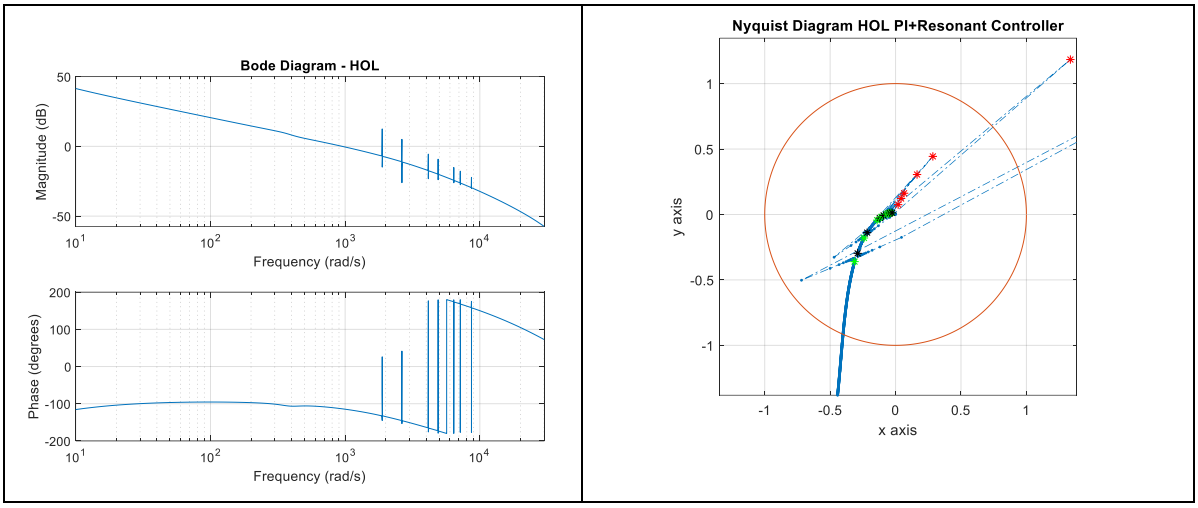

Figure 4.25: Impact of the low pass filter into the Nyquist plot of the H_{OL} transfer function without damping.

4.6.3 Voltage tracking and Output Impedance

The expression for v_c, as a function of v_{ref} and the load current i_0 is given by:

$$V_c = \left(\frac{A(s)B(s)}{1 + A(s)B(s)C(s)}\right)V_{c\_ref} - \left(\frac{B(s)}{1 + A(s)B(s)C(s)}\right)I_0 \tag{107}$$

$$V_c = MV_{c\_ref} - \mathrm{N}I_0 \tag{108}$$

The values of $A(s)$, $B(s)$, and $C(s)$ are the same shown in Figure 4.5 and they are repeated below:

$$A(s) = \frac{PI(s)}{1 + T_{eq,i}s} \tag{109}$$

$$B(s) = \frac{1}{sC} + R_c \tag{110}$$

$$C(s) = \frac{LPFC(s)}{PI(s)}\left\{PI(s)LPF(s) - \left[k_d\left(\frac{RC(s)_5}{K_{V5}} + \frac{RC(s)_7}{K_{V7}} + \cdots \frac{RC(s)_h}{K_{Vh}}\right) - \left(k_d + RC(s)\right)\right]HPF(s)\right\} \tag{111}$$

Ideally, the component M has the form of a close loop transfer function and as such, it should have a straight line around zero up to the crossover frequency. However, in this

case, it has as peak, shown in Figure 4.27. The reason is the same as explained before, it is the dq low pass filter acting as a resonant controller in the $\alpha\beta$ frame.

The output impedance has the same behaviour, but something more might be important to notice; with an output impedance transfer function with a value close to 1.0 means that the full load current is affecting the capacitor voltage reducing it which is the logical result of the inverter trying to provide its rated current to the grid, which has been assumed as a large grid that can maintain its voltage fixed. Thus, the voltage drop caused by the rated inverter current will inevitably cause a reduction in the capacitor voltage.

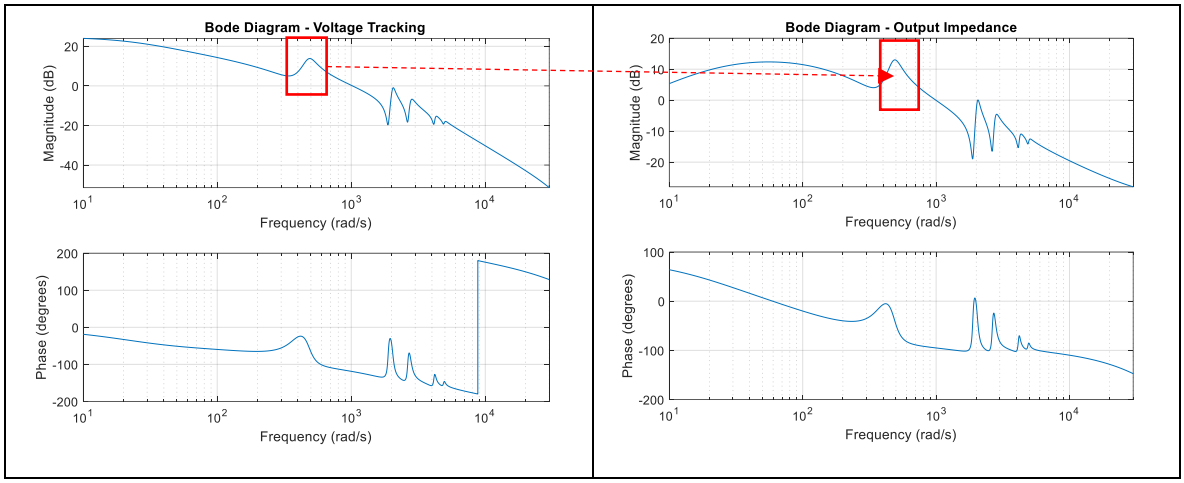

Figure 4.26: Bode Plot of Voltage tracking transfer function M and output impedance N for a resonant controller implemented with damping.

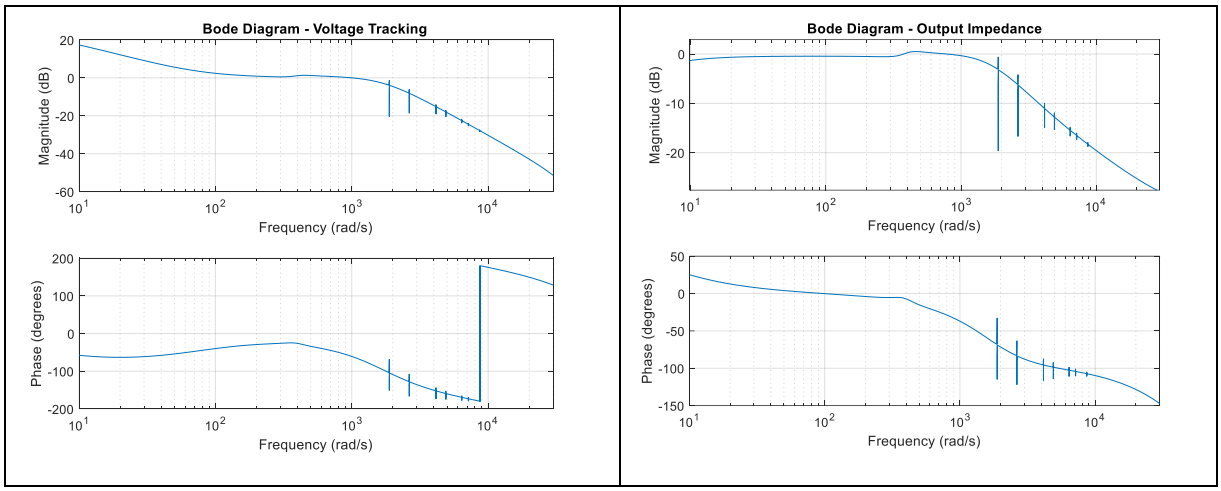

Figure 4.27: Bode Plot of Voltage tracking transfer function M and output impedance N for a resonant controller implemented without damping.

The Figure 4.27 shows that, for the harmonic terms, the closed-loop transfer function of the voltage is following the reference and resonates for the harmonic terms. The output impedances become very low (gains in the Bode plots lower than zero) at the harmonic terms, which is cancelling the load current I_0, which in fact allows the controller follows the reference. However, it is important to note that the load current is not completely cancelled. There will be in fact, a load drop in the capacitor voltage, caused by the load current. A better following of the reference by the controller could be obtained using also a resonant controller for the fundamental harmonic value.

The Figure 4.28 is essentially similar in the case of a resonant controller with delay compensation but without damping and as expected the impact of the resonant controllers is limited at the resonant frequencies.

In the Section 5, the simulation results will show how the voltage control loop works.

5 Simulation Results

In order to compare the performance of the different implementations with and without damping and with and without delay compensation, 5 cases have been assessed. The analysis of the result is given in Section 6. The following magnitudes are verified:

- Converter current before LCL filter
- Converter current after LCL filter
- Capacitor Voltage
- Non-linear load
- Current supplied to grid
- Frequency variation at capacitor point

The cases are:

- Case 0: No resonant controller and with/without damping
- Case 1: Resonant Controller without relative damping factor but including delay compensation and active damping
- Case 2: Resonant Controller with relative damping factor and without delay compensation, with z transform and active damping
- Case 3: Resonant Controller with relative damping factor and without delay compensation, implemented using a delta operator and active damping
- Case 4: Resonant Controller with relative damping factor and delay compensation, implemented using a delta operator and active damping

The purpose of Case 0 is to have a reference case to compare the performance of the different implementation of resonant controllers. For that reason, no resonant controllers are used in this case. Only the K_{P_T} and K_I are maintained equal and all resonant controllers and active damping is deactivated. A different selection of K_{P_T} and K_I can be chosen to optimize its performance, however it is maintained equal for comparative purposes.

5.1 Case 0

With the active damping activated and the resonant controller deactivated the system looks stable. The response can be seen in Figure 5.1. When the active damping is deactivated the system is completely unstable.

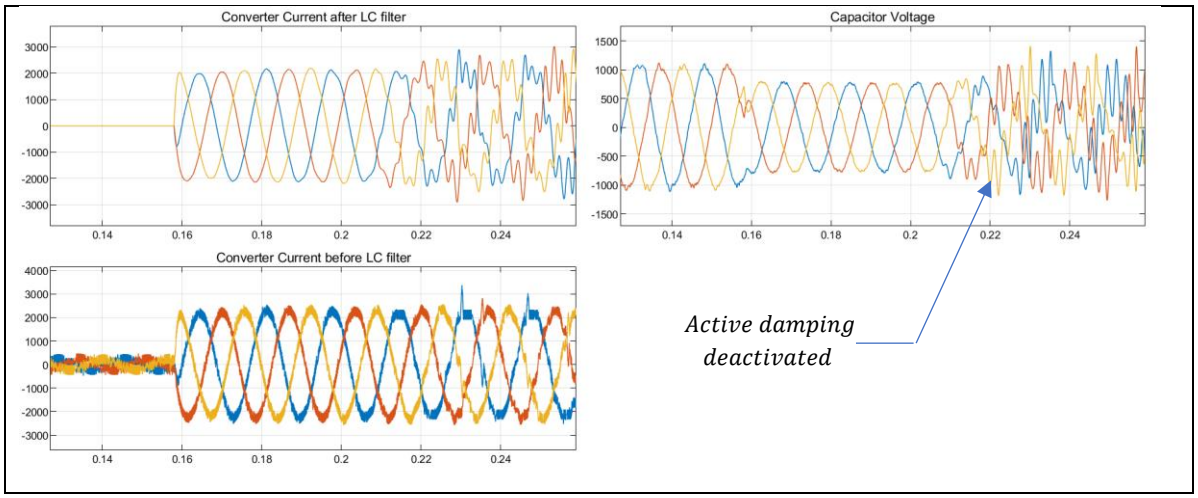

Figure 5.1: System response without resonant controllers and with/without active damping Case 0.

5.2 Case 1

In this case the system is stable, with no problems and good balance. In Figure 5.2 it is seen that the converter current shows the action of the hysteresis current controller, but the filtering action of the converter side inductor is reflected comparing the converter current before and after the LCL filter. The transient state in the capacitor voltage because of the circuit breaker closing is quite smooth even for such a change in the converter current from $0.10\,p.u.$ to $1.00\,p.u.$ The rated current is measured at the output of the converter, and includes the necessary current to charge the capacitor. The capacitor voltage shows some of the high frequency harmonics present in the converter current before the converter side inductance, but overall seems good.

In Figure 5.3, some unbalanced is observed in the converter current, but the impact is minimum in the THD.

In Figures 5.4 and 5.5 it is observed the transient in the α and β components of the capacitor voltage, it is seen that the error difference between the reference voltage $v_{c\_ref\_\alpha}$ and the α component of the capacitor voltage becomes very close to zero within two cycles, which is really good.

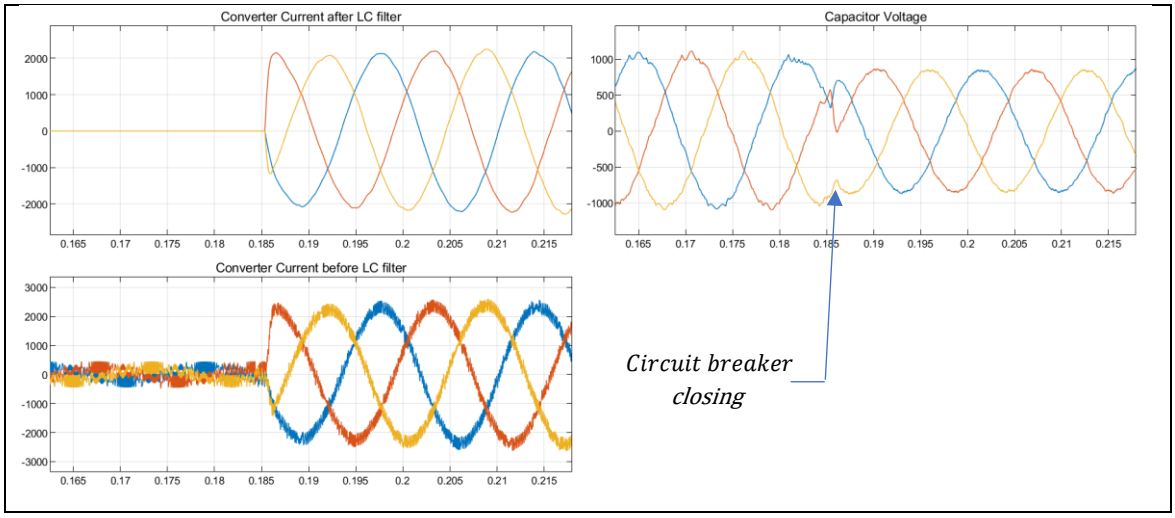

Figure 5.2: System response with active damping and resonant controller case 1.

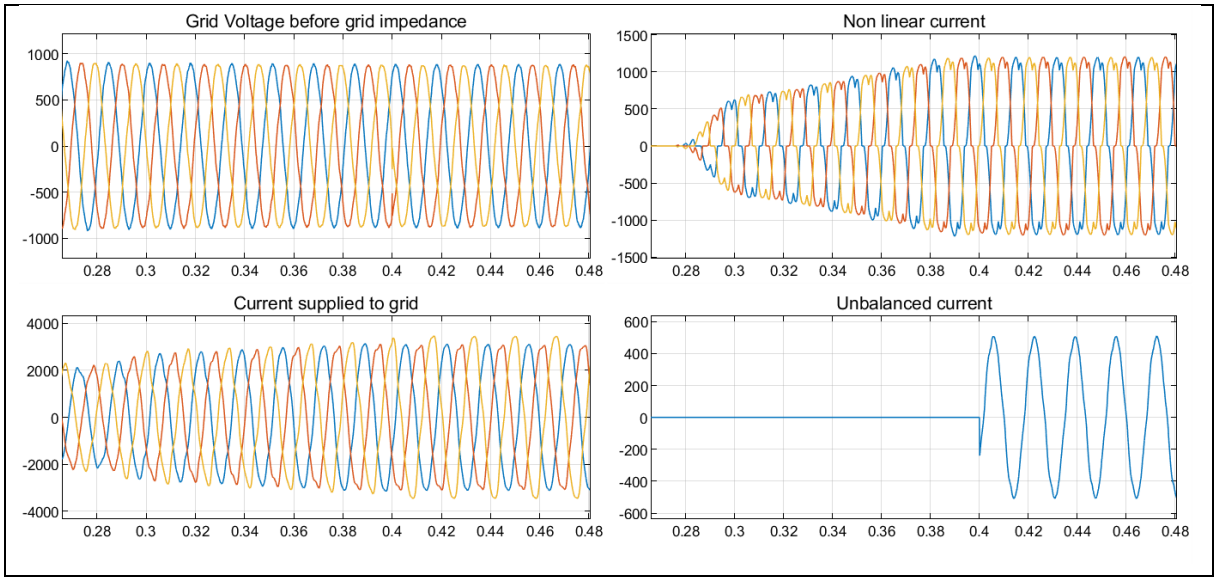

Figure 5.3: System response with active damping and resonant controller case 1.

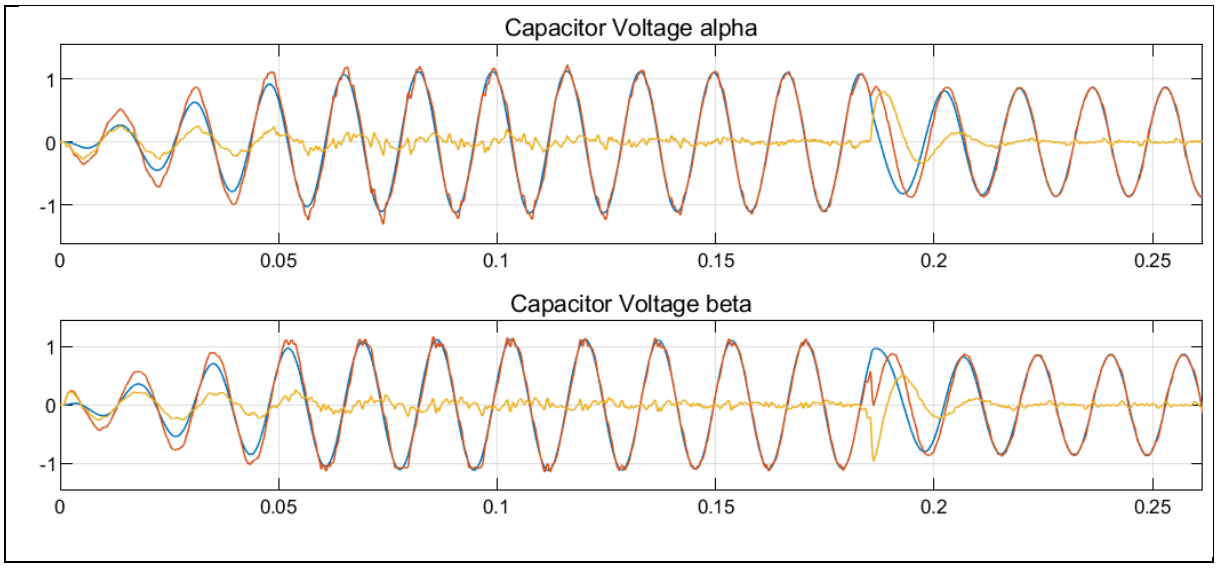

Figure 5.4: Capacitor voltage $\alpha\beta$ frame case 1.

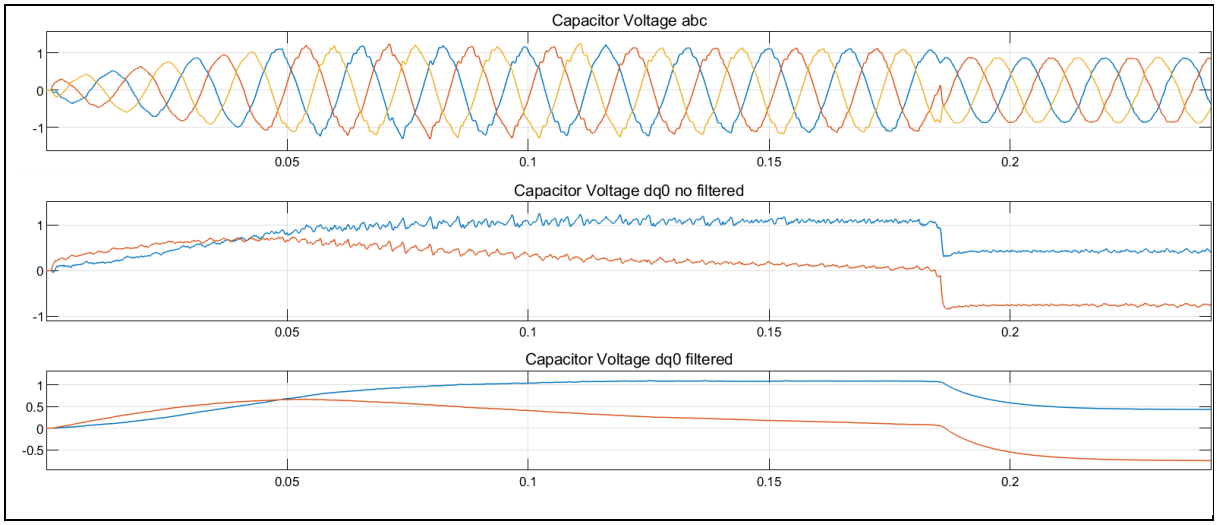

Figure 5.5: Capacitor voltage abc and dq frame case 1.

5.3 Case 2

The performance is very similar to case 1.

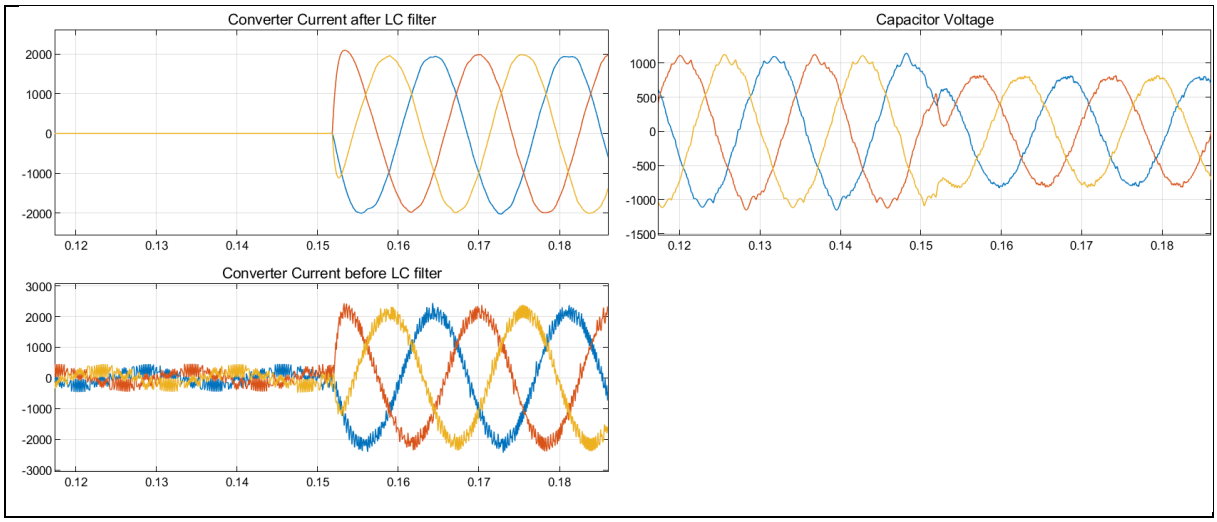

Figure 5.6: System response with active damping and resonant controller case 2.

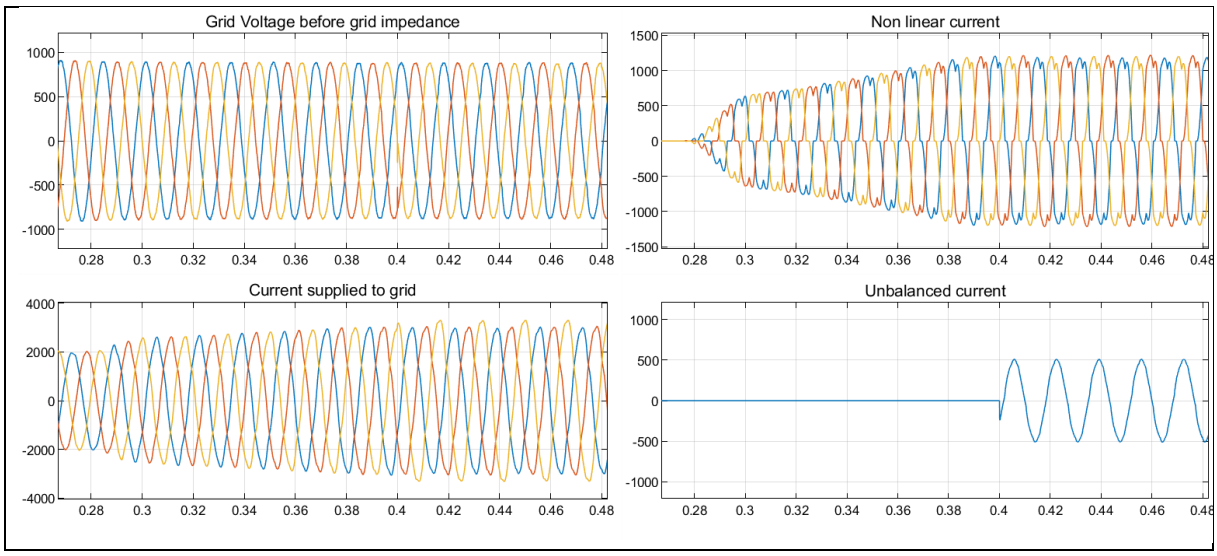

Figure 5.7: System response with active damping and resonant controller case 2.

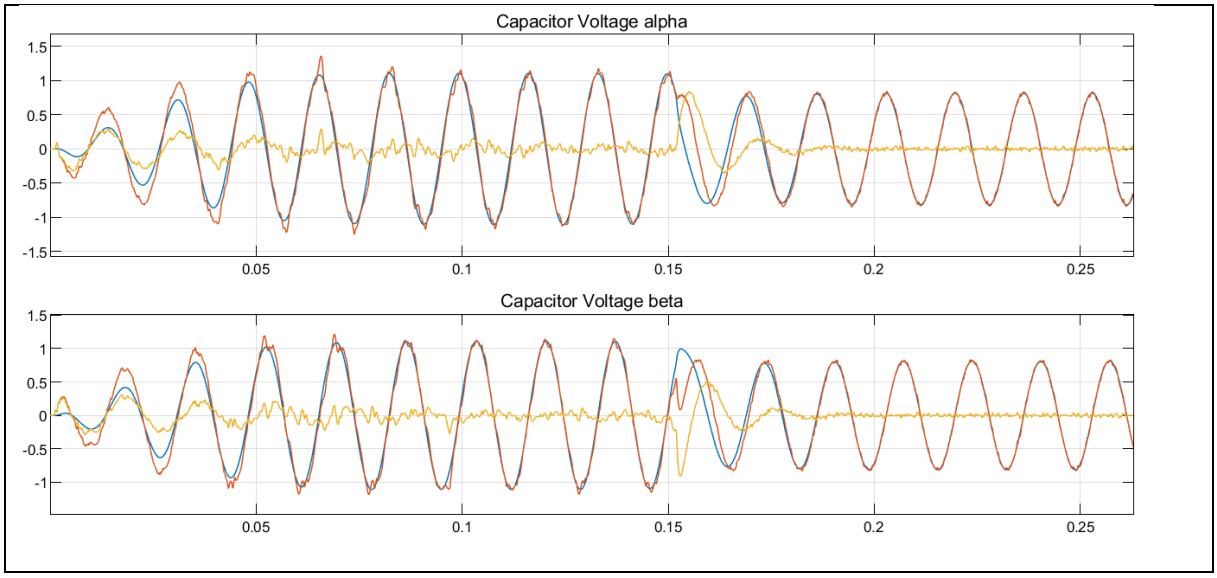

Figure 5.8: Capacitor voltage $\alpha\beta$ frames case 2.

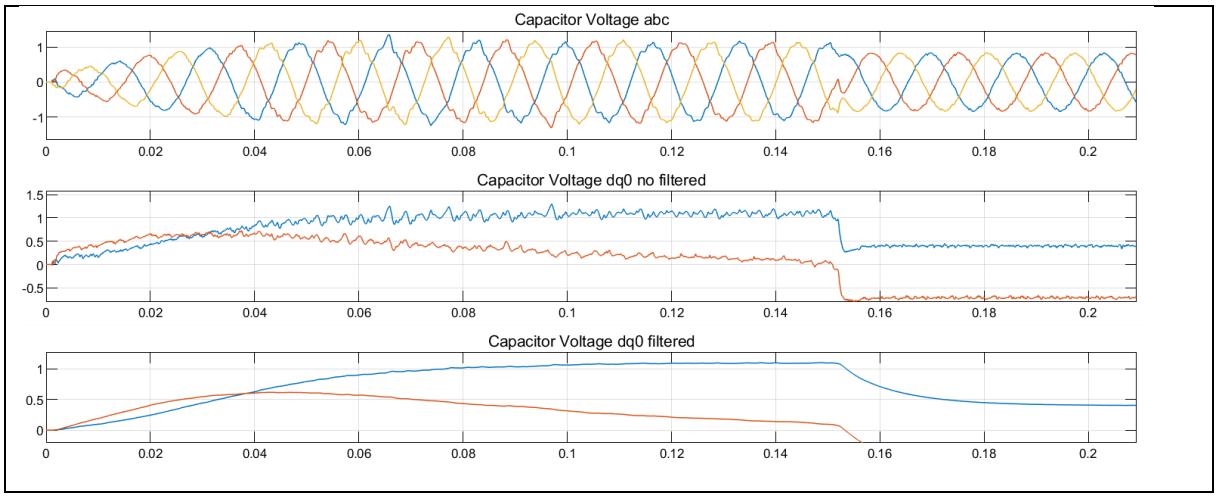

Figure 5.9: Capacitor voltage dq frame case 2.

5.4 Case 3

The performance is very similar to case 1.

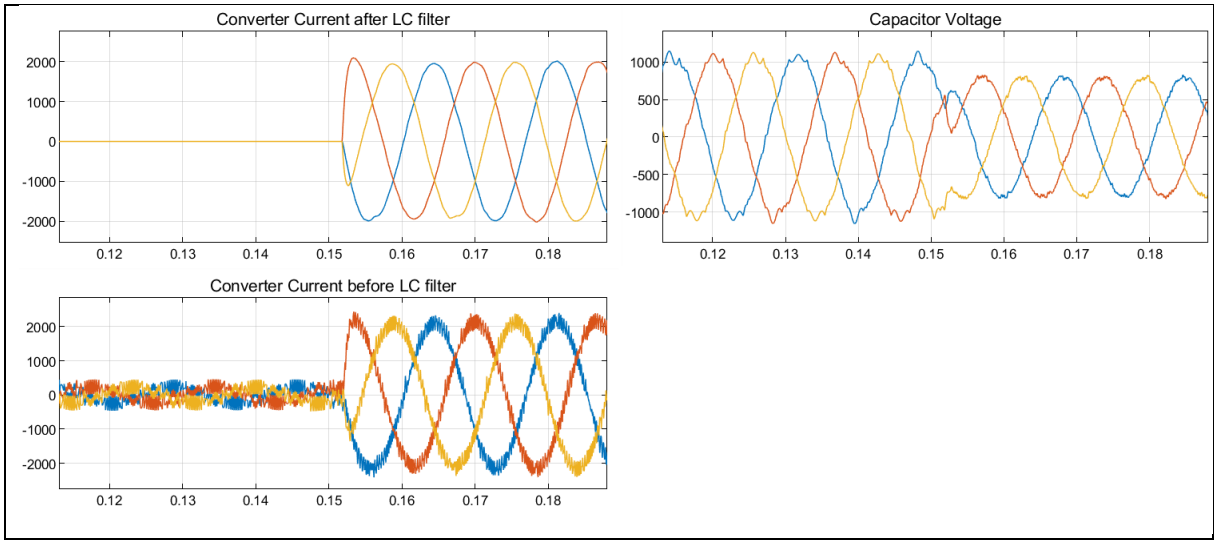

Figure 5.10: System response with active damping and resonant controller case 3.

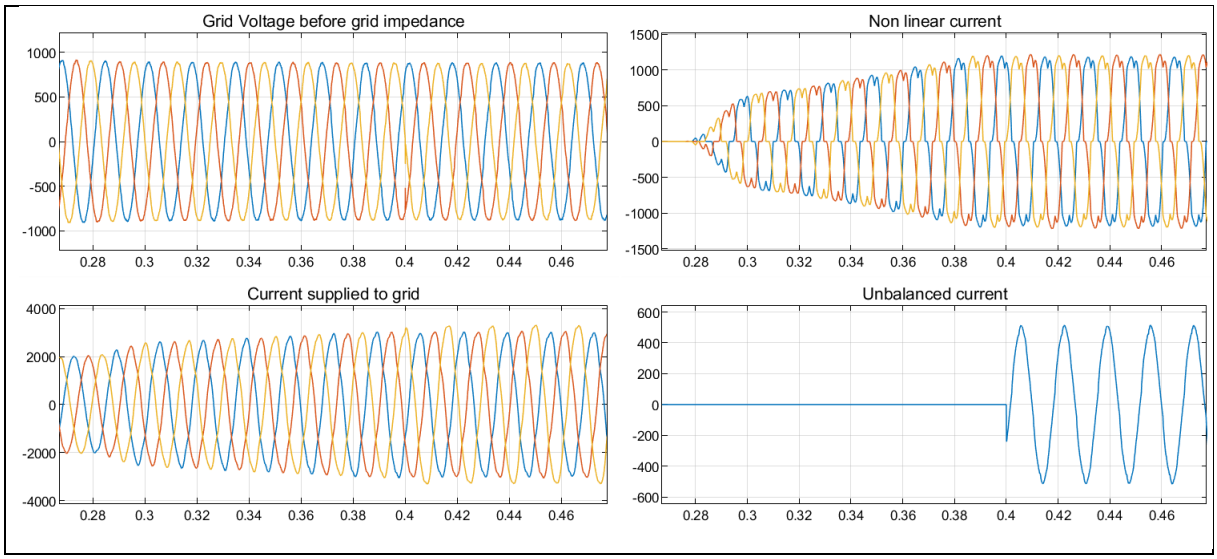

Figure 5.11: System response with active damping and resonant controller case 3.

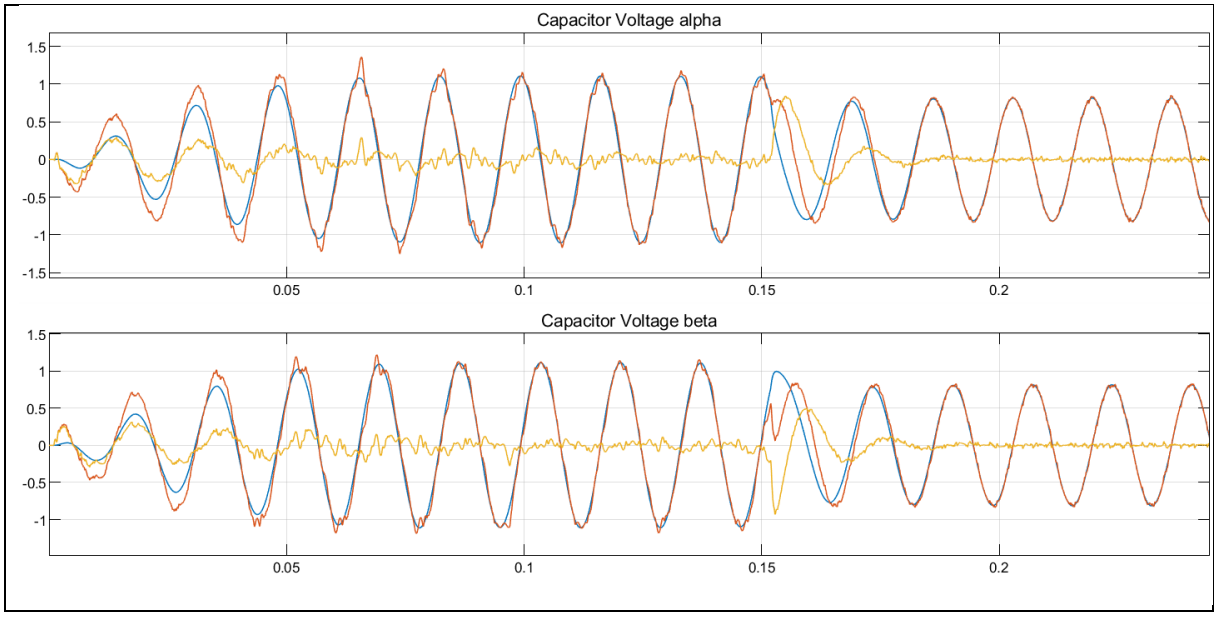

Figure 5.12: Capacitor voltage $\alpha\beta$ frames case 3.

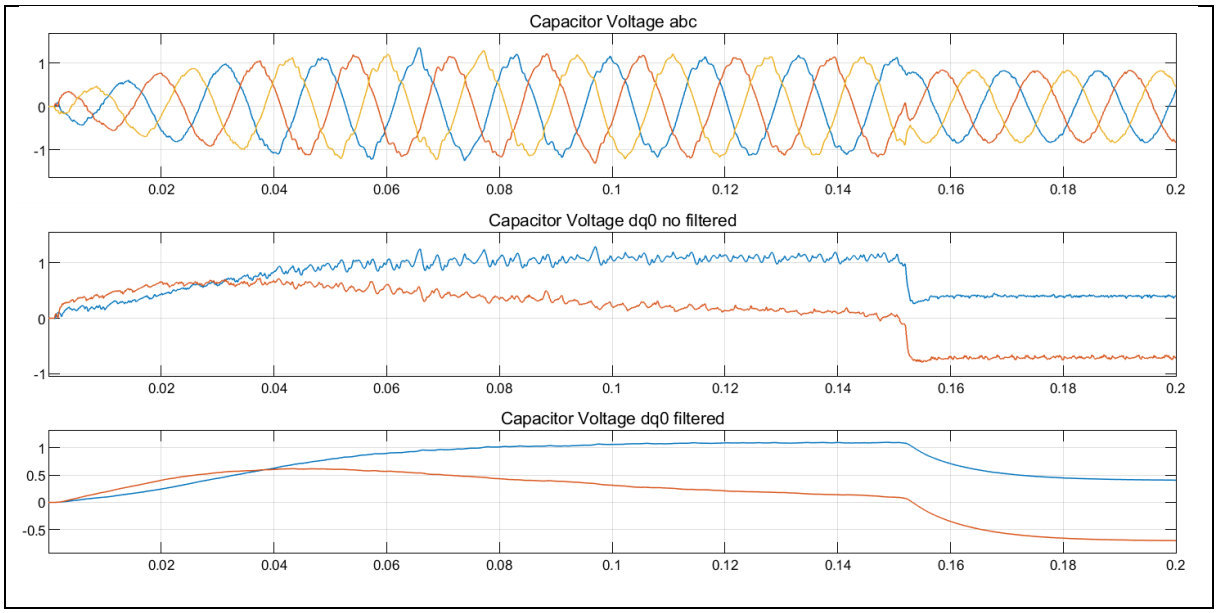

Figure 5.13: Capacitor voltage dq frame case 3.

5.5 Case 4

The performance is very similar to case 1. In this case system is also stable, with no problems and good balance. To compare with the other previous solutions, a case with twice the grid impedance has been simulated, to see the impact in the harmonic levels in the grid.

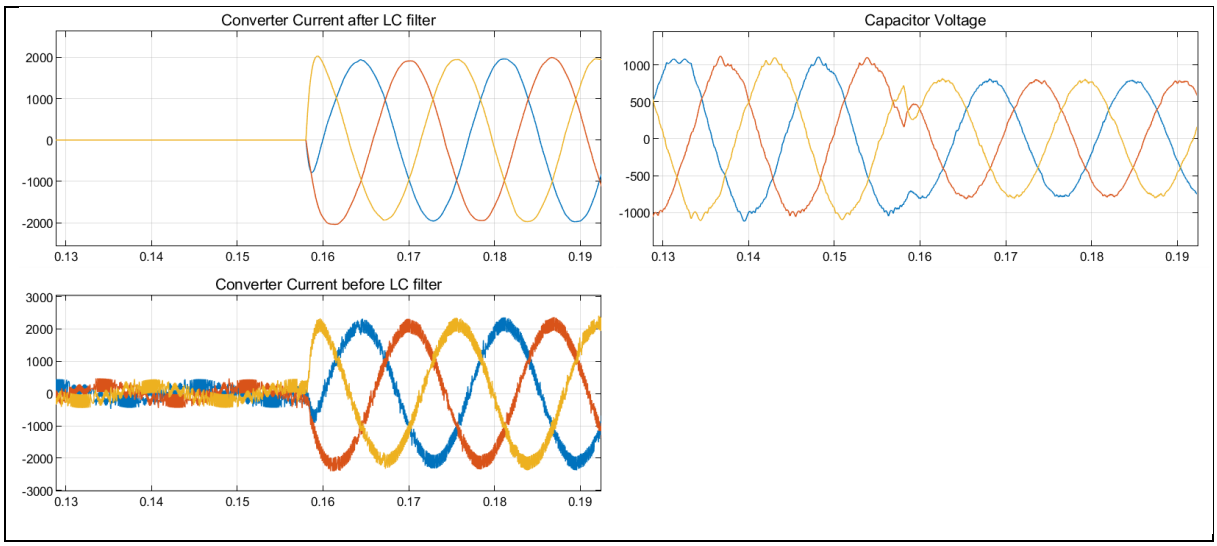

Figure 5.14: System response with active damping and resonant controller case 4.

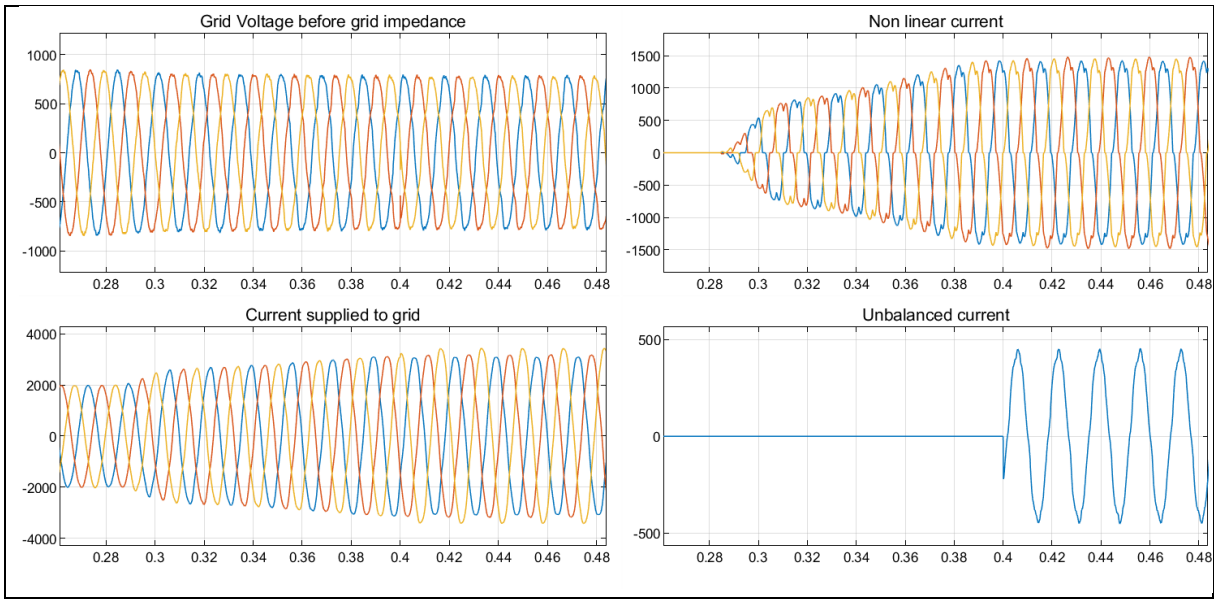

Figure 5.15: System response with active damping and resonant controller case 4.

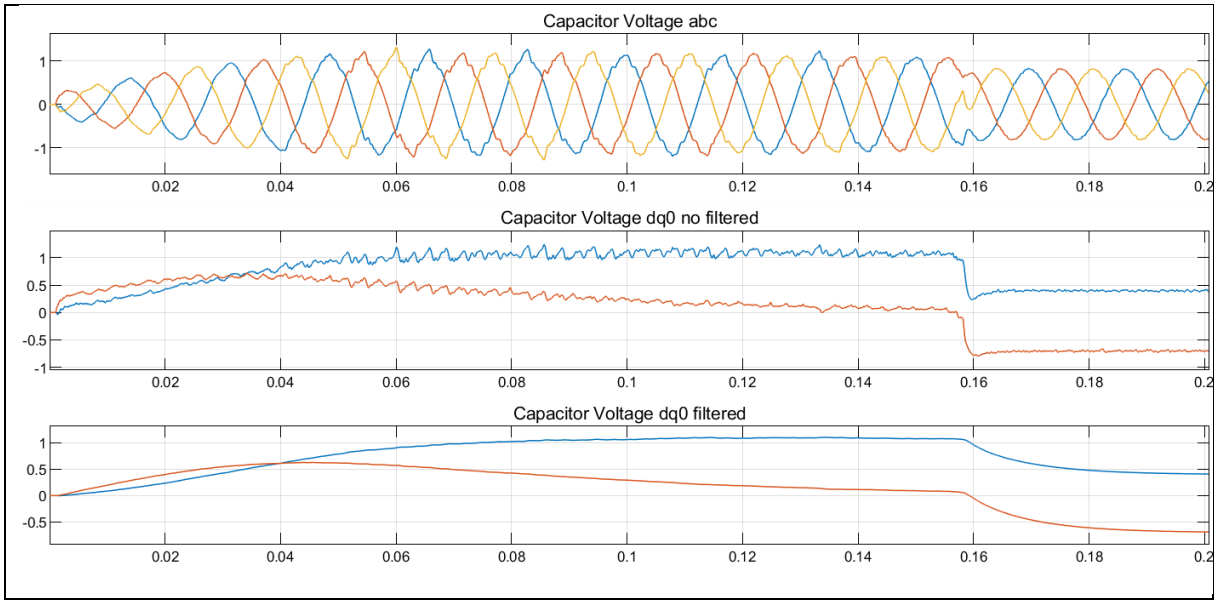

Figure 5.16: Capacitor voltage dq frames case 4.

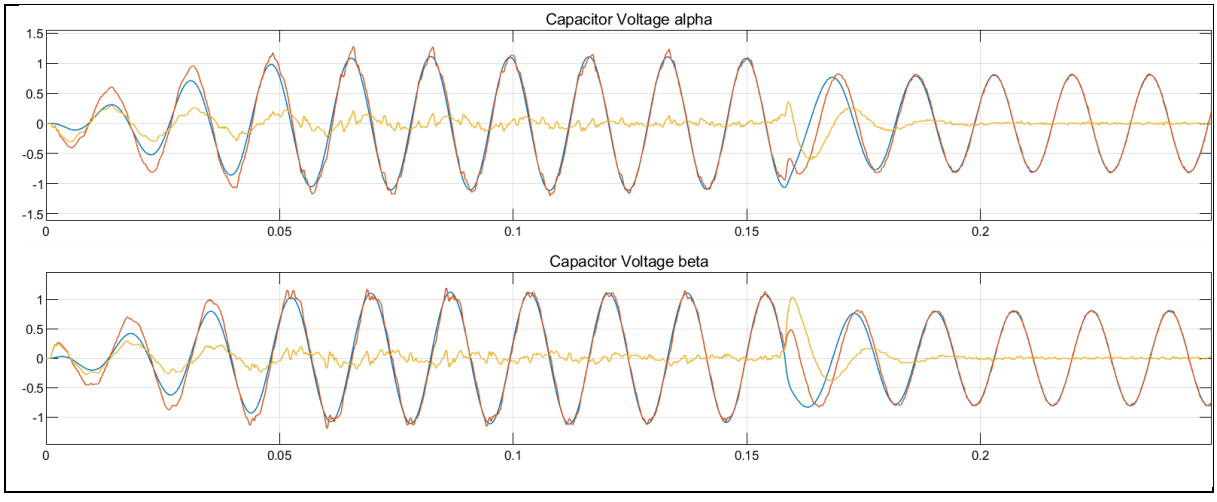

Figure 5.17: Capacitor voltage $\alpha\beta$ frame case 4.

6 Discussion

6.1 Simulation results

The total harmonic distortion factor for the 5 cases simulated is found in Table 6.1. The Figure 4.3 is repeated below to easy following of the Table 6.1:

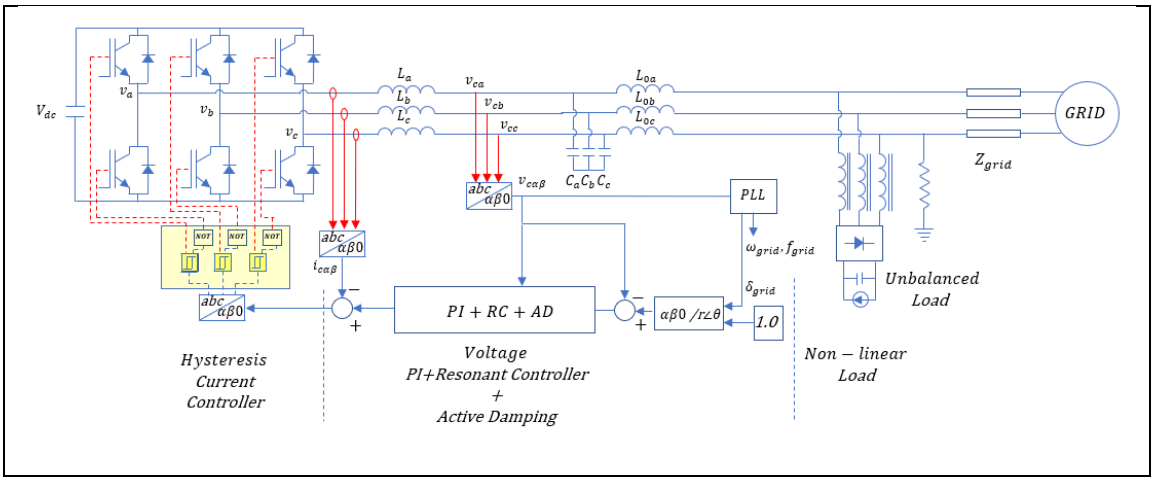

Figure 6.1: General Power and Control Circuit of the closed-loop VSI

Case #	Description	THD (%)				Grid Frequency Variation (%)
		Non-linear current load	Current Supplied to grid	Converter Current after LCL filter	Capacitor Voltage	
0	No resonant controller and with active damping k_d	7.94	2.22	4.75	4.97	12%
1	Resonant Controller without relative damping factor ζ but including delay compensation ϕ_h and active damping k_d	12.40	5.34	5.08	4.89	12%
2	Resonant Controller with relative damping factor ζ and without delay compensation ϕ_h, with z transform and active damping k_d	12.79	4.27	3.25	5.06	9%
3	Resonant Controller with relative damping factor ζ and without delay compensation ϕ_h, implemented using a delta operator and active damping k_d	12.82	4.05	3.26	4.63	9%
4A	Resonant Controller with relative damping factor ζ and delay compensation ϕ_h, implemented using a delta operator and active damping k_d, using double grid impedance	9.04	3%	4.75	6.4%	9%

Table 6.1: Total Harmonic Distortion and grid frequency variation for different resonant controller implementations

In the case 0, without the active damping the system is unstable with a high harmonic level. This is of course a non-desirable situation. If the system is started without the active damping, the system stability is indeed worst.

A completely different situation is observed with the active damping incorporated. In all cases a minimum oscillatory behavior is observed, and the system is stable in all cases 1, 2,3 and 4. This brings into discussion whether the delay compensation is in fact necessary for the stable operation of the converter. It can be seen a reduction in the grid frequency variation, but all the implementations seem to work properly.

The harmonic level of the non-linear load stays within the expected range that it is not transferred into the grid. It seems that the AFE is supplying part of the non-linear current to the non-linear load, avoiding the pollution of the grid. This is a desired situation.

The unbalanced load is added, and some part of that current is supplied from the grid, as it can be seen in several Figures in the Section 5 whereas some part is supplied from the AFE converter. It is not expected that the AFE converter handles unbalanced currents in these cases, because not resonant controllers are used to control the fundamental frequency.

In such case, the control loop should be modified as in Figure 6.2 and the tuning procedure should be adjusted to reflect this change.

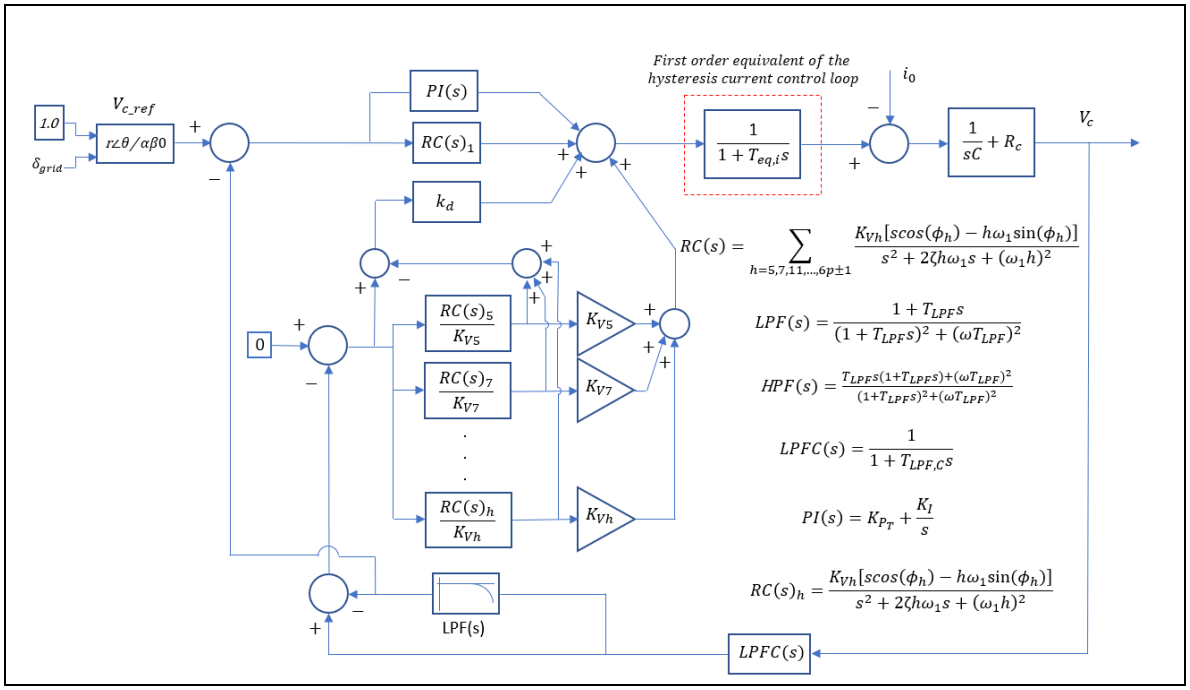

Figure 6.2: Voltage control loop with resonant controller for fundamental frequency

However, the controller should still contain an integral term to handle the DC offset, but of course, with a different integral gain.

The procedure to tune the controller in this case should be similar, get the simplified control loop and apply the same methodology to obtain a different K_{P_T} and new delay compensation angles ϕ_h for each harmonic to be controlled.

Overall it seems that the harmonics levels have been reduced in some cases and increased in others and the non-linear loads do not pollute the grid with harmonic levels. The capacitor voltage contains some harmonics but the harmonic level is still acceptable.

6.2 Sensitivity analysis of the solution

The tuning process has helped to understand how the system works and how the different variables influence stability, voltage tracking features and voltages drops obtained. A summary of probable impacts on modifying design variables is described below:

6.2.1 Influence of the crossover frequency over kp

The crossover frequency $\omega_c$has a direct influence in the value of K_{P_T}. In Section 2.20 it was explained that the K_{P_T} selection for a current controller was done considering the crossover frequency 10 times smaller than the switching frequency $\omega_c = \frac{\omega_{sw}}{10}$. For the voltage controller, the criterion is 10 times smaller than the crossover frequency of the current control loop, i.e. $\omega_c = \frac{\omega_{sw}}{100}$, as standard practice in control engineering. The results obtained indicate that the K_{P_T} becomes smaller when ω_c reduces. As very small K_{P_T} could be stable but may complicate that the current controller follows its reference. Therefore, the system should be tested with the K_{P_T} obtained and verify if the current controller is indeed following the reference and adjust the K_{P_T} value accordingly, if necessary.

6.2.2 Influence of the active damping over stability

The active damping moves the locus of the open loop transfer function H_{OL} away from the instability point, therefore it should be always be included to facilitate the design process. It is a good feature and simplifies tuning. Some authors [37] have proposed solutions without damping but active damping is a well-known control technique and therefore it is not a problem to have it in a practical design.

6.2.3 Influence of the damping factor on resonant controller over stability

A suitable value of relative damping factor helps with the frequency adaptability of the resonant controller. A very small value moves the locus of the H_{OL} away from the instability point but the frequency adaptability is lost. A very large damping factor affects the performance of the resonant controller. It should be considered only the relative damping factor necessary to achieve the frequency adaptability desired.

6.2.4 Influence of kp over delay compensation

The delay compensation is mostly affected by the plant model itself and the computational delay time T_d rather than the K_{P_T} value. However, it is recommended to always verify how K_{P_T} affects the delay compensation on each specific case.

6.2.5 Impact of harmonic gain factor over general stability

A high harmonic gain K_{Vh} will affect the general stability of the controller. The circumference that the resonant controller forms in the z plane increases with the increase of the harmonic gain and when there are resonant controllers for several harmonics, in contrast to what happens in a Bode Plot, interact with each other. This is characteristic not usually recognized in several publications, being the usual approach the tuning of resonant controllers with the same gain for all harmonic frequencies [13, 34-36]. It seems to be the rule with resonant controllers without damping. Only [42] mention that it could be desirable to tune the harmonic gains proportionally to its percentage of THD to minimize the total error convergence rate. In this sense, it would be an overkill and additional computational time to set all harmonic gains to the same value. As explained in Section 3, the lowest order harmonic will form the largest circumference and the circumference radius will decrease according to the increase of the harmonic order. Therefore, considering only the most significant harmonics and adjusting the gains in a somewhat proportional way to the THD is a good approach to get a stable solution.

6.2.6 Impact of integral gain factor over general stability

Provided that the K_I factor is obtained by standard methods, there is not much concern on how to get K_I to help stability. Lots of methods already exist. It is important to assure that the PI controller does not have to deal with harmonic current, that it cannot control.

6.2.7 Impact of harmonic gain and damping factor voltage tracking ability and harmonic cancellation on load current

The harmonic gain causes that the voltage tracking and output impedance transfer functions have very low gain values at the harmonic frequencies, which is in fact the desired situation. This means that the harmonic components of current and voltages are attenuated (not eliminated) at those frequencies. The undesired peak close to the fundamental frequency is related to the filter, as explained in Section 4.9

6.2.8 Impact of resonant frequency of LCL filter over control loop

The resonant frequency of the LCL filter considered in the design is 897 Hz. When the grid impedance is doubled, as a way of assessing grid variation, the resonance frequency changes from $15\omega_1$ to $14.8\omega_1$. This is a large harmonic and in this case harmonic 15^{th} is not expected.

6.2.9 Impact of changes in grid impedance over operation of inverter

A weak grid has a larger impedance than a strong grid. If the converter is connected to a weak grid, the converter may take more of the non-linear currents than the grid itself. In that sense, it is recommended to assess how the converter would work under weak grid conditions, to see if it performs according to it is expected.

7 Conclusions and Further Work

7.1 Conclusions

- The use of the classical robust control theory and the Nyquist diagrams has been used to develop a sequence to tune resonant controllers considering the most important features such as delay compensation, filtering, discretization.
- The resonant controllers without damping provides low stability margins and limited frequency adaptation, although they provide good voltage tracking. Even with a good discretization method, the bandwidth of the resonant controller is somewhat narrow, and it may be affected by regular frequency deviations. In that sense, the resonant controllers with damping have a better performance.
- Regarding the discretization methods, the implementations using z transform and delta operator did not show significant difference in the results, although some time difference was observed in the time used for the simulations, being the implementation with the delta operator faster in most of the cases.
- The tuning method for resonant controllers with damping becomes very similar to the method proposed [13] in when a very small relative damping factor is used. In that sense, it could be said that the method proposed in [13] is a particular case of the method proposed.
- Active damping is a well-known method and it helps on getting a stable solution with reasonable effort. Then it is recommended to include it whenever possible.
- A systematic methodology to tune the resonant controller has been proposed by maximizing distance of the HOL locus to the instability point for the fundamental frequency and harmonic frequencies.
- The LCL resonance frequency was high in this case and therefore it was not critical for the tuning of the resonant controller. This resonant frequency should always be checked.
- K_{P_T} is the most important factor when tuning P+R controllers and its maximum value is dependent on the crossover frequency ω_c. Once the maximum K_{P_T} is obtained, it should be adjusted to make sure that the current controller follows the reference.
- K_{P_T} is the most important factor when tuning resonant controllers. A high K_{P_T}reduces stability and a low K_{P_T} hinders performance.
- K_I is less important regarding stability, that guarantees smaller settling time.
- Harmonic gain K_{Vh} is less important regarding tuning but it impacts in the reduction of THD.
- Harmonic gain can be considered proportional to the harmonic components to help in minimizing harmonic and at the same time guarantee stability.
- Delay compensation is more important for less values of K_{P_T} than for high values of K_{P_T}. For some converters, a delay compensation scheme may be less important.
- Unbalanced current or voltage can be controlled if a resonant controller is implemented for fundamental frequency. Alternatively, an unbalance compensation scheme could be implemented in the active and reactive control loop, as suggested in [41].

7.2 Further Work

- The angle θ is variable and depend on the plant and controller parameters. The value of $\theta = \theta$ has been used as a conservative estimation with good results. If this is equal to $\theta = \frac{\pi}{2}$, the delay compensation scheme is the same as [13]. An assessment of the limits of θ value that are dependent on the resonant controller and the elements in the control loop should be done to improve the accuracy of the delay compensation. The idea is to develop a methodology that can be replicated in any voltage control loop rather than one exact formulation, since the control structures and philosophies change among designs. Most of the tuning recommendations reviewed are based on simplified equivalent models which complicates its use in new applications.
- Study how the control loop proposed behaves under grid fault conditions
- Verify which other elements in the control systems must be adaptative in the system to work with changing frequency.
- Test the controls in islanded operation mode.
- Continue the development of the outer loop that contain the active and reactive power control and other features such as synthetic inertia, virtual impedance, unbalance compensation.
- Prepare the implementation of the control loop in a processor either a DSP or FPGA.
- Perform testing in a laboratory of the AFE control loops.
- Test of the complete system, i.e. the AFE converter controls together with the adjustable speed drive with a synchronous generator.

References

1. Wu, B. and M. Narimani, *High-power converters and AC drives*. Vol. 59. 2017: John Wiley & Sons.
2. Anaya-Lara, O., et al., *Offshore wind energy generation: control, protection, and integration to electrical systems*. 2014: John Wiley & Sons.
3. Mohan, N. and T.M. Undeland, *Power electronics: converters, applications, and design*. 2007: John wiley & sons.
4. Holmes, D.G. and T.A. Lipo, *Pulse width modulation for power converters: principles and practice*. Vol. 18. 2003: John Wiley & Sons.
5. Nilsen, R., *Electric Drives*. 2018, Trondheim, Norway: Department of Electric Power Engineering, NTNU.
6. Teodorescu, R., M. Liserre, and P. Rodriguez, *Grid converters for photovoltaic and wind power systems*. Vol. 29. 2011: John Wiley & Sons.
7. Midtsund, T., *Control of Power Electronic Converters in Distributed Power Generation Systems: Evaluation of Current Control Structures for Voltage Source Converters operating under Weak Grid Conditions*. 2010, Institutt for elkraftteknikk.
8. Adapa, R., *High-wire act: Hvdc technology: The state of the art.* IEEE power and energy magazine, 2012. **10**(6): p. 18-29.
9. Blaabjerg, F., *Control of Power Electronic Converters and Systems*. Vol. 2. 2018: Academic Press.
10. Suul, J.A., et al., *Synchronous reference frame hysteresis current control for grid converter applications.* IEEE transactions on industry applications, 2011. **47**(5): p. 2183-2194.
11. Jena, S., B.C. Babu, and L. Sahu. *Experimental study on adaptive hysteresis current controller for inverter-interfaced 1-Φ grid connected system*. in *2011 Annual IEEE India Conference*. 2011. IEEE.
12. Nachiappan, A., K. Sundararajan, and V. Malarselvam. *Current controlled voltage source inverter using Hysteresis controller and PI controller*. in *2012 International Conference on Power, Signals, Controls and Computation*. 2012. IEEE.
13. Yepes, A.G., *Digital resonant current controllers for voltage source converters.* University of Vigo, 2011.
14. Liserre, M., F. Blaabjerg, and S. Hansen, *Design and control of an LCL-filter-based three-phase active rectifier.* IEEE Transactions on industry applications, 2005. **41**(5): p. 1281.
15. Holter, A.S., *Design and Analysis of Stationary Reference Frame Controllers for Active Front End Converter*. 2016, NTNU.
16. Ruan, X., et al., *Control techniques for LCL-type grid-connected inverters*. 2018: Springer.
17. Park, K.-B., et al., *Weight minimization of LCL filters for high-power converters: impact of PWM method on power loss and power density.* IEEE Transactions on Industry Applications, 2017. **53**(3): p. 2282-2296.
18. Liserre*, M., F. Blaabjerg, and A. Dell'Aquila, *Step-by-step design procedure for a grid-connected three-phase PWM voltage source converter.* International journal of electronics, 2004. **91**(8): p. 445-460.
19. Zhong, Q.-C. and T. Hornik, *Control of power inverters in renewable energy and smart grid integration*. Vol. 97. 2012: John Wiley & Sons.
20. Teodorescu, R., et al., *Proportional-resonant controllers and filters for grid-connected voltage-source converters.* IEE Proceedings-Electric Power Applications, 2006. **153**(5): p. 750-762.

21. Yepes, A.G., et al., *High-performance digital resonant controllers implemented with two integrators.* IEEE Transactions on Power Electronics, 2011. **26**(2): p. 563-576.
22. Ogata, K., *Modern Control Engineering. United State, America*. 2010, PEARSON.(5 th Edi.).
23. Das, J., *Power system harmonics and passive filter designs*. 2015: John Wiley & Sons.
24. Landau, I.D. and G. Zito, *Digital control systems: design, identification and implementation*. 2007: Springer Science & Business Media.
25. Newman, M.J. and D.G. Holmes, *Delta operator digital filters for high performance inverter applications.* IEEE Transactions on Power Electronics, 2003. **18**(1): p. 447-454.
26. Ogata, K., *Discrete-time control systems*. Vol. 2. 1995: Prentice Hall Englewood Cliffs, NJ.
27. Yepes, A.G., et al., *Effects of discretization methods on the performance of resonant controllers.* IEEE Transactions on Power Electronics, 2010. **25**(7): p. 1692-1712.
28. Nilsen, R., *Lecture 5-Digital Signal Processing*, in *ELK-21: Electronics for Power Conversion*. 2018, Department of Electric Power Engineering, NTNU: Trondheim, Norway.
29. Tan, P., P. Loh, and D. Holmes, *High-performance harmonic extraction algorithm for a 25 kV traction power quality conditioner.* IEE Proceedings-Electric Power Applications, 2004. **151**(5): p. 505-512.
30. Sharifabadi, K., et al., *Design, control, and application of modular multilevel converters for HVDC transmission systems*. 2016: John Wiley & Sons.
31. Kjøsnes, E.M.A., *Adaptive Resonant Controllers in a Modular Multilevel Converter-An Analytical Study of the Circulating Current Suppressing Controller*. 2018, NTNU.
32. Acharya, A.B., et al. *Frequency Adaptive Digital Filter Implementation of Proportional-Resonant Controller for Inverter Applications*. in *2018 IEEE 19th Workshop on Control and Modeling for Power Electronics (COMPEL)*. 2018. IEEE.
33. Harnefors, L., *Implementation of resonant controllers and filters in fixed-point arithmetic.* IEEE Transactions on Industrial Electronics, 2008. **56**(4): p. 1273-1281.
34. Harnefors, L., et al., *Passivity-based stabilization of resonant current controllers with consideration of time delay.* IEEE Transactions on Power Electronics, 2014. **29**(12): p. 6260-6263.
35. Xie, C., et al., *A New Tuning Method of Multiresonant Current Controllers for Grid-Connected Voltage Source Converters.* IEEE Journal of Emerging and Selected Topics in Power Electronics, 2019. **7**(1): p. 458-466.
36. Shen, G., et al., *A new feedback method for PR current control of LCL-filter-based grid-connected inverter.* IEEE Transactions on Industrial Electronics, 2010. **57**(6): p. 2033-2041.
37. Pérez-Estévez, D., et al., *Enhanced resonant current controller for grid-connected converters with LCL filter.* IEEE Transactions on Power Electronics, 2017. **33**(5): p. 3765-3778.
38. Mo, O., M. Hernes, and K. Ljøkelsøy. *Active damping of oscillations in LC-filter for line connected, current controlled, PWM voltage source converters*. in *Proc. 10th European Conf. Power Electron. Applicat*. 2003.
39. Bahrman, M.P. and B.K. Johnson, *The ABCs of HVDC transmission technologies.* IEEE power and energy magazine, 2007. **5**(2): p. 32-44.
40. Amin, M., et al., *Nyquist Stability Criterion and its Application to Power Electronics Systems.* Wiley Encyclopedia of Electrical and Electronics Engineering, 2019: p. 1-22.
41. Guerrero, J. *Connecting renewable energy sources into the smartgrid*. in *2011 IEEE International Symposium on Industrial Electronics*. 2011.

42. Yang, Y., et al., *Phase compensation multiresonant control of CVCF PWM converters.* IEEE Transactions on Power Electronics, 2012. **28**(8): p. 3923-3930.

Appendices

Appendix 1: Matlab Code for Tuning a Voltage Control Loop

Appendix 1: Matlab Code for Tuning a Voltage Control Loop

```
%Delay compensation considering the inner current controller as a first
%order equivalent and the filter of the capacitor voltage feedback loop
clear;
close all;
clc;
f=60;
Teq=350*10^(-6);% Equivalent time constant
Tsamp=1/15000;  % Sampling time
Rc=0.02;      % Capacitor resistance
Cap=990*10^(-6);
zeta = 0.000002;  % damping factor or 0 (zero)
w0 = 2*pi*f;    % system angular frequency
Tfc=50*10^(-6); % Filter in capacitor voltage control loop
T_LP=(1/(2*pi*15)); % Low pass filter in the active damping loop
%Filter data
Rf=0.001;
Lf=0.5*83*10^(-6);
% Kp and Ki of PI and resonant controller
kp=0:0.05:50;%
ki=85;
%Active damping
k_d=1;
kn=numel(kp);
%Plant model including filter installed in the capacitor voltage control
%loop
w0Ts=2*pi/99.3;%Crossover frequency
w=(0.5:0.5:31500);%Plotting frequencies up to 5000 Hz
wn=numel(w);
z=exp(1j*w*Tsamp);
z1=exp(1j*w0Ts);
s=(w./(tan(w*Tsamp/2))).*(z-1)./(z+1);
s1=(w0./(tan(w0*Tsamp/2))).*(z1-1)./(z1+1);
%Low Pass Filters to separate fundamental capacitor voltage and harmonic
%capacitor voltage
LPF=(1+T_LP*s)./((1+T_LP*s).^2+(w0*T_LP)^2);
HPF=(T_LP*s.*(1+T_LP*s)+(w0*T_LP)^2)./((1+T_LP*s).^2+(w0*T_LP)^2);
LPF1=(1+T_LP*s1)./((1+T_LP*s1).^2+(w0*T_LP)^2);
HPF1=(T_LP*s1.*(1+T_LP*s1)+(w0*T_LP)^2)./((1+T_LP*s1).^2+(w0*T_LP)^2);
%Initialization of all variables
P=zeros(kn,wn);
PI=zeros(kn,wn);
A_P=zeros(kn,wn);
A_PI=zeros(kn,wn);
R_C_h=zeros(kn,wn);
R_C_h_nk=zeros(kn,wn);
C_P=zeros(kn,wn);
C_PI=zeros(kn,wn);
C=zeros(kn,wn);
CC=zeros(kn,wn);
HOL_P=zeros(kn,wn);
HOL_PI=zeros(kn,wn);
HOL=zeros(kn,wn);
HV=zeros(kn,wn);
HI=zeros(kn,wn);
HOLX=zeros(kn,wn);
a_HOL_P=zeros(kn,wn);
a_HOL_PI=zeros(kn,wn);
a_HOL=zeros(kn,wn);
a_D_P=zeros(kn,wn);
```

```
a_D_PI=zeros(kn,wn);
a_D=zeros(kn,wn);
a_D_RL=zeros(kn,wn);
D_P=zeros(kn,wn);
S_P=zeros(kn,wn);
D_PI=zeros(kn,wn);
S_PI=zeros(kn,wn);
D=zeros(kn,wn);
S=zeros(kn,wn);
d_angle_P=zeros(kn,wn);
d_angle_PI=zeros(kn,wn);
%Calculation of Kpt to avoid interference with current control
%Creation of PI controller for calculation
for ii=1:kn
        P1(ii)=kp(ii);
        PI1(ii)=kp(ii)+ki./s1;
        A1_P(ii)=(1/Cap)*(Tsamp*z1^(-1)/(1-z1^(-1))-Teq*(1-exp(-
Tsamp/Teq))*z1^(-1)/(1-exp(-Tsamp/Teq)*z1^(-1)))*P1(ii);
        A1_PI(ii)=(1/Cap)*(Tsamp*z1^(-1)/(1-z1^(-1))-Teq*(1-exp(-
Tsamp/Teq))*z1^(-1)/(1-exp(-Tsamp/Teq)*z1^(-1)))*PI1(ii);
end
B1=1/(Cap)*Tsamp*z1^(-1)/(1-z1^(-1));
%Note: Resonant controller not included in calculation of Kp
for ii=1:kn
    C1_P(ii)=1./((1+Tfc*s1)*P1(ii)).*(P1(ii)*LPF1+k_d*HPF1);
    C1_PI(ii)=1./((1+Tfc*s1)*PI1(ii)).*(PI1(ii)*LPF1+k_d*HPF1);
end

for ii=1:kn
    HOL1_P(ii)=A1_P(ii).*C1_P(ii);
    HOL1_PI(ii)=A1_PI(ii).*C1_PI(ii);
end

f_kp_P=1-abs(HOL1_P);
f_kp=1-abs(HOL1_PI);

for ii=1:kn-1
    if f_kp_P(ii)>0 && f_kp_P(ii+1)<0
        ikp_P=ii;
    else
        ikp_P=1;
    end
    if f_kp(ii)>0 && f_kp(ii+1)<0
        ikp=ii;
    end
end
ikp_P=ikp_P;%-3
kp(ikp_P)
ikp=ikp%-3
kp(ikp)
%Creation of P and PI controller
for ii=1:kn
    for jj=1:wn
        P(ii,jj)=kp(ii);
        PI(ii,jj)=kp(ii)+ki./s(jj);
        A_P(ii,jj)=(1/Cap)*(Tsamp*z(jj)^(-1)/(1-z(jj)^(-1))-Teq*(1-exp(-
Tsamp/Teq))*z(jj)^(-1)/(1-exp(-Tsamp/Teq)*z(jj)^(-1)))*P(ii,jj);
        A_PI(ii,jj)=(1/Cap)*(Tsamp*z(jj)^(-1)/(1-z(jj)^(-1))-Teq*(1-exp(-
Tsamp/Teq))*z(jj)^(-1)/(1-exp(-Tsamp/Teq)*z(jj)^(-1)))*PI(ii,jj);
    end
end
```

```
B=1/(Cap)*Tsamp*z.^(-1)./(1-z.^(-1));

for ii=1:kn
    for jj=1:wn

C_P(ii,jj)=1./((1+Tfc*s(jj)).*P(ii,jj)).*(P(ii,jj).*LPF(jj)+k_d*HPF(jj));

C_PI(ii,jj)=1./((1+Tfc*s(jj)).*PI(ii,jj)).*(PI(ii,jj).*LPF(jj)+k_d*HPF(jj))
;
    end
end

for ii=1:kn
    for jj=1:wn
        HOL_P(ii,jj)=A_P(ii,jj).*C_P(ii,jj);
        HOL_PI(ii,jj)=A_PI(ii,jj).*C_PI(ii,jj);
        a_HOL_P(ii,jj)=180/pi*angle(HOL_P(ii,jj));
        a_HOL_PI(ii,jj)=180/pi*angle(HOL_PI(ii,jj));
    end
end

for ii=1:kn
    for jj=1:wn
        %Creation of all z plant models
        a_D_P(ii,jj)=180/pi*angle(1+HOL_P(ii,jj));
        a_D_PI(ii,jj)=180/pi*angle(1+HOL_PI(ii,jj));
        %Creation of all sensitivity functions
        D_P(ii,jj)=abs(1+HOL_P(ii,jj));
        S_P(ii,jj)=20*log(1./D_P(ii,jj));
        D_PI(ii,jj)=abs(1+HOL_PI(ii,jj));
        S_PI(ii,jj)=20*log(1./D_PI(ii,jj));
    end
end

low_S=20*log(1-1./abs(1-z.^(-1)));
upp_S=20*log(1+1./abs(1-z.^(-1)));

for ii=1:wn
    if abs(imag(low_S(ii)))>0
       low_S(ii)=NaN;
    end
    if abs(imag(low_S(ii)))>0
       upp_S(ii)=NaN;
    end
end

for ii=1:kn
    D_min_P(ii)=min(D_P(ii,:));
    D_min_PI(ii)=min(D_PI(ii,:));
end

%Calculation of n_p min with P an PI controller
n_p_P=D_min_P(ikp_P);
n_p_PI=D_min_PI(ikp);
for ii=1:kn
    for jj=1:wn
        if S_P(ii,jj)>20*log(1/n_p_P)
            S_P(ii,jj)=NaN;
        end
```

```
        if S_PI(ii,jj)>20*log(1/n_p_PI)
            S_PI(ii,jj)=NaN;
        end
%         if S(ii,jj)>20*log(1/n_p)
%             S(ii,jj)=NaN;
%         end
    end
end

%Strategy to get only absolute values of atan(x) (tricky)
count1=0;
count2=0;

%For P controller only
for ii=1:kn
    for jj=1:wn-1
        if abs((a_HOL_P(ii,jj+1)-a_HOL_P(ii,jj)))>6
            a_HOL_P(ii,jj+1)=a_HOL_P(ii,jj+1)-360;
            count1=1;
        end
        if abs((a_HOL_P(ii,jj+1)-a_HOL_P(ii,jj)))>6 && count1>0
            a_HOL_P(ii,jj+1)=a_HOL_P(ii,jj+1)-360;
        end
    end
end
%For PI controller only. Not relevant for resonant controllers
for ii=1:kn
    for jj=1:wn-1
        if abs((a_HOL_PI(ii,jj+1)-a_HOL_PI(ii,jj)))>170
            a_HOL_PI(ii,jj+1)=a_HOL_PI(ii,jj+1)-360;
            count2=1;
        end
    end
end

%Obtention of compensation angles
for ii=1:kn
    for jj=1:wn
        d_angle_P(ii,jj)=-(-a_HOL_P(ii,jj)+a_D_P(ii,jj))+0.5*90;
        d_angle_PI(ii,jj)=-(-a_HOL_PI(ii,jj)+a_D_PI(ii,jj))+0.5*90;
     end
end

%Creation of Resonant Controllers for all cases
Kih=9.5;
Kih_s=1;
k1=Kih*2*zeta*1*w0*0;
k3=Kih*2*zeta*3*w0*0;
k5=Kih*2*zeta*5*w0;
k7=Kih*2*zeta*7*w0*0.75;
k11=Kih*2*zeta*11*w0*0.5;
k13=Kih*2*zeta*13*w0*0.25;
k15=Kih*2*zeta*15*w0*0;
k17=Kih*2*zeta*17*w0*0;
k19=Kih*2*zeta*19*w0*0;
k23=Kih*2*zeta*23*w0*0;
Kih_m=[k5,k7,k11,k13,k17,k19,k23];
hk=[5,7,11,13,17,19,23];
hkn=numel(hk);%Harmonics for resonant controllers
for ii=1:hkn
            d_angle_c(ii)=-0*d_angle_PI(ikp,377*hk(ii)*2)*pi/180;
```

```
    end
d_angle_c
for ii=1:hkn
    for jj=1:wn
        R_C_h(ii,jj)=Kih_m(ii)*(s(jj)*cos(d_angle_c(ii))-
hk(ii)*w0*sin(d_angle_c(ii))./(s(jj).^2+2*zeta*hk(ii)*w0*s(jj)+(hk(ii)*w0)
^2);
        R_C_h_nk(ii,jj)=Kih_s*(s(jj)*cos(d_angle_c(ii))-
hk(ii)*w0*sin(d_angle_c(ii))./(s(jj).^2+2*zeta*hk(ii)*w0*s(jj)+(hk(ii)*w0)
^2);
        R_C_h_nd(ii,jj)=Kih*s(jj)./(s(jj).^2+(hk(ii)*w0)^2);
    end
end
R_C_wk=sum(R_C_h);
R_C_nk=sum(R_C_h_nk);

for ii=1:kn
    for jj=1:wn
        PI(ii,jj)=kp(ii)+ki./s(jj);
        A_PI(ii,jj)=(1/Cap)*(Tsamp*z(jj)^(-1)/(1-z(jj)^(-1))-Teq*(1-exp(-
Tsamp/Teq))*z(jj)^(-1)/(1-exp(-Tsamp/Teq)*z(jj)^(-1)))*PI(ii,jj);
        C(ii,jj)=1./((1+Tfc*s(jj)).*PI(ii,jj)).*(PI(ii,jj).*LPF(jj)-
(k_d*R_C_nk(jj)-(k_d+R_C_wk(jj))).*HPF(jj));
    end
end

for ii=1:kn
    for jj=1:wn
        HOL(ii,jj)=A_PI(ii,jj).*C(ii,jj);
        a_HOL(ii,jj)=180/pi*angle(HOL(ii,jj));
    end
end

for ii=1:kn
    for jj=1:wn
        %Creation of all z plant models
        a_D(ii,jj)=180/pi*angle(1+HOL(ii,jj));
        %Creation of all sensitivity functions
        D(ii,jj)=abs(1+HOL(ii,jj));
        S(ii,jj)=20*log(1./D(ii,jj));
    end
end

for ii=1:kn
    D_min(ii)=min(D(ii,:));
end

%Calculation of n_p min with P an PI controller
n_p=D_min(ikp);
for ii=1:kn
    for jj=1:wn
        if S(ii,jj)>20*log(1/n_p)
            S(ii,jj)=NaN;
        end
    end
end

%Obtention of compensation angles
for ii=1:kn
    for jj=1:wn
```

```
        d_angle(ii,jj)=-(-a_HOL(ii,jj)+a_D(ii,jj))+0.5*90;
    end
end

y3=180/pi*(-2*w*Tsamp);

figure(1)
plot(w/(2*pi),a_D_P(ikp_P,:),'--');hold on;
plot(w/(2*pi),-90*ones(63000,1),'--');hold on;
plot([60 60],[0 -350],'--')
plot([1380 1380],[0 -350],'-')
title('D angle P');
xlabel('Frequency [Hz]');
ylabel('Phase [degrees]');
xlim([0 5200]);hold on; grid on;

figure(2)
plot(w/(2*pi),a_D_PI(ikp,:),'--');hold on;
plot(w/(2*pi),-90*ones(63000,1),'--');hold on;
plot([60 60],[0 -350],'--')
plot([1380 1380],[0 -350],'-')
title('D angle PI');
xlabel('Frequency [Hz]');
ylabel('Phase [degrees]');
xlim([0 5200]);hold on; grid on

figure(3)
plot(w/(2*pi),y3);hold on;
plot(w/(2*pi),a_HOL_P(ikp_P,:),'--');hold on;
plot(w/(2*pi),-90*ones(63000,1),'--');hold on;
plot([60 60],[0 -350],'--')
plot([1380 1380],[0 -350],'-')
title('HOL angle P');
xlabel('Frequency [Hz]');
ylabel('Phase [degrees]');
xlim([0 5200]);hold on; grid on;

figure(4)
plot(w/(2*pi),y3);hold on;
plot(w/(2*pi),a_HOL_PI(ikp,:),'--');hold on;
plot(w/(2*pi),-90*ones(63000,1),'--');hold on;
plot([60 60],[0 -350],'--')
plot([1380 1380],[0 -350],'-')
title('HOL angle PI');
xlabel('Frequency [Hz]');
ylabel('Phase [degrees]');
xlim([0 5200]);hold on; grid on;

figure(5)
plot(w/(2*pi),y3);hold on;
plot(w/(2*pi),d_angle_P(ikp_P,:),'--');hold on;
plot(w/(2*pi),-90*ones(63000,1),'--');hold on;
plot([60 60],[0 -350],'--')
plot([1380 1380],[0 -350],'-')
title('Delay Compensation P');
xlabel('Frequency [Hz]');
ylabel('Phase [degrees]');
legend({'Two Samples Project','Project','90 degrees','60 Hz','h=23 (1380
Hz)'},'Location','northeast')
xlim([0 5200]);hold on; grid on;
```

```
figure(6)
plot(w/(2*pi),y3);hold on;
plot(w/(2*pi),d_angle_PI(ikp,:),'--');hold on;
plot(w/(2*pi),-90*ones(63000,1),'--');hold on;
plot([60 60],[0 -350],'--')
plot([1380 1380],[0 -350],'-')
title('Delay Compensation PI');
xlabel('Frequency [Hz]');
ylabel('Phase [degrees]');
legend({'Two Samples Project','Project','90 degrees','60 Hz','h=23 (1380
Hz)'},'Location','northeast')
xlim([0 5200]);hold on; grid on;

figure(7)
plot(w/(2*pi),y3);hold on;
for ii=1:kn
    if kp(ii)<kp(ikp+1)
        plot(w/(2*pi),d_angle(ii,:),'--');hold on;
    end
end
plot(w/(2*pi),-90*ones(wn,1),'--');hold on;
plot([60 60],[0 -350],'--')
plot([1380 1380],[0 -350],'-')
line([60 60], [0 -350]); hold on;
title('Delay Compensation PI+R');
xlabel('Frequency [Hz]');
ylabel('Phase Delay [degrees]');
legend({'Two Samples Project','Project','90 degrees','60 Hz','h=23 (1380
Hz)'},'Location','northeast')
xlim([0 5000]);hold on; grid on;

figure(8)
plot(kp,f_kp);hold on;
title({'Best Kpt to avoid interference of commutation','harmonics with
current control PI'});
xlabel('Kpt');
ylabel('f(Kpt)=1 - |HOL(exp(2*pi/100))|');
plot([kp(ikp) kp(ikp)],[-2 2],'--');
grid on;

figure(9)
plot(w/(2*pi),D_P(ikp_P,:),'--');hold on;
title({'Minimum Distance D(z) of the OL transfer','function to the critical
point (-1,0j) P'} );
xlabel('Frequency [Hz]');
ylabel('D [p.u.]');
xlim([0 5000]);hold on;
ylim([0 2]);hold on;
grid on;

figure(10)
% for ii=1:kn
plot(w/(2*pi),D_PI(ikp,:),'--');hold on;
% end
title({'Minimum Distance D(z) of the OL transfer','function to the critical
point (-1,0j) PI'} );
xlabel('Frequency [Hz]');
ylabel('D [p.u.]');
xlim([0 5000]);hold on;
```

```
ylim([0 2]);hold on;
grid on;

figure(11)
for ii=1:kn
  plot(w/(2*pi),D(ikp,:),'--');hold on;
end
title({'Minimum Distance D(z) of the OL transfer','function to the critical
point (-1,0j) PI+R'} );
xlabel('Frequency [Hz]');
ylabel('D [p.u.]');
xlim([0 5000]);hold on;
ylim([0 2]);hold on;
grid on;

figure(12)
plot(kp,D_min_P,'--');hold on;
plot(kp,ones(kn,1),'--');hold on;
plot(kp,n_p_P*ones(kn,1),'--');hold on;
plot([kp(ikp_P) kp(ikp_P)],[0 1.1],'--');
title('Minimum D(z) as a function of Kpt P');
xlabel('Kp [p.u.]');
ylabel('D(z) [p.u.]');
grid on;

figure(13)
plot(kp,D_min_PI,'--');hold on;
plot(kp,ones(kn,1),'--');hold on;
plot(kp,n_p_PI*ones(kn,1),'--');hold on;
plot([kp(ikp) kp(ikp)],[0 1.1],'--');
title('Minimum D(z) as a function of Kpt PI');
xlabel('Kp [p.u.]');
ylabel('D(z) [p.u.]');
grid on;

figure(14)
plot(kp,D_min,'--');hold on;
plot(kp,ones(kn,1),'--');hold on;
plot(kp,n_p*ones(kn,1),'--');hold on;
plot([kp(ikp) kp(ikp)],[0 1.1],'--');
title('Minimum D(z) as a function of Kpt PI+R');
xlabel('Kp [p.u.]');
ylabel('D(z) [p.u.]');
grid on;

figure(15)
plot(w/(2*pi),20*log(1/n_p_P*ones(1,wn)),'--');hold on;
plot(w/(2*pi),low_S,'--');hold on;
plot(w/(2*pi),upp_S,'--');hold on;
plot(w/(2*pi),S_P(ikp,:),'-');hold on;
title('Output Sensitivity Function Template P');
xlabel('Operating Frequency [Hz]');
ylabel('Magnitude [dB]');
legend({'Modulus Margin','Lower Delay Margin=Ts','Upper Delay
Margin=Ts','Output Sensitivity Function'},'Location','northeast')
xlim([0 5000]);hold on;
ylim([-50 50]);hold on;
grid on;

figure(16)
```

```
plot(w/(2*pi),20*log(1/n_p_PI*ones(1,wn)),'--');hold on;
plot(w/(2*pi),low_S,'--');hold on;
plot(w/(2*pi),upp_S,'--');hold on;
plot(w/(2*pi),S_PI(ikp,:),'-');hold on;
title('Output Sensitivity Function Template PI');
xlabel('Operating Frequency [Hz]');
ylabel('Magnitude [dB]');
legend({'Modulus Margin','Lower Delay Margin=Ts','Upper Delay
Margin=Ts','Output Sensitivity Function'},'Location','northeast')
xlim([0 5000]);hold on;
ylim([-50 50]);hold on;
grid on;

figure(17)
plot(w/(2*pi),20*log(1/n_p*ones(1,wn)),'--');hold on;
plot(w/(2*pi),low_S,'--');hold on;
plot(w/(2*pi),upp_S,'--');hold on;
plot(w/(2*pi),S(ikp,:),'-');hold on;
title('Output Sensitivity Function Template PI+R');
xlabel('Operating Frequency [Hz]');
ylabel('Magnitude [dB]');
legend({'Modulus Margin','Lower Delay Margin=Ts','Upper Delay
Margin=Ts','Output Sensitivity Function'},'Location','northeast')
xlim([0 5000]);hold on;
ylim([-50 50]);hold on;
grid on;

figure(18)
plot(real(HOL_P(ikp_P,:)),imag(HOL_P(ikp_P,:)),'.-.');hold on;grid on;
xCenter = 0;
yCenter = 0;
theta = 0 : 0.01 : 2*pi;
radius = 1;
x = radius * cos(theta) + xCenter;
y = radius * sin(theta) + yCenter;
plot(x, y);
axis square;
axis equal;
xlim([-2 2]);hold on;
ylim([-2 2]);hold on;
title('Nyquist Diagram HOL only P');
xlabel('x axis');
ylabel('y axis');

figure(19)
plot(real(HOL_PI(ikp,:)),imag(HOL_PI(ikp,:)),'.-.');hold on;grid on;
xCenter = 0;
yCenter = 0;
theta = 0 : 0.01 : 2*pi;
radius = 1;
x = radius * cos(theta) + xCenter;
y = radius * sin(theta) + yCenter;
plot(x, y);
axis square;
axis equal;
xlim([-2 2]);hold on;
ylim([-2 2]);hold on;
title('Nyquist Diagram HOL only PI');
xlabel('x axis');
ylabel('y axis');
```

```
figure(20)
plot(real(HOL(ikp,:)),imag(HOL(ikp,:)),'.-.');hold on;

for ii=1:hkn

plot(real(HOL(ikp,round(377*hk(ii)/0.5*0.95))),imag(HOL(ikp,round(377*hk(ii
)/0.5*0.95))),'g*');hold on;

plot(real(HOL(ikp,377*hk(ii)/0.5)),imag(HOL(ikp,377*hk(ii)/0.5)),'r*');hold
on;

plot(real(HOL(ikp,round(377*hk(ii)/0.5*1.05))),imag(HOL(ikp,round(377*hk(ii
)/0.5*1.05))),'k*');hold on;
end
grid on;
xCenter = 0;
yCenter = 0;
theta = 0 : 0.01 : 2*pi;
radius = 1;
x = radius * cos(theta) + xCenter;
y = radius * sin(theta) + yCenter;
plot(x, y);
axis square;
axis equal;
xlim([-4 3]);hold on;
ylim([-2 5]);hold on;
title('Nyquist Diagram HOL PI+Resonant Controller');
xlabel('x axis');
ylabel('y axis');

figure(21)
for ii=1:hkn
    plot(real(R_C_h(ii,:)),imag(R_C_h(ii,:)));hold on;

plot(real(R_C_h(ii,round(377*hk(ii)/0.5*0.95))),imag(R_C_h(ii,round(377*hk(
ii)/0.5*0.95))),'g*');hold on;grid on;

plot(real(R_C_h(ii,round(377*hk(ii)/0.5))),imag(R_C_h(ii,round(377*hk(ii)/0
.5))),'r*');hold on;grid on;

plot(real(R_C_h(ii,round(377*hk(ii)/0.5*1.05))),imag(R_C_h(ii,round(377*hk(
ii)/0.5*1.05))),'k*');hold on;grid on;
end
xCenter = 0;
yCenter = 0;
theta = 0 : 0.01 : 2*pi;
radius = 1;
x = radius * cos(theta) + xCenter;
y = radius * sin(theta) + yCenter;
plot(x, y);
axis square;
axis equal;
xlim([-50 60]);hold on;
ylim([-30 60]);hold on;
title('Nyquist Diagram of Resonant Transfer Function with Damping');
xlabel('x axis');
ylabel('y axis');

    for jj=1:wn
        HOL(ikp,jj)=A_PI(ikp,jj).*C(ikp,jj);
        HV(ikp,jj)=A_PI(ikp,jj)./(1+A_PI(ikp,jj).*C(ikp,jj));
```

```
        HI(ikp,jj)=B(jj)./(1+A_PI(ikp,jj).*C(ikp,jj));
    end

figure(22)
%Bode Digital Resonant Controller
subplot(2,1,1)
semilogx(w,20*log10(abs(R_C_wk)));hold on;grid on;
title('Bode Diagram - Resonant Controllers');
xlabel('Frequency (rad/s)');
ylabel('Magnitude (dB)');
xlim([0.5 3*10^4]);hold on;

subplot(2,1,2)
semilogx(w,180/pi*angle(R_C_wk));hold on;grid on;
xlabel('Frequency (rad/s)');
ylabel('Phase (degrees)');
xlim([0.5 3*10^4]);hold on;

figure(23)
%Bode HOL
subplot(2,1,1)
semilogx(w,20*log10(abs(HOL(ikp,:))));hold on;grid on;
title('Bode Diagram - HOL');
xlabel('Frequency (rad/s)');
ylabel('Magnitude (dB)');
xlim([10 3*10^4]);hold on;
subplot(2,1,2)
semilogx(w,180/pi*angle(HOL(ikp,:)));hold on;grid on;
xlabel('Frequency (rad/s)');
ylabel('Phase (degrees)');
xlim([10 3*10^4]);hold on;

figure(24)
%Bode HV
subplot(2,1,1)
semilogx(w,20*log10(abs(HV(ikp,:))));hold on;grid on;
title('Bode Diagram - Voltage Tracking');
xlabel('Frequency (rad/s)');
ylabel('Magnitude (dB)');
xlim([10 3*10^4]);hold on;
subplot(2,1,2)
semilogx(w,180/pi*angle(HV(ikp,:)));hold on;grid on;
xlabel('Frequency (rad/s)');
ylabel('Phase (degrees)');
xlim([10 3*10^4]);hold on;

figure(25)
%Bode HI
subplot(2,1,1)
semilogx(w,20*log10(abs(HI(ikp,:))));hold on;grid on;
title('Bode Diagram - Output Impedance');
xlabel('Frequency (rad/s)');
ylabel('Magnitude (dB)');
xlim([10 3*10^4]);hold on;
subplot(2,1,2)
semilogx(w,180/pi*angle(HI(ikp,:)));hold on;grid on;
xlabel('Frequency (rad/s)');
ylabel('Phase (degrees)');
xlim([10 3*10^4]);hold on;
```

```
figure(26)
%Bode LPF
subplot(2,2,1)
semilogx(w,20*log10(abs(LPF)));hold on;grid on;
title({'Bode Diagram','alpha-beta Low Pass Filter'});
xlabel('Frequency (rad/s)');
ylabel('Magnitude (dB)');
xlim([10 3*10^4]);hold on;
subplot(2,2,3)
semilogx(w,180/pi*angle(LPF));hold on;grid on;
xlabel('Frequency (rad/s)');
ylabel('Phase (degrees)');
xlim([10 3*10^4]);hold on;
%Bode HPF
subplot(2,2,2)
semilogx(w,20*log10(abs(HPF)));hold on;grid on;
title({'Bode Diagram','alpha-beta High Pass Filter'});
xlabel('Frequency (rad/s)');
ylabel('Magnitude (dB)');
xlim([10 3*10^4]);hold on;
subplot(2,2,4)
semilogx(w,180/pi*angle(HPF));hold on;grid on;
xlabel('Frequency (rad/s)');
ylabel('Phase (degrees)');
xlim([10 3*10^4]);hold on;
```

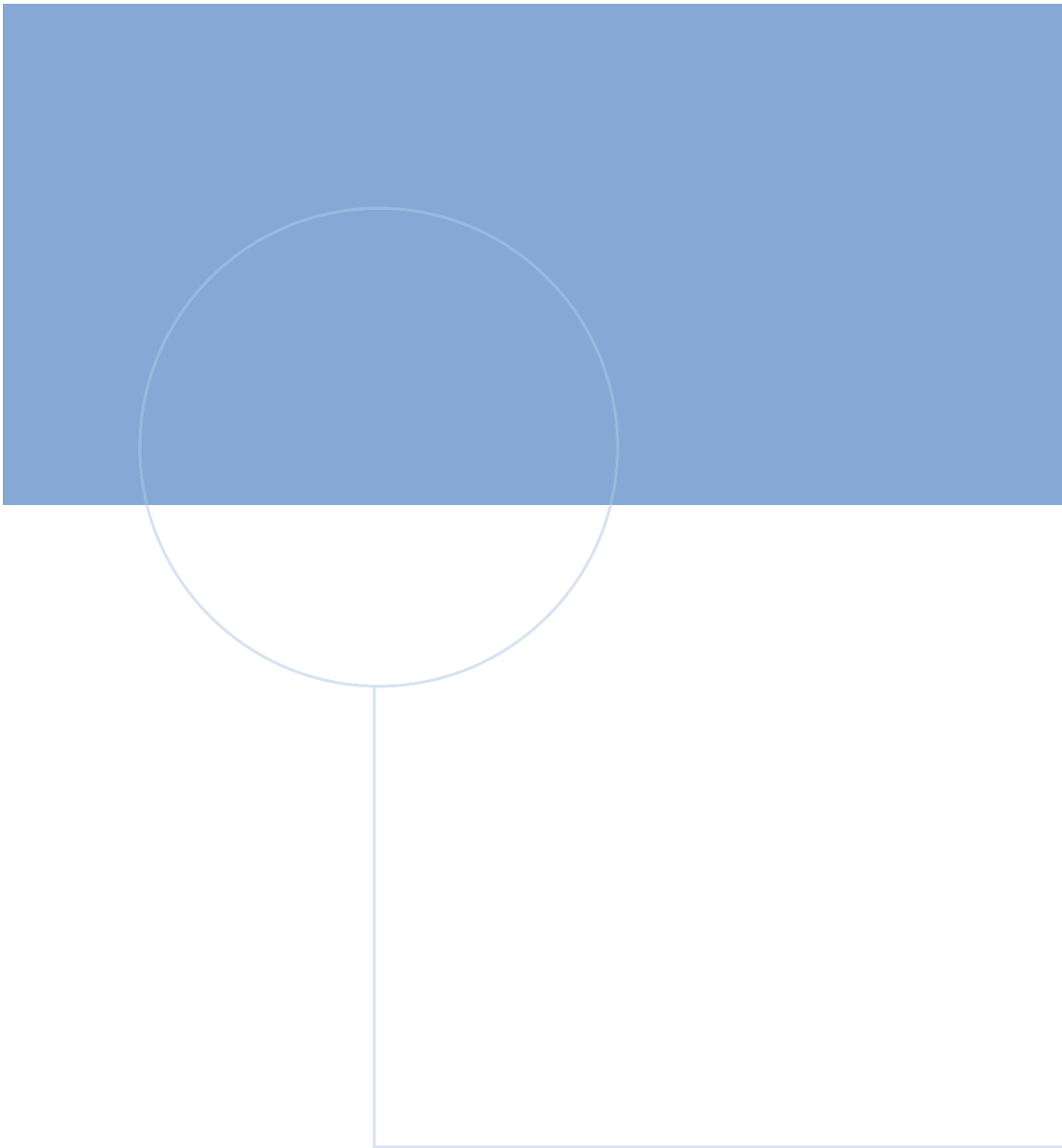

NTNU
Norwegian University of
Science and Technology